

---

# 27<sup>th</sup> RAU

## ANNUAL USERS MEETING LNLS/CNPq

---

November 22<sup>nd</sup> - 24<sup>th</sup>, 2017

**ABSTRACT BOOK**

[pages.cnpq.br/rau](http://pages.cnpq.br/rau)



MINISTÉRIO DA  
CIÊNCIA, TECNOLOGIA,  
INOVAÇÕES E COMUNICAÇÕES



Organization



Support

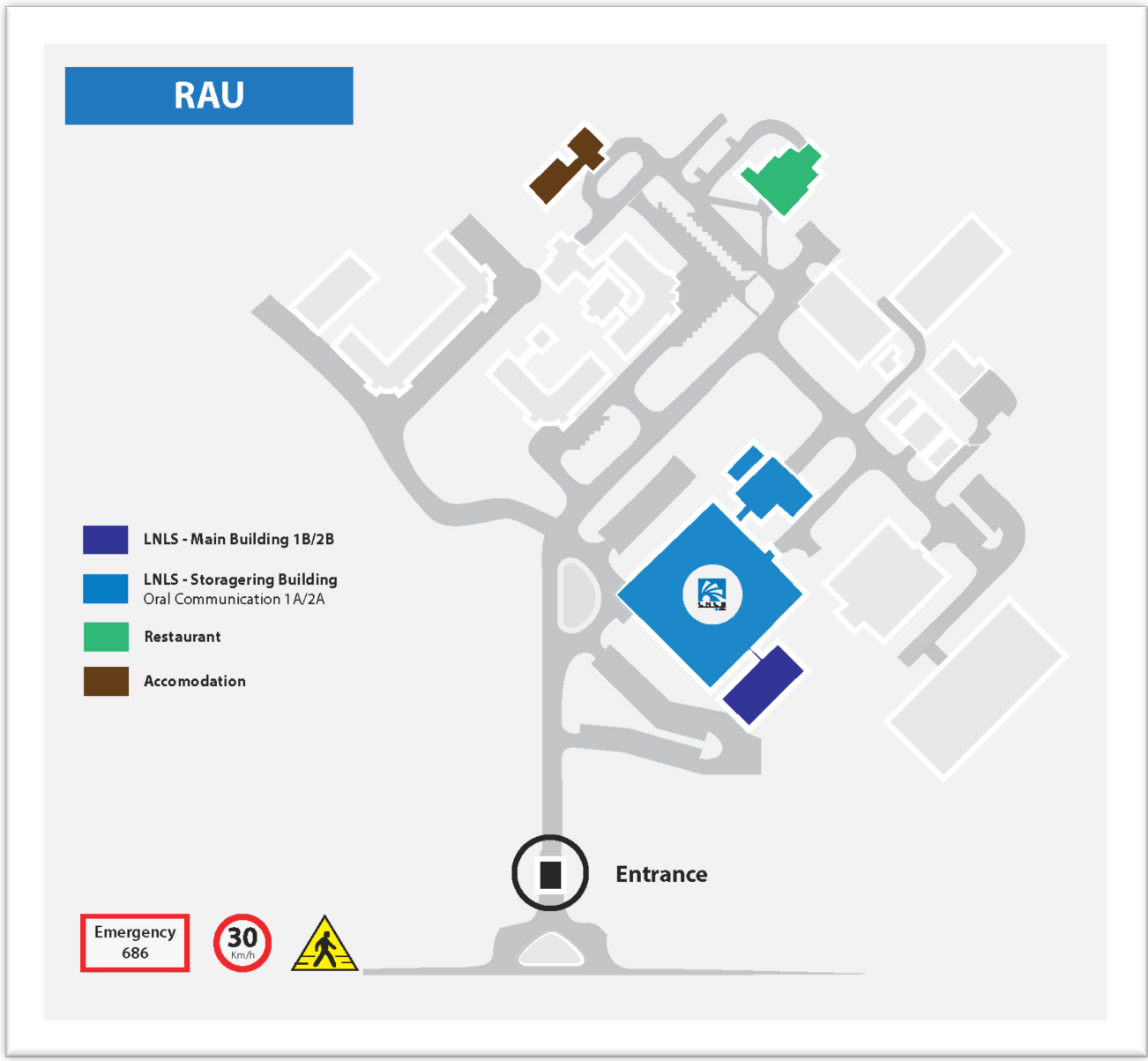


Sponsors



**Agilent Technologies**





**CNPEM – Campus Map**

# SUMMARY

**13 Presentation**

**14 Organization | scientific and local committees**

**15 Program**

**19 Speakers**

**22 Abstracts**

**23 XAFS Study of Inorganically Coated Colloidal Quantum Dots**

Acebróna, M., Herrera, F. C., Mizrahi, M., Requejo, F. G., Juarez, B. H.

**24 Copper-Doped Zinc Oxide Nanoparticles Synthesis by a Fast Polymer Precursor Based Method**

Almeida, D. F. De, Garcia, L. A., Kiminami, R. H. G. A., Klein-Gunnewiek, R. F. K.

**25 Bismuth ferrite crystallization from a  $V_2O_5 - Bi_2O_3 - Fe_2O_3$  glass matrix**

Almeida, N. P. De, Cassanjes, F. C., Klein-Gunnewiek, R. F. K.

**26 Water Adsorption in Layered Material**

Altoé, M. A. S., Michels, L., Santos, E. C. Dos, Droppa Jr., R., Grassi, G., Ribeiro, L., Knudsen, K. D., Bordallo, H. N., Fossun, J.O., Silva, G.J. Da.

**27 Particle size effects on structural and optical properties of  $BaF_2$  nanoparticles**

A B. Andrade<sup>1</sup>, Nilson S. Ferreira<sup>1,2</sup> And M. E. G. Valerio<sup>1</sup>.

**28 Cluster models  $Cu_{20}$  obtained by FSA and DFT strategies and XANES simulated spectrum by FDMNES**

Andrini, L., Soldano, G.J., Mariscal, M., Requejo, F.G., Joly, Y.

**30 Phosphate fertilization effects on phosphorus speciation in an Oxisol under no till evaluated by P-XANES**

Antonangelo, J. A., Firmano, R. F., Colzato, M., Abdala, D. B., Oliveira Jr., A., Carvalho, H. W. P., Alleoni, L. R. F., Zhang, H.

**32 Structural and Vibrational Properties of  $Co_3O_4$  Films Deposited by Reactive DC Magnetron Sputtering**

Azevedo Neto, N. F., Affonço, L.J., Angélico, J.C., Zanatta, A.R., Pereira, A.L.J., Soares, M. M., Silva, J.H.D. Da.

**34 Chemical speciation of Sulphur in petroleum asphaltenes using XANES spectroscopies**

Bava, Y. B., Geronés, M., Andrini, L., Giovanetti, L., Erben, M. F.

**35 An alternative paradigm for EUVL resists: hybrid n-cars-design principles and photodynamics**

Belmonte, G. K., Moura, C. A. S., Reddy, G., Gonsalves, K. E., Weibel, D. E.

**37 PDF Phama research team: high-energy X-ray characterization of amorphous solid drugs using synchrotron radiation**

- Bezzon, V. D. N., Araujo, G. L. B. De.
- 39 Study about luminescence in doped cayal3o7 using VUV**  
Bispo, G. F. C., Andrade, A. B., Teixeira, V. C., Novais, S. M. V., Macedo, Z. S., Valerio, M. E. G.
- 41 Modelling the structure of Nafion membranes by using small angle x-ray scattering**  
Bordín, S.P. F., Andrada, H., Carreras, A., Castellano, G., Oliveira, R., Galván, V.
- 42 Sodium Caseinate/Sunflower Oil Nanoemulsion-Based Gels Analyzed by SAXS**  
Borroni, V., Oca-Avalos, J. M. M. De, Candal, R., Herrera, M. L.
- 43 Insights into Aminotransferases From The Biosynthesis Pathway of Aminoglycosides Antibiotics**  
Bury, P.S., Huang, F., Sun, Y., Cerrone, N., Leadlay, P., Dias, M. V. B.
- 44 Analysis of sugarcane bagasse particles by X-ray microtomography**  
Cabellero, D. M. Y., Ling, L. Y., Archilha, N. L., Ferreira, J. E., Driemeier, C.
- 45 Polymeric precursor based fast-synthesis of lanthanum-doped bismuth ferrite nanoparticles**  
Cancellieri, I. C., Perdomo, C. P. F., Klein-Gunnewiek, R. F.
- 46 Structural Characterization of Sodium Caseinate Aerogels**  
Candal, R.J., Oca Avalos, J. M. M. De, Borroni, M.V., Herrera, M.L.
- 47 Microwave induced mineralogical transformation in copper ore**  
Cardoso, A. L. F., Klein-Gunnewiek, R. F., Magalhães Filho, T. A., Perdomo, C. F., Kiminami, R.
- 50 A versatile setup in reflection mode for in situ diffraction patterns acquisition from flat polycrystalline specimens bathed in a liquid medium**  
Carezzato, G. L., Couto, C. P., Rossi, J. L., Martinez, L. G., Turrillas, X.
- 51 Magnetic and structural behavior of Ca<sub>2</sub>MnReO<sub>6</sub> under pressure**  
Cavichini, A. S., Orlando, M. T. D., Depianti, J. B., Passamai Jr, J. L., Granado, E.
- 52 Production and initial crystallographic studies of 2,5-furandicarboxylic acid decarboxylase 1 enzyme from Paraburkholderia xenovorans LB400**  
Chagas, B. C. A., Rocha, R., Costa, M. A. F., Rodrigues, F. T. G., Nagem, R. A. P.
- 55 Internal structures of Thoropa miliaris tadpole using phase-contrast synchrotron microtomography**  
Colaço, m.v., fidalgo, g., braz, d., nogueira, l.p., colaço, g., silva, h.r., bar, r.c.
- 56 XAS and XPS studies of Zn<sub>1-x</sub>co<sub>x</sub>o thin films applied as gas sensors**  
Colmenares, N., Mastelaro, V. R., Correr, W.

- 59 Magnetic Field Induces Nanoparticles Structuring. A SAXS Application: Instrumental Development at LNLS and Data Analysis**  
Coral, D. F., Mendoza Zélis, P., Polli, J. M., Fernández Van Raap, M. B.
- 60 Structuring Of Magnetic Nanoparticles In Living Cells**  
 Coral, D. F., Soto, P., Muñoz, G. A., Setton, P., Sánchez, F. H., Fernández Van Raap, M.B.
- 61 Study of the partial substitution of Ni by Nb in perovskite based catalysts applied on partial oxidation of methane using XPD line**  
Costa, D. S., Brandão, S. T., Rodella, C. B., Gomes, R. S.
- 63 In vivo XANES for determination of the chemical environment of Zn in the stem of kidney beans treated with zno nanoparticles**  
Cruz, T. N. M. Da, Savassa, S. M., Picolla, C. D., Carvalho H. W. P. De.
- 66 Structure and Properties of Siloxane-Polyether Hybrid Organic-Inorganic Materials for Drug Delivery of Salicylic Acid**  
Dahmouche, K., Barcelos, E. I., Gomes, A De S.
- 67 Catalytic Nanoparticles sitting on top of Graphene: The heterojunction interaction with H<sub>2</sub> gas followed by in-situ GISAXS Experiments**  
 Dalfovo, M. C., Huck-Iriart., C., Giovanetti, L. J., Ibañez, F.J.,
- 68 BI-Reforming of Biogas for Hydrogen Production Using lanio<sub>3</sub>/cexzr<sub>1-xo2</sub>(x = 1; 0.75; 0.5) as Precursor Material**  
Dos Santos, D. B. L., Noronha, F. B., Hori, C. E.
- 69 Complex structural arrangements of ceramide lipids is produced by asymmetric molecular shape**  
Dupuy, F., Pérez Bordín, S., Pusterla J., Gasperini, A., Maggio, B., Oliveira, R.
- 70 M-XANES and X-ray tomography uncovering the effects of nanoparticles on Phaseolus vulgaris seeds**  
Duran, N. M., Costa Júnior, G. T., Santos, J. R. P., Carvalho, H. W. P.
- 73 Synthesis and structural characterization of new ion-conducting PVA/Clay/ionic liquid nanocomposite membranes**  
Dutra Filho, J. C., Dahmouche, K., Gomes, A. S.
- 74 In-situ study of formation and phase transition using x-ray absorption and diffraction in (Y.RT)cro<sub>3</sub>+γ compounds**  
Fabian, F. A., Barbosa, C. C. S., Duque, J. G. S., Meneses, C. T.
- 75 Study of structural properties of Heavy Fermion compound ybfe<sub>2</sub>zn<sub>20</sub> doped with Cd.**  
Fahl, A. L., Cabrera-Baez, M., Avila, M. A., Adriano, C., Giles, C., Silva, D. R. G., Granado, E.

- 76 Mixed nimo, niw and nimow Sulfides Obtained from Idhs**  
Faro Jr., A. C., Arias, S., Licea, Y., Eon, J. G., Palacio, L.
- 77 [1]Benzothieno[3,2-b]benzothiophenes derivatives: influence in the molecular orientations and charge delocalization process**  
Fernández, A. B., Veigala, A. G. Da, Alev, A., Geerts, Y. H., Rocco, M. L.
- 78 Structural characterization of Sb-based type II superlattices**  
Ferreira, S. O., Deneke, C., Zamrı, M., Cavallo, F.
- 79 Physicochemical properties of nanostructured Pd/lanthanide-doped ceria spheres with high catalytic activity for CH<sub>4</sub> combustion**  
Fuentes, R. O., Acuña, L. M., Leyva, A. G., Baker, R. T., Pan, H., Chen, X., Delgado-Jaén, J. J.
- 82 Cobalt-dopped Zinc Oxide Nanoparticles Synthesis by a Fast Polymer Precursor Based Method**  
Garcia, L. A., Almeida, D. F. De, Perdomo, C. P. F., Klein-Gunnewiek, R. F.
- 83 Advanced Modeling and Data Analysis of In-Situ SAXS investigations of silver nanoparticles nucleation**  
Garcia, P. R. A. F., Grasmik, V., Pappert, K., Prymak, O., Epple, M., Oliveira, C. L. P.
- 84 Unravelling the nature of NIR plasmonic nanoprisms**  
Giovanetti, L., Huergo, M. A., Moreno, M. S., Maier, C. M., Requejo, F. G., Salvarezza, R. C., Vericat, C.
- 85 In Vivo Evaluation of Zinc Foliar Absorption Applied by Sources with Different Solubility in Soybean**  
Gomes, M. H. F., Rodrigues, E. S., Duran, N. M, Almeida, E, Otto, R., Carvalho, H. W. P.
- 88 Mapping Out the Dynamics of Cation Exchange by Means of Synchrotron XRD**  
Grassi, G., Michels, L., Altoé, M. A. S., Fonsêca C. L. S. Da, Droppa Jr., R., Fossum, J.O., Silva, G.J. Da.
- 89 Synthesis and structural characterization using synchrotron X-ray Powder Diffraction (S-XRD) of  $\text{NdBa}_2\text{Cu}_3\text{O}_{6+\delta}$  with energy applications**  
Grassi, J., Macías, M., Suescun, L.
- 92 Spectrochemical analysis of metals in gingival fluid of patients with dental implants and different prosthetic materials**  
Grenón, M., Fuks, D., García, M., Oliva, F., Ibañez, J. C., Ibañez, M. C., Juaneda, M. A., Pérez, C. A., Sánchez, H. J.
- 93 Impact of the crystallization conditions on the polymorphism and crystalline size domain of Efavirenz**  
Gumarães, R., Cuffini, S. L., Kuznetsov, A., Rocha, H. V. A.

- 94 Born Again vs. Isgisaxs: Application of these popular softwares in the characterization of nanopores embedded in zno films**  
Heredia, E., Bojorge, C., Cánepa, H.
- 95 Structure of Sodium Caseinate-Stabilized Nanoemulsions Studied by Laser Scanning Confocal Microscopy and Small Angle X-Ray Scattering**  
Herrera, M.L., Oca Ávalos, J.M. M. De, Borroni, M.V., Candal, R.J.
- 96 In situ synchrotron radiation evaluation of hydrogen embrittlement in stainless steels and of severe plastic deformation at cryogenic temperatures in metals**  
Hoyos, J. J., Craidy, P., Paes, M. T. P., Ramírez, A. J., Tschiptchin, A., Cintho, O.
- 97 Isolation and characterization of nitrososulphide species (SNO-/SNOH) stabilized by coordination to iridium (III)**  
Huck-Iriart, C., Foi, A., Andriani, L., Lopez, J. R., Joly, Y., Di Salvo, F., Doctorovich, F.
- 98 Mn-Zn ferrite nanoparticles probed by synchrotron pair distribution function analysis and anomalous X-ray scattering**  
Ichikawa, R. U., Parra J., Vallcorba, O., Peral, I., Yoshito, W. K., Saeki, M. J., Turrillas, X., Martinez, L. G.
- 99 Crystal Structures of  $\text{BaFe}_2\text{As}_2$  and  $\text{Sr}(\text{Fe}_{0.08}\text{Co}_{0.20})_2\text{As}_2$  under Magnetic Field**  
Kaneko, U. F., Piva, M., Saleta, M. E., Pagliuso, P. G., Granado, E.
- 100 Chemical speciation of size-segregated aerosol samples collected at an urban location in Central Argentina**  
Lanzaco, B. L., López, M. L., Olcese, L.E., Toselli, B. M.
- 103 Core-shell starch nanoparticles-co-p(NIPAM) hybrid microgels**  
Leite, D. C., Silveira, N. P.
- 104 The Surface Atomic Structure of Black Phosphorus Studied by Photoelectron Diffraction**  
Lima, L. H. De, Barreto, L., Landers, R., Siervo, A. De
- 105 Crystallographic and Kinetic Analysis of nahk Mutants: A Decarboxylase from the Naphthalene Degradation Pathway**  
Marins, K. S., Guimarães, S. L., Nagem, R. P.
- 108 In situ XRD studies of Copper-based methanol synthesis catalysts activation**  
Mello, M. I. S. De, Vinaches, P., Rodella, C., Pergher, S. B. C.
- 109 Synthesis and characterization of ligand-free Ni nanoclusters**

Mizrahi, M., Peinetti, A. S., Buceta, D., Ramallo-López, J. M., González, G., Requejo, F., López-Quintela, A., Battaglini, F.

**112 Structure-property relations of polurea elastomers prepared by sol-gel process**

Molina, E. F., Bonattini, V. H.

**113 Changes in the Structural Characteristics of Titania Photocatalysts Probed by Multivariate Analysis Applied to SAXS Profiles and FT-IR Spectra**

Moreno, Y. P., Ferrão, M., Dos Santos, J. H. Z.

**114 Calculation of Two-Dimensional Scattering Patterns for Oriented Systems**

Oliveira, C. L. P., Alves, C., Pedersen, J. S.

**115 Grazing incidence X-ray off specular scattering on biomembrane Langmuir monolayers**

Oliveira, R., Pusterla, J., Gasperini, A., Puentes-Martinez, X., Cavalcanti, L.

**116 Study of the profile of layer formed in plasma nitrated Austenitic stainless steel**

Olzon-Dionysio, D., De Souza, S. D., Martinez, L. G., Campos, M., Da Silva, E. H., Olzon-Dionysio, M.

**117 Studying the 4f electrons in the Kondo lattice antiferromagnet  $Ce_2RhIn_8$**

Pakuszewski, K. R., Silva, W. S., Giles, C., Rodolakis, F., Cezar, J. C., Campuzano, J. C., Pagliuso, P. G., Adriano, C.

**118 Coal-terephthalate hydrotalcite materials with high aluminum contents**

Palacio, L., Coelho, T., Arias, S., Licea, Y., Faro, A.

**121 Cooling induces phase separation in isolated Central Nervous System myelin membranes**

Pusterla, J., Schneck, E., Funari, S., Demé, B., Tanaka, M., Oliveira R.

**122 The structure of Co species in novel active and selective Co/MCM41 catalyst in the coprox reaction prepared by supercritical CO<sub>2</sub> reactive deposition**

Ramallo-López, J. M., Mizrahi, M., Aspromonte, S., Alonso, E., Boix, A.

**123 Mesoporous silica: in situ SAXS investigation of synthesis processes**

Rasmussen, H. Ø., Neto, F. M., Fantini, M. C. A., Oliveira, C. L. P.

**124 Specific procedures for experiments of multiple diffraction at XRD2 beamline (LNLS) applicated to micro organic crystals**

Remédios, C. M. R., Morelhão, S. L.

**125 Stability and reactivity of copper clusters with five atoms**

Requejo, F. G., Giovanetti, L. J., Ramallo-López, J. M., Iriart, C. H., Escudero-Rodríguez, C., Buceta, D., López-Quintela, M. A.

- 126 Effects of B4C Addition on Microstructure and Mechanical Properties of a Beta Titanium Alloy**  
Rielli, V. V., Contieri, R. J.
- 127 Compact XRF spectrometer for CARNAUBA beamline at SIRIUS**  
Robledo, J. I., Pérez, C. A., Ribeiro, R., Honnicke, M., Sánchez, H. J.
- 128 Molecular Orientation and Ultrafast Charge Transfer Dynamics Studies on the P3HT:PCBM Blend**  
Rocco, M. L. M., Borges, B.G.A.L., Veiga, A. G., Tzounis, L., Laskarakis, A., Logothetidis, S.
- 129 Lectins from Parkia biglobosa and Parkia platycephala: A comparative study of structure and biological effects**  
Rocha, B. A. M., Bari, A. U., Santiago, M. Q., Osterne, V. J. S., Pinto-Júnior, V. R., Pereira, L. P., Silva-Filho, J. C., Debray, H., Delatorre, P., Teixeira, C. S., Neto, C. C., Assreuy, A. M. S., Nascimento, K. S., Cavada, B. S.
- 130 Mapping of elemental distribution of Cu, Fe and Zn in human prostatic carcinoma cell spheroid culture using synchrotron radiation based on Microbeam X-ray Fluorescence**  
Rocha, K. M. J., Leitão, R. G., Oliveira-Barros, E. G., Oliveira, M. A., Canellas, C. G. L., Anjos, M. J., Nasciutti, L. E., Lopes, R. T.
- 132 Advances in the Red/NIR-persistent luminescence materials design with VUV luminescence spectroscopy**  
Rodrigues, L. C. V., Santos, D. O. A., Barbará, M. A. S. G., Fritzen, D. L., Bezzan, O. P., Teixeira, V. C.
- 134 Impact of oxidized lipid in the structural parameters of biological model membranes as seen by Small Angle X-Ray Scattering (SAXS)**  
De Rosa, R.
- 135 Study of hydration of sulphoaluminate cement by in situ synchrotron diffraction**  
Rossetto, C. M., Martinez, L. G., Ichikawa, R. U., Carezzato, G. L., Carvalho, A. M. G., Turrillas, X.
- 136 Local structure on bafe2as2: formation of nanotwins studied by atomic pair distribution function**  
Saleta, M. E., Tobia, D., Piva, M. M., Jesús, C. B. R., Rosa, P. F., Urbano, R. R., Granado, E., Pagliuso, P.G.
- 138 Pressure-induced Phase Transition and Phonon Anomalies in Sr2IrO4**  
Samanta, K., Rigitano, D. S., Ardito, F. M., Souza-Neto, N. M., Granado, E.
- 139 Copper Chemical Environment in Daphnia magna exposed to copper nanoparticles**  
Santos, J. R. P., Costa Jr, G. T., Gomes, M. H. F., Monteiro, R. T. R., Carvalho, H. W.

- 140  $\mu$ -XANES analysis for understanding of the interaction of zno nanoparticles in seeds of common bean**  
Savassa, S. M., Duran, N. M., Rodrigues, E. S., Pereira De Carvalho, H.W.
- 141 Structure of coo thin films under mechanical stress**  
Sborz, J., Bordin, A., Soares, M. M.
- 142 Study of the zeolitic precursor (P)MCM-22: nucleation and growth**  
Schwanke, A. J., Vinaches, P., Meneau, F., Morgado Jr., E., Pergher, S. B. C.
- 143 Magnetite nanoparticles for hyperthermia cancer treatment**  
Shigeyosi, W. T., Costa, F. C., Kobarg, J., Cardoso, M. B.
- 144 Qualitative Structure and Strain Determination of ceo2 Nanoparticles Using Atomic Pair Distribuiton Function Analysis**  
Silva, F. P., Silva, M. S., Ferreira, N. S.
- 145 A study of M-type mfe12o19 (M=Ba and Sr) nanoparticles by X-ray diffraction and atomic pair distribution function**  
Silva, F. P., Silva, M. S., Ferreira, N. S.
- 146 Micelles and hybrid silicas formation with tripropylammonium surfactants and different hydrophobic tails**  
Silva, L. L. Da, Zapelini, I. W., Modesto, P. P., Campos, A. F. P., Oliveira, L. B. De, Silva, J. F. Da, Cardoso, D.
- 147 Long-term drug release using sio2-Poly(oxypropylene)hybrid matrix: correlation between the release mechanism and the physical-chemical characteristics**  
Silva, R., Dahmouche, K., Santilli, C. V.
- 148 Radiation damage caused by soft X-rays in sulfur tripeptides in solution: Why should we care?**  
Simões, G., Gonzalez, J. C., Bernini, R. B., Coutinho, L. H., De Souza, G. G. B.
- 149 Thermo-mechanical stability of austenite in post weld heat treated supermartensitic stainless steel weld metal**  
Svoboda, H. G., L. Tufaro, S. Zappa
- 150 New method in the growth of thin films of Ag2Se and structural study through Synchrotron radiation X-ray grazing incidence diffraction with in situ heating**  
Taborda, J. A. P., Briones, F., Gonzales, M. S. M.
- 151 Magnetic Structures and Transitions of rnsi3 (R = Gd-Ho)**  
Tartaglia, R., Giraldo, D. V. A., Avila, M. A., Granado, E.
- 152 In-situ electrochemical cell for lithium ion batteries and X-ray absorption studies**

---

Thomas, J. E., Giovanetti, L. J., Sanservino, M. A., Azevedo, G., Requejo, F. G.,  
Visitin, A.

**153 X-Ray Absorption Study on Native Defects of Cu<sub>2</sub>O**

Tumelero, M. A., Brandt, I. S., Pasa, A. A.

**154 Properties of hybrid silicas synthesized using different cationic surfactants  
with cyclic head**

Zapelini, I. W., Silva, L. L. Da, Modesto, P. P., Fukuda, P. M., Franke, K. N.,  
Vasconcellos, M. S., Caroso, D.

**155 Tambo Colorado pigments: a archaeometric study by synchrotron X-ray  
diffraction**

Zeballos-Velásquez, E., Wright, V., Suescun, L., Asto, E.

---

# PRESENTATION

Dear Colleague,

On behalf of the organizers, I welcome all the participants of the 27<sup>th</sup> Annual Users Meeting of the Brazilian Synchrotron Light Laboratory (RAU/LNLS).

As the construction of the new synchrotron light source (SIRIUS) evolves steadily, the broad scientific horizon offered by such state-of-the-art machine attracts an increasing interest by the LNLS present and future users community. Amongst other gains, there is little doubt that the record-low emittance of SIRIUS will have a particularly huge impact on the attainable spacial resolution, which will drop to the nanometer scale in some beamlines. This opens an avenue to combine imaging with spectroscopy and diffraction, offering the possibility to characterize and understand the structure and dynamics of increasingly complex and inhomogeneous samples.

In this year's meeting, the scientific program was devised to highlight the new science and technical challenges brought by this exciting development. Tobias Schulli (ESRF, France) and Rainer Hillenbrand (Nanoscience Cooperative Research Center – CIC nanoGUNE, Spain) will deliver invited talks showing their experiences in using imaging and spectroscopy/scattering in very different regions of the electromagnetic spectrum, namely x-rays and Infrared/THz, respectively. Also, the LNLS scientific computation group will expose the advances and planning in handling, treating, restoring and reconstructing images, amongst other advances that will be essential to optimize the use of the new facility. The scientific program will be complemented by a LNLS Presentation, Oral and Poster sessions, visit to SIRIUS civil works, a LNLS Thematic session, meeting with beamline coordinators, and will be finalized with a round table with the users.

The scientific and local committees are acknowledged for their decisive contributions to the organization of this meeting. We are also indebted to the sponsors and main funding agencies Fapesp, CNPq and CAPES, which made this important event possible.

**Eduardo Granada**

Chair of the 27<sup>th</sup> RAU

---

# ORGANIZATION

- **SCIENTIFIC COMMITTEE**

Eduardo Granado Monteiro da Silva (Unicamp) – **Chairperson**  
Hélio Cesar Nogueira Tolentino (LNLS – CNPEM) – **Local Coordinator**  
Felix Requejo (UNPL / Argentina)  
Izabel Riegel Vidotti (UFPR)  
Leopoldo Suescun (UDELAR / Uruguai)  
Maria do Carmo Martins Alves (UFRGS)  
Maria Luiza Rocco (UFRJ)  
Mônica Alonso Cotta (Unicamp)  
Rafael Guido (USP)

- **LOCAL COMMITTEE**

Dora Marques (CNPEM)  
Graziela Esteves (LNLS – CNPEM)  
Luciana Noronha (CNPEM)  
Priscila Alves (LNLS – CNPEM)  
Renata Mioshi (SAU – CNPEM)  
Thaís Capovilla (LNLS – CNPEM)  
Vilmara Congilio (SAU – CNPEM)  
Renan Picoreti (LNLS – CNPEM)  
Lucas Dias (CNPEM)  
Murilo Oliveira (CNPEM)  
Gabriela Campeão (CNPEM)

# PROGRAM

<b>22nd November 2017</b>	
<b>10:00 – 11:00</b>	<b>Reception / Registrations / Welcome Coffee</b>
<b>11:00 – 12:45</b>	<b>LNLS Presentation:</b> Dr. Antonio José Roque da Silva [LNLS Director] and Dr. Harry Westfahl [LNLS Scientific Director]
<b>12:45 – 13:00</b>	<b>Official Photo</b>
<b>13:00 – 14:00</b>	<b>Lunch</b>
<b>14:00 – 15:00</b>	<b>Plenary 1:</b> “X-ray scattering under imaging conditions: merging spectroscopy, reciprocal and real space” ( <b>Dr. Tobias Schulli, ESRF</b> )
<b>15:00 – 18:00 (simultaneously)</b>	<b>Meeting with beamline coordinators</b> <b>Visit to Sirius civil works (groups leaving at 15H / 16H / 17H)</b>
<b>18:00</b>	<b>Social gathering</b>

<b>23rd November 2017</b>	
<b>08:30 – 09:30</b>	<b>Plenary 2:</b> Sirius IT infrastructure ( <b>Dennis Massaroto Campos, CNPEM</b> ) Sirius Beamlines Control and Data Acquisition ( <b>James Piton, LNLS</b> ) Beamline Data Processing and Visualization Strategies for Sirius ( <b>Eduardo Miqueles, LNLS</b> )
<b>09:30 – 11:00</b>	<b>Oral Communication 1 (two parallel sessions – 1A and 1B)</b>
<b>11:00 – 11:30</b>	<b>Coffee Break</b>
<b>11:30 – 13:00</b>	<b>Poster Session 1</b>
<b>13:00 – 14:30</b>	<b>Lunch</b>
<b>14:30 – 15:30</b>	<b>Plenary 3:</b> “IR and THz nanoimaging and nanospectroscopy – Emerging analytical tools for science and technology” ( <b>Dr. Rainer Hillenbrand, CIC nanoGUNE</b> )
<b>15:30 – 16:00</b>	<b>Coffee Break</b>
<b>16:00 – 17:30</b>	<b>Oral Communication 2 (two parallel sessions – 2A and 2B)</b>

## 24th November 2017

<b><i>08:30 – 10:30</i></b>	<b>LNLS Tematic Session: UVX and Sirius</b>
<b><i>10:30 – 12:00</i></b>	<b>Poster Session 2</b>
<b><i>12:00 – 13:15</i></b>	<b>Round Table with users</b>
<b><i>13:15 – 14:00</i></b>	<b>Lunch</b>
<b><i>End</i></b>	

## Storage Ring Auditorium - November 23<sup>rd</sup>

### Oral Communication 1 A

<b>09:30</b>	<b>Cristiano Luis Pinto Oliveira</b>	<b>Calculation of Two-Dimensional Scattering Patterns for Oriented Systems</b>
<b>09:45</b>	<b>José Carlos Dutra Filho</b>	<b>Synthesis and structural characterization of new ion-conducting PVA/Clay/ionic liquid nanocomposite membranes</b>
<b>10:00</b>	<b>Nádyá Silveira</b>	<b>Core-shell starch nanoparticles-co-p(NIPAM) hybrid microgels</b>
<b>10:15</b>	<b>Roberto Jrge Candal</b>	<b>Structural Characterization of Sodium Caseinate Aerogels</b>
<b>10:30</b>	<b>Jaime Andres Perez Taborda</b>	<b>New method in the growth of thin films of Ag<sub>2</sub>Se and structural study through Synchrotron radiation X-ray grazing incidence diffraction with in situ heating</b>
<b>10:45</b>	<b>Paulo Ricardo de Abreu Furtado Garcia</b>	<b>Advanced Modeling and Data Analysis of In-Situ SAXS investigations of silver nanoparticles nucleation</b>

### Oral Communication 2 A

<b>16:00</b>	<b>Cláudio Márcio Rocha Remédios</b>	<b>Specific procedures for experiments of multiple diffraction at XRD2 beamline (LNLS) applicated to micro organic crystals</b>
<b>16:15</b>	<b>Ulisses Kaneko</b>	<b>Crystal Structures of BaFe<sub>2</sub>As<sub>2</sub> and Sr(Fe<sub>0.08</sub>Co<sub>0.20</sub>)<sub>2</sub>As<sub>2</sub> under Magnetic Field</b>
<b>16:30</b>	<b>Martín Eduardo Saleta</b>	<b>Local structure on BaFe<sub>2</sub>As<sub>2</sub>: formation of nanotwins studied by atomic pair distribution function</b>
<b>16:45</b>	<b>Kevin Raduenz Pakuszewski</b>	<b>Studying the 4f electrons in the Kondo lattice antiferromagnet Ce<sub>2</sub>RhIn<sub>8</sub></b>
<b>17:00</b>	<b>Kousik Samanta</b>	<b>Pressure-induced Phase Transition and Phonon Anomalies in Sr<sub>2</sub>IrO<sub>4</sub></b>
<b>17:15</b>	<b>Carlos Basilio Pinheiro</b>	<b>Hard X-ray-Induced Valence Tautomeric Interconversion in a Cobalt Complex</b>

## LNLS Auditorium - November 23<sup>rd</sup>

### Oral Communication 1 B

<b>09:30</b>	<b>Rodolfo Oscar Fuentes</b>	Physicochemical properties of nanostructured Pd/lanthanide-doped ceria spheres with high catalytic activity for CH <sub>4</sub> combustion
<b>09:45</b>	<b>Francisco Ibañez</b>	Catalytic Nanoparticles and their interaction with H <sub>2</sub> gas followed by in-situ GISAXS Experiments
<b>10:00</b>	<b>Felix G. Requejo</b>	Stability and reactivity of copper clusters with five atoms
<b>10:15</b>	<b>Milton Andre Tumelero</b>	X-Ray Absorption Study on Native Defects of Cu <sub>2</sub> O
<b>10:30</b>	<b>Carlos William Galdino</b>	On the Co electronic states of the ludwigite Co <sub>3</sub> O <sub>2</sub> BO <sub>3</sub> - an x-ray absorption spectroscopy study
<b>10:45</b>	<b>Marcos Henrique Feresin Gomes</b>	In Vivo Evaluation of Zinc Foliar Absorption Applied by Sources with Different Solubility in Soybean

### Oral Communication 2 B

<b>16:00</b>	<b>Cristián Huck Iriart</b>	Isolation and characterization of nitrososulphide species (SNO-/SNOH) stabilized by coordination to iridium (III)
<b>16:15</b>	<b>Daniel Weibel</b>	An alternative paradigm for EUVL resists: hybrid n-CARs-design principles and photodynamics
<b>16:30</b>	<b>Jose Ignacio Robledo</b>	Compact XRF spectrometer for CARNAUBA beamline at SIRIUS
<b>16:45</b>	<b>Luis Henrique de Lima</b>	The Surface Atomic Structure of Black Phosphorus Studied by Photoelectron Diffraction
<b>17:00</b>	<b>Daison Manuel Yancy Caballero</b>	Analysis of sugarcane bagasse particles by X-ray microtomography
<b>17:15</b>	<b>Lucas Carvalho Veloso Rodrigues</b>	Advances in the Red/NIR-persistent luminescence materials design with VUV luminescence spectroscopy

---

# 27<sup>th</sup> RAU

## ANNUAL USERS MEETING LNLS/CNPEM

---

November 22<sup>nd</sup> - 24<sup>th</sup>, 2017

**ABSTRACTS**

[pages.cnpem.br/rau](http://pages.cnpem.br/rau)



MINISTÉRIO DA  
CIÊNCIA, TECNOLOGIA,  
INOVAÇÕES E COMUNICAÇÕES



## **X-ray scattering under imaging conditions: merging spectroscopy, reciprocal and real space**

*T. Schülli a Head of the X-ray Nanoprobe group a ESRF, Grenoble, France  
schulli@esrf.fr*

X-ray diffraction and X-ray imaging have for one century mostly been regarded as two distinct applications of the same type of radiation. Traditionally x-ray diffraction is considered as a method with poor spatial resolution yielding only spatial averages as useful results. Very recent developments in the use of highly focused beams produced on the most advanced synchrotron sources show however a great and rapidly developing potential of diffraction imaging techniques. These are much improving the resolution of traditional x-ray imaging and topography but are as well combined with x-ray diffraction. In this way a new portfolio of techniques emerges, coupling the information of strain and texture with spatial information. As so far most of these new imaging techniques are brilliance limited they are naturally developed at synchrotrons. With the rapid development of the availability of synchrotron radiation throughout Europe and in interaction with the very active user community in this field, new imaging techniques rapidly gain practically all fields of materials science and biomedicine. While x-ray optics typically limit today's resolution to about 100 nm, technological progress in this field, as well as the use of reconstruction techniques pave already the way towards nanometric resolution in space while preserving the structural information available through diffraction. With new source projects at the horizon these exciting imaging techniques will be established on a growing number of beamlines. With the completion of the first phase of the upgrade of the European Synchrotron Radiation Facility (ESRF), several spectro-nanoprobes and diffraction imaging beamlines have returned successfully to user operation. Offering scanning microscopy with x-ray beams focused down to 20 nm, full field x-ray microscopy using compound refractive lenses or parallel beam techniques, and with the use coherent Bragg diffractive imaging applications the ESRF can supply a vast spectrum of techniques for high resolution (strain) imaging.

## **IR and THz nanoimaging and nanospectroscopy – Emerging analytical tools for science and technology**

*Rainer Hillenbrand CIC nanoGUNE, San Sebastian, Spain  
r.hillenbrand@nanogune.eu*

With the development of scattering-type scanning near-field optical microscopy (s-SNOM) and nanoscale Fourier transform infrared spectroscopy (nano-FTIR), the analytical power IR and THz radiation has been brought to the nanometer scale. It opens a new era in modern nanoanalytics, including the chemical identification of organic and inorganic materials, protein secondary structure mapping, free-carrier profiling in semiconductors, or mapping of plasmon polaritons in 2D materials such as graphene, all with a spatial resolution of about 10 - 20 nm. s-SNOM and nano-FTIR are based on elastic light scattering at an atomic force microscope tip, employing either monochromatic laser illumination or broadband illumination from a glow bar, a supercontinuum laser or a synchrotron. Acting as an optical antenna, the tip converts the illuminating field into a strongly concentrated near field at the very tip apex (nanofocus), which provides a means for local excitation of molecule vibrations, plasmons or phonons in the sample surface. Recording of the tip-scattered field as a function of sample position (employing monochromatic illumination) yield nanoscale-resolved IR and THz images, while Fourier-transform spectroscopy of the tip-scattered field (employing broadband illumination) allows for nanoscale IR point spectroscopy and IR hyperspectral nanoimaging. In this talk, recent developments, trends and applications in materials sciences and nanophotonics will be discussed.

---

# 27<sup>th</sup> RAU

## ANNUAL USERS MEETING LNLS/CNPq

---

November 22<sup>nd</sup> - 24<sup>th</sup>, 2017

[pages.cnpem.br/rau](http://pages.cnpem.br/rau)



CNPq

MINISTÉRIO DA  
CIÊNCIA, TECNOLOGIA,  
E INOVAÇÃO



# XAFS Study of Inorganically Coated Colloidal Quantum Dots

M. Acebróna<sup>1</sup>, F. C. Herrera<sup>2</sup>, M. Mizrahi<sup>2</sup>, F. G. Requejo<sup>2</sup>, B. H. Juárez<sup>1,3</sup>

<sup>1</sup> IMDEA Nanoscience, Faraday 9, Cantoblanco, 28049, Madrid

<sup>2</sup> Instituto de Investigaciones Fisicoquímicas Teóricas y Aplicadas (INIFTA), CONICET and FCE, UNLP, CC/16, suc 4, 1900 La Plata, Argentina.

<sup>3</sup> Applied Physical Chemistry Department. Universidad Autónoma de Madrid, Cantoblanco, 28049. Madrid.

Felix.requejo@inifta.unlp.edu.ar

The dielectric nature of organic ligands capping semiconductor colloidal nanocrystals (NCs) makes them incompatible with optoelectronic applications. For this reason, these ligands are regularly substituted through ligand-exchange processes by shorter (even atomic), or inorganic ones. In this work, an alternative path is proposed to obtain inorganically coated NCs. Differently to a regular ligand exchange processes, the here reported method produces core-shell NCs simultaneously to the removal of the original organic shell. The insulating organic ligands and the higher solubility in polar media turns these structures very attractive for their further integration into optoelectronic devices. In this work two different sulfur precursors were used, namely: thioacetamide (TA) and thiocarbamide (TC) which, despite of their structural similarities, yield NCs with different optical properties and thickness coverages. The nature of the inorganic shell has been elucidated by X-ray Absorption Near Edge Structure (XANES), Extended X-ray Absorption Fine Structure (EXAFS). XAS experiments were measured at the SXS (S and Cd edges) and XAFS2 (Zn and Se edges) beamlines at the LNLS (Laboratorio Nacional de Luz Sincrotron), Campinas, Brazil.

According to the S-K edge spectra a combination of sulfides and sulfates seems feasible, although out of these spectra, clear identification to ZnS and/or CdS cannot be ascribed univocally and the contribution of Cd or Zn sulfides and sulfates cannot be distinguishable from these results. samples drastically differ from CdSO<sub>4</sub>. Cd XANES spectra corresponding to our samples are very close to the already reported for CdS.[1]

[1] G. Van der Snickt, J. Dik, M. Cotte, K. Janssens, J. Jaroszewicz, W. De Nolf, J. Groenewegen, L. Van der Loeff, *Analytical Chemistry* 2009, 81, 2600.

*Acknowledgements:* This work was supported by FIS2015-67367-C2-1-P from the Spanish Ministry of Economy and Competitiveness. BHJ, FCH, MM ad FGR thank CEAL-AL/2015-15 from UAM-Banco Santander FCH, MM and FGR also acknowledge to CONICET (Project PIP 1035). XAFS experiments were partially supported by Project XAFS2-20150061 (LNLS, Campinas, Brazil). The authors acknowledge to Dr. L. Giovanetti and Dr. C. Huck-Iriart for SAXS experiments, which were performed at INIFTA thanks to project "Nanopymes" (EropeAid/132184/D/ SUP/AR-Contract-896).

# Copper-Doped Zinc Oxide Nanoparticles Synthesis by a Fast Polymer Precursor Based Method

Diógenes Ferreira de Almeida<sup>1</sup>, Leonardo Abreu Garcia<sup>1</sup>, Ruth Herta Goldschmidt Aliaga Kiminami<sup>2</sup>, Rodolfo Foster Klein Gunnewiek<sup>1</sup>

<sup>1</sup>Universidade Federal de Alfenas, 37715-400, Campus Avançado de Poços de Caldas, Brazil;

<sup>2</sup>Universidade Federal de São Carlos, 13565-905, Departamento de Engenharia de Materiais, São Carlos, Brazil.

*diogenesdm@hotmail.com*

Nanostructured doped ZnO synthesis have recently received attention due the enhanced and new properties showed by the nanoparticles, which can be applied in UV detector, varistor, gas sensor, photocatalytic properties, optics, anti-bactericidal activity, among others. The doping of this material with effective metal elements can modify the grain size, crystalline structure, phase and also improve as optical and electromagnetic properties, exhibiting ferromagnetism at room temperature<sup>[1]</sup>. In the present work, nanostructured Cu doped-ZnO was synthesized by a modified fast polymeric precursor method based on soluble polymer. This method involved a water-based complexation of Zn and Cu by soluble polyacrylate<sup>[2]</sup>, with concentration of Cu ranging from 0.1 to 5.0%-mol. The solution was dried and calcined by 120 minutes at 400, 450, 500 and 550 °C. The temperatures or thermal decomposition were determined using Differential Scanning Calorimetry (DSC). A Fourier-Transform Infra-Red Spectroscopy (FTIR) was proceeded to determine how was the calcination process and the molecular structures of calcined by-products. The stoichiometry was confirmed by X-ray fluorescence, performed at LNLS (FRX beamline). X-Ray Diffraction was performed at LNLS (XRD1 beamline), showing very crystalline pattern, specially the powders thermally decomposed at 550 °C. Using Scherrer inference calculated from diffractogram peaks, nanoparticles under 50 nm are present. Scanning Electron Microscopy was also employed to study the morphology of the particles. This process yielded the synthesis of nanoparticles in very short time of about six hours, faster than conventional polymeric precursor methods as Pechini and sol-gel, and no ageing step was needed.

[1] S. Siriam, K. C. Lalithambika, A. Thayumanavan, *Optik - International Journal for Light and Electron Optics*, 139, (2017) 299–308.

[2] R. F. K. Gunnewiek, C. F. Mendes, R. H. G. A. Kiminami, *Advanced Powder Technology*. 27, (2016) 1056-1061.

*Acknowledgements:* This work was supported by CNPEN LNLS (proposals number 20160362 (FRX) and 20160371 (XRD1)), CAPES and FAPEMIG and the authors would like to thank the CNPEN LNLS beamline coordinators Carlos A. Pérez and Alexandre M. G. Carvalho.

## **Bismuth ferrite crystallization from a $V_2O_5 - Bi_2O_3 - Fe_2O_3$ glass matrix**

Natã Pereira de Almeida<sup>1</sup>, Fábria Castro Cassanjes<sup>1</sup> and Rodolfo Foster Klein-Gunnewiek<sup>1</sup>

<sup>1</sup> Universidade Federal de Alfenas, Instituto de Ciência e Tecnologia, 37715-400, Poços de Caldas, Brasil.

natapereira15@gmail.com

Bismuth ferrite is a widely studied and promising material due to its unique combination of ferroelectric and ferromagnetic properties and its possible application as sensors, actuators and solid state memories. The synthesis of this material, however, is problematic, due to the frequent formation of undesired secondary phases. One line of study developed to try to solve this problem is the obtention of bismuth ferrite via crystallization from a glass state precursor[1,2]. In this work, the possibility of obtention of bismuth ferrite from a  $V_2O_5 - Bi_2O_3 - Fe_2O_3$  glass system was evaluated. The processing temperatures used here were lower than previous reported studies, ranging from 850°C to 1050°C. X-ray diffraction (XRD) measures performed at the XRD1 beamline of LNLS confirmed the formation of a glass state for the studied compositions. Differential scanning calorimetry (DSC) was employed to study the crystallization process and determine the optimal temperature for the thermal treatment. The phases were determined using XRD and Rietveld analysis was employed to calculate the percentage of crystalline phase formed. The multiferroic properties of the material were studied using impedance spectroscopy and magnetometry.

[1] EGORYSHEVA, A. V. et al. Magnetic glass-ceramics containing multiferroic  $BiFeO_3$  crystals. **Solid State Sciences**, v.40, p. 31-35, 2014.

[2] TAKAHASHI, Y. et al. Multiferroic  $BiFeO_3$  glass-ceramics: Phase formation and physical property. **Applied Physics Letters**, v. 104, 2014.

*Acknowledgements:* The authors would like to thank CAPES for the financial support and CNPEM – LNLS (Proposal 20160680) for the opportunity to use the synchrotron beamline and the financial support.

## Water Adsorption in Layered Material

M.A.S. Altoé<sup>1</sup>, L. Michels<sup>2</sup>, E.C. dos Santos<sup>2,3</sup>, R. Droppa Jr<sup>4</sup>, G. Grassi<sup>5</sup>, L. Ribeiro<sup>6</sup>,  
K.D. Knudsen<sup>7,2</sup>, H.N. Bordallo<sup>3,8</sup>, J.O. Fossum<sup>2</sup> and G.J. da Silva<sup>5</sup>

<sup>1</sup> Departamento de Química e Física, Universidade Federal do Espírito Santo, 29.500-000, Alegre, ES, Brazil

<sup>2</sup> Department of Physics, Norwegian University of Science and Technology, NO 7495, Trondheim, Norway

<sup>3</sup> Niels Bohr Institute, University of Copenhagen, 2100, Copenhagen, Denmark

<sup>4</sup> Centro de Ciências Naturais e Humanas, Universidade Federal do ABC, 09.210-580, Santo André, SP, Brazil

<sup>5</sup> Instituto de Física, Universidade de Brasília, 70.919-970, Brasília, DF, Brazil

<sup>6</sup> Câmpus de Ciências Exatas e Tecnológicas, Universidade Estadual de Goiás, 75.132-903, Anápolis, GO, Brazil

<sup>7</sup> Physics Department, Institute for Energy Technology (IFE), P.O.Box 40, N-2027 Kjeller, Norway

<sup>8</sup> European Spallation Source, Tunavägen 24, 22100, Lund, Sweden  
mario.altoe@ufes.br

The water adsorption isotherms of Ni-fluorohectorite have been obtained from the relative humidity dependence of X-ray diffraction intensities, and continuous transitions between the stable hydration states were observed. This behavior is significantly different from previous studies of Na-fluorohectorite and Li-fluorohectorite smectites. It was also observed that the environmental history of the clay mineral samples is important for the behavior displayed by these isotherms. In addition, based on thermogravimetric and differential scanning calorimetry measurements, it was observed that a complete Ni-fluorohectorite dehydrated state can only be reached at long times (several hours) at 70 °C, or at shorter times (minutes) above 150 °C. Our observations are consistent with the existence of various forms of Ni<sup>2+</sup>-H<sub>2</sub>O complexes in Ni-fluorohectorite, and we suggest that the present results can be extended to other smectites with transition metals as interlayer charge compensating cations, and consequently have significant practical consequences in materials science and other areas.

*Acknowledgements:* The authors acknowledge the Brazilian Synchrotron Light Laboratory (LNLS) technical staff at the XRD2 beam line. We also wish to thank Antônio Gasperini, Fabio Zambello and Vinícius Fonseca for their helpful assistance at LNLS, also J.E.M. Pereira for assistance in the TGA measurements. M.A.S. Altoé acknowledges CAPES for PDSE Scholarship, process number BEX 4792/14-9. L. Michels, E. C. dos Santos, K. D. Knudsen, and J. O. Fossum appreciate the support from the Research Council of Norway (SYNKNØYT grant number 228551). H. N. Bordallo acknowledges support from the Carlsbergfond grant Ref: 2013-01-0589.

# Particle size effects on structural and optical properties of BaF<sub>2</sub> nanoparticles

A B. Andrade<sup>1</sup>, Nilson S. Ferreira<sup>1,2</sup> and M. E. G. Valerio<sup>1</sup>

<sup>1</sup> Universidade Federal de Sergipe, Departamento de Física, 49100-000, São Cristovão - SE, Brazil; <sup>2</sup> Universidade Federal do Amapá, 68902-280, Macapá - AP, Brazil.  
Email\_abandrade1@gmail.com

Barium fluoride (BaF<sub>2</sub>) nanoparticles (NPs) with different sizes were produced through a hydrothermal microwave method (HTMW) [1]. The microstructural and electronic properties of the synthesized BaF<sub>2</sub> NPs were investigated using X-ray powder diffraction combined with the Rietveld refinement method and Williamson–Hall formalism, scanning electron microscopy (SEM X-ray and photoemission spectroscopy (XPS). From the Rietveld method, we have found that the lattice parameter of BaF<sub>2</sub> NPs is smaller than that observed for BaF<sub>2</sub> in its crystal bulk form. These results demonstrated that the lattice parameter shows dependence on size of particle, increasing for larger particles, reducing strain-surface effects. XPS analyses showed that no other elements were present in the material. Photoluminescence (PL) studies were performed using synchrotron radiation at the Brazilian light source synchrotron radiation (LNLS) in the Thoroidal Grating Monochromator (TGM) beamline, in the vacuum ultraviolet (VUV) and visible (VIS) to investigate the luminescence properties. The PL results showed a slight shift in the self-trapped exciton (STE) edge for samples with higher particle sizes. In addition, the band gap energy ( $E_g$ ) was found to be around 10.5 eV for all samples. The observed lattice contraction/expansion was in concordance with the bond-order-length strength (BOLS) correlation mechanism [2,3]. Therefore, we concluded that this behavior was purely due to surface stress as a result of particle size decreasing.

[1] S. Komarneni, R. Roy and Q. H. Li, Mater. Res. Bull., 1992, 27, 1393–1405.

[2] C. Q. Sun, Prog. Solid State Chem., 2007, 35, 1–159.

[3] C. Q. Sun, B. K. Tay, X. T. Zeng, S. Li, T. P. Chen, J. Zhou, H. L. Bai and E. Y. Jiang, J. Phys. Condens. Matter, 2002, 14, 7781.

*Acknowledgements:* The authors gratefully acknowledge to financial support from the CAPES and CNPq, Brazilian agencies. The authors thank the Brazilian National Laboratories, Synchrotron Light Laboratory(LNLS) and Nanotechnology Laboratory (LNNano) under research proposals TGM – No. 16209/13, TGM – No. 17070/14 and XPS – No. 17752. The authors also thank the Multiuser Center for Nanotechnology of the Federal University of Sergipe (CMNano/UFS), under proposals # 35 – JSM7500F and # 56 –JSM7500F.

# Cluster models Cu<sub>20</sub> obtained by FSA and DFT strategies and XANES simulated spectrum by FDMNES

Leandro Andrini<sup>1</sup>, G.J. Soldano<sup>2</sup>, M. Mariscal<sup>2</sup>, F.G. Requejo<sup>1,3</sup> and Y. Joly<sup>4</sup>

<sup>1</sup> UNLP-CONICET, Departamento de Química, Instituto de Fisicoquímica Teórica y Aplicada (INIFTA), 1900, La Plata, Argentina; <sup>2</sup> Universidad de Córdoba, Facultad de Ciencias Químicas, Departamento de Matemática y Física, Córdoba, Argentina; <sup>3</sup> Université de Grenoble Alpes, CNRS, Institut Neel, 38042, Grenoble, France.  
andrini@fisica.unlp.edu.ar

From those years, considerable progress in the knowledge in clusters[1] were done, but due to the production and characterization difficulties, many questions remain opened. It can be said that the studies of clusters are divided into four main stages[1,2]: *calculus* methods and theoretical cluster predictions, physical-chemistry cluster generation, cluster detection, and cluster experiments where the cluster are probed in its applications and tested with multiple techniques. The involved cluster sizes, ranging from some atoms and the nano-meter radius up, to some millions of atoms, make their evidence at the limit of the detection techniques.

Another aspect is that, copper nanoclusters (Cu-NCs), for example, are difficult to stabilize because of atom-specific electron configuration, in contrast with intermetallic, such as Au<sub>m</sub>Ag<sub>n</sub> or Au<sub>m</sub>Cu<sub>n</sub> isolable, which are monodisperse and with atomically precise nature.

On other hand, some authors argue that the structure is probably the most fundamental property of a cluster and is important for understanding all aspects of chemical and physical behaviour[3] while others argue that it is the electronic structure.[4] We will thus use in this context both absorption edges, *i.e.* XANES, to get both kinds of information.

We present *ab initio* simulations of X-ray Absorption Near-Edge Structure spectra, performed on model Cu-NCs built by fast simulated annealing (FSA) and optimized by Density Functional Theory (DFT) minimization. By comparison with experiments and the analysis of the simulated spectrum shapes, we show the sensitivity of the technique on the number of atoms *n*, around 20, and on the morphology of the Cu<sub>*n*</sub> nano-clusters. For this study we used both L3 and K edges and found the former more sensitive. We also get a good agreement with previous predictions on the HOMO-LUMO gaps.

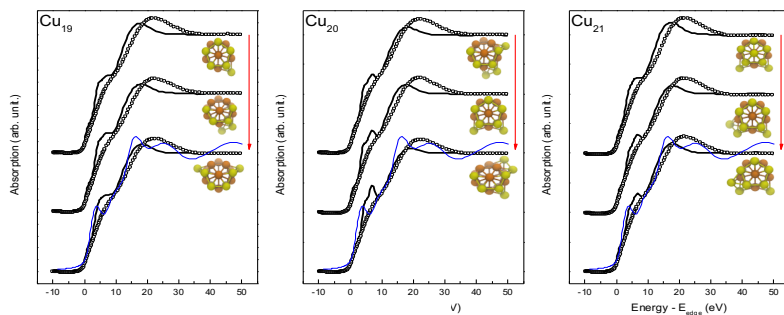


**Figure.** Cu<sub>19</sub>. Cu<sub>20</sub>. Cu<sub>21</sub> FSA clusters. The red arrow indicates the structure more stable to less stable. The black full line are FDM simulations and the circle are MST simulations. In all cases the calculation is non-SFC. E<sub>edge</sub> = 8979 eV

[1] P. Jena, B.K. Rao, S.N. Khanna, Physics and chemistry of small clusters (Springer Science & Business Media, 1987).  
 [2] A. Kaldor, D.M. Cox, M.R. Zakin, Molecular Surface Chemistry: Reactions of Gas-Phase Metal Clusters (Wiley, 2009).  
 [3] V. Bonačić-Koutecký, J. Burda, R. Mitrić, M. Ge, G. Zampella, P. Fantucci, J. Chem. Phys. 117, 3120 (2002).  
 [4] L.S. Kau, K.O. Hodgson, E.I. Solomon, J. Am. Chem. Soc. 111, 7103 (1989).

*Acknowledgements:* This work was supported by PICT: ANPCyT (PICT 2015-2285).

## Phosphate fertilization effects on phosphorus speciation in an Oxisol under no till evaluated by P-XANES

João A. Antonangelo<sup>1</sup>, Ruan F. Firmano<sup>2</sup>, Marina Colzato<sup>2</sup>, Dalton B. Abdala<sup>3</sup>, Adilson Oliveira Junior<sup>4</sup>, Hudson W. P. Carvalho<sup>5</sup>, Luís R. F. Alleoni<sup>2</sup> and Hailin Zhang<sup>1</sup>

<sup>1</sup> Oklahoma State University, Plant and Soil Sciences Department, 74078, Stillwater, OK, United States; <sup>2</sup> Universidade de São Paulo, Escola Superior de Agricultura Luiz de Queiroz, Departamento de Ciência do Solo, 13418-900, Piracicaba, SP, Brasil; <sup>3</sup> Laboratório Nacional de Luz Síncrotron, 13083-100, Campinas, SP, Brasil; <sup>4</sup> Brazilian Agricultural Research Corporation, National Soybean Centes, 86001-970, Londrina, PR, Brasil; <sup>5</sup> Universidade de São Paulo, Centro de Energia Nuclear na Agricultura, Laboratório de Instrumentação Nuclear, 13416-000, Piracicaba, SP, Brasil.

ruanff@usp.br

With the advent of no-till in tropical agro-systems, the greatest soil organic matter conservation changes phytoavailable phosphorus (P) species. In highly weathered soils, the long-term P rates may interfere in such species and in the crystallinity of Fe and Al oxides associated therewith. The aim was to identify P species in solid state through XANES technique. Therefore, we combined P *K-edge* XANES,  $\mu$ -XRF, XRD and conventional chemical analysis in order to evaluate the effects of no-till in conjunction

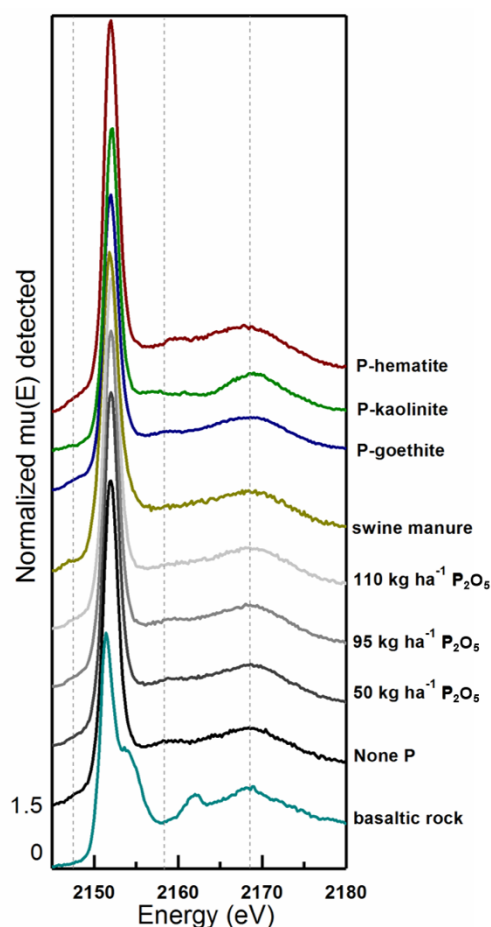


**Fig. 1.** P K-XANES of P adsorbed in hematite, kaolinite and goethite, soil samples amended with swine manure, 110 kg ha<sup>-1</sup> P<sub>2</sub>O<sub>5</sub>, 95 kg ha<sup>-1</sup> P<sub>2</sub>O<sub>5</sub>, 50 kg ha<sup>-1</sup> P<sub>2</sub>O<sub>5</sub> and none P, and basaltic rock sample.

with P rates on the solid speciation of P in soil samples from long-term field experiment. Soil was sampled in a Rhodic Hapludox<sup>[1]</sup> developed on a basalt spill submitted to P rates during more than 20 years under no-till. X-ray Absorption Near Edge Structure (XANES) data were collected at SXS beamline at the Brazilian Synchrotron Light Laboratory (LNLS) and Micro X-ray fluorescence ( $\mu$ -XRF) at the Nuclear Instrumentation Laboratory at the Center for Nuclear Energy in Agriculture (CENA). Those were compared with soil chemical and mineralogical attributes. A soil sample from an experiment amended with swine manure were included for comparison, as well as a basaltic rock sample, representing the parent material of the Rhodic Hapludox. The proportions and crystallinities of P-bearing minerals have been changed with long-term P rates under no-till, then contributed to more crystalline Fe oxides being the most responsible for P adsorption. The features that allowed the identification of changes in proportions were the intensities at the top of white line, collected at 2158 eV and at 2169 eV. These results will be further complemented with chemical fractionation to endorse linear combination fitting.

---

[1] Soil Survey Staff. Soil Taxonomy: A basic system of soil classification for making and interpreting soil surveys. 2<sup>nd</sup> ed. USDA-NRCS, (U.S. Gov. Print. Office, 1999), p 436.

*Acknowledgements:* The authors thank the Coordination for the Improvement of Higher Education Personnel (CAPES) and the São Paulo Research Foundation by the financial support (process n° 2015/19121-8), as well as the Brazilian Agriculture Research Corporation – Soybeans national study center by the concession of the experimental area, LNI-CENA (Laboratory of Nuclear Instrumentation – Centre for Nuclear Energy in Agriculture) for assistance in this study, and University of São Paulo and Oklahoma State University by the research assistantship.

# Structural and Vibrational Properties of Co<sub>3</sub>O<sub>4</sub> Films Deposited by Reactive DC Magnetron Sputtering

N.F. Azevedo Neto<sup>1</sup>, L.J. Affonço<sup>1</sup>, J.C. Angélico<sup>1</sup>, A.R. Zanatta<sup>2</sup>, A.L.J. Pereira<sup>4</sup>,  
M.M. Soares<sup>3</sup> and J.H.D. da Silva<sup>1</sup>

<sup>1</sup> Universidade Estadual Paulista, 17033-360, Bauru, Brazil

<sup>2</sup> Universidade de São Paulo, IFSC, 13566-590, São Carlos, Brazil

<sup>3</sup> Laboratório Nacional de Luz Síncrotron, 13083-970, Campinas, Brazil

<sup>4</sup> Universidade Federal da Grande Dourados, 79804-970, Dourados, Brazil  
nilton@fc.unesp.br

The main stable phases of cobalt oxide are CoO, with rock-salt structure, and Co<sub>3</sub>O<sub>4</sub>, cubic spinel structure. Both CoO and Co<sub>3</sub>O<sub>4</sub> are known as direct transition p-type semiconductors [1]. Recent developments in the growth of high quality Co<sub>3</sub>O<sub>4</sub> epitaxial thin films have been by several methods, including PLD, molecular beam epitaxy and atomic layer deposition [2]. Alternatively, we propose the growth of these phases using reactive sputtering. This technique presents some advantages, as versatility and relatively low operating cost. In order to investigate the influence of different substrates on the structural properties of cobalt oxide epitaxial films, we have grown Co<sub>3</sub>O<sub>4</sub> films onto LaAlO<sub>3</sub> and c-Al<sub>2</sub>O<sub>3</sub> (0001) substrates by reactive DC reactive magnetron sputtering. The films were characterized by high-resolution X-ray diffraction using synchrotron radiation, at the LNLS-XRD2 beamline. The  $\theta$ -2 $\theta$  XRD diffractograms of the samples showed only Co<sub>3</sub>O<sub>4</sub> phase and the diffraction peaks shift to lower angles indicating tensile strain. Different substrates resulted in different crystal orientation of the films.  $\omega$ -Scan of the film Co<sub>3</sub>O<sub>4</sub> (111) on c-Al<sub>2</sub>O<sub>3</sub> showed FWHM 0.233°, while the FWHM of Co<sub>3</sub>O<sub>4</sub> (220) on LaAlO<sub>3</sub> 0.208°. The  $\phi$ -scan of the (333) reflection of Co<sub>3</sub>O<sub>4</sub> film deposited onto c-Al<sub>2</sub>O<sub>3</sub> showed regular symmetric peaks and exhibit FWHM of 1.06°, indicating that Co<sub>3</sub>O<sub>4</sub> films were epitaxially grown on the c-Al<sub>2</sub>O<sub>3</sub> (0001) substrate. The position of the Raman peaks showed a blue shift of the order of 2 cm<sup>-1</sup> for all active modes related with compressive biaxial stress. The observation of selection rules for the Co<sub>3</sub>O<sub>4</sub> (111) surfaces in polarized Raman experiments indicate high ordering of the films in agreement with the XRD experiments. The results suggest that it was possible to grow Co<sub>3</sub>O<sub>4</sub> oriented crystalline films with good structural properties by DC reactive magnetron sputtering, and the c-sapphire is more effective concerning the production of epitaxial films.

[1] K.J. Kormondy, et al, Journal of Applied Physics. 115, 243708 (2014).

[2] C.A.F. Vaz, V.E. Henrich, C.H. Ahn and E.I. Altman, Journal of Crystal Growth. 311, 2648 (2009).

*Acknowledgements:* LNLS (proposal ID 20160103) and LNNano (proposal ID 9841)

# Chemical speciation of Sulphur in petroleum asphaltenes using XANES spectroscopies

Y. B. Bava<sup>1</sup>, M. Geronés<sup>1</sup>, L. Andrini<sup>2</sup>, L. Giovanetti<sup>2</sup> and M. F. Erben<sup>1</sup>

<sup>1</sup>CEQUINOR (UNLP, CCT-CONICET La Plata). Departamento de Química, Facultad de Ciencias Exactas, Universidad Nacional de La Plata. Blvd. 120 N° 1465, CC 962, La Plata (CP 1900), Argentina.

<sup>2</sup>INIFTA (UNLP, CCT-CONICET La Plata). Departamento de Química, Facultad de Ciencias Exactas, Universidad Nacional de La Plata. La Plata, Argentina.

ybava@quimica.unlp.edu.ar

Asphalthenes are complex mixture of heteroatom rich aromatic hydrocarbons that are present as a solid suspension in crude oils. The asphaltenes are the fraction of oil insoluble in heptane (or pentane) but soluble in toluene. All asphaltene chemical properties, excepting elemental composition, had been the subject of debate, specially their molecular weight and structure. The most probable composition of asphaltenes are a complex mixtures of polycyclic aromatic hydrocarbons groups (PAHs) of seven fused aromatic rings (7FAR) with a width of three to ten fused aromatic rings (3FAR-10FAR) with substituted alkyl chains with heteroatoms functional groups. Sulphur is the most abundant heteroatom in the oil, present in the heavier fractions: asphaltenes (about 0.5 to 7 wt%,) and resins. Thus, the knowledge of the sulphur chemistry in petroleum helps in the mitigation of sulphur induced problems in resource utilization. Sulfur speciation varies greatly in asphaltenes from different locations representing different source and reservoir rocks. Besides sulfur is a good marker of the alteration of oils because it is very sensitive to oxidation, and exhibits a range of oxidation states from -2 to +6. [1, 2] The XANES spectroscopy is an appropriated technique for the speciation of chemical species and provide qualitative and quantitative information about the sulphur chemistry in asphaltenes. [3, 4]

Three samples of asphaltenes were extracted from different Argentinian crude oils by precipitation with n-pentane, n-hexane and n-heptane, using a solvent to the bitumen ratio of 40:1 volume/weight. The precipitated asphaltenes were separated from malthenes by filtration and then the resins coprecipitated were removed with a Soxhlet extraction with the respective n-alkane. The XANES measurements were performed in the SXS beamline at LNLS. The commercial standard models used for the experiment were sodium sulfide, pyrite, dibenzyl sulfide, dibenzyl disulfide, diphenyl disulfide, dibenzothiophene, dibenzothiophene sulfona, thianthrene, tetraphenylthiophene, dimethyl sulfone, diphenyl sulfoxide, diphenyl sulfone, and potassium sulfate.

The spectra of asphaltenes can be describe in terms of three different sulfur structures as sulfide, thiophene and sulfate. It has been possible to observe a major contribution of sulfide structure in asphaltenes coprecipitated with resins compare to the spectra of asphantenes. It is well know that the precipitation in n-heptano is selective for asphaltenes of highest molecular weight, and in this case, the XANES spectra show a different shape according to the solvent. An increase in the contribution of more oxidated sulphur form as thiophenic and sulfone group were observed.

[1] Mullins, O. C.; Sheu, E. Y.; Hammami, A.; Marshall, A. G. *Asphaltenes, Heavy Oils, and Petroleomics*; 2007.

[2] Mullins, O. C. *Annu. Rev. Anal. Chem.* 2011, 4, 393–418.

[3] Pomerantz, A. E.; Bake, K. D.; Craddock, P. R.; Kurzenhauser, K. W.; Kodalen, B. G.; Mitra-kirtley, S.; Bolin, T. B. *Org. Geochem.* 2014, 68, 5–12.

---

[4] George, G. N.; Gorbaty, M. L. J. Am. Chem. Soc 1989, 111, 3182–3186.

*Acknowledgements:* This work has been supported by LNLS under Proposals SXS-20160690. The authors thank Facultad de Ciencias Exactas, Universidad Nacional de La Plata, CONICET.

# An alternative paradigm for EUVL resists: hybrid n-CARs-design principles and photodynamics

G. K. Belmonte<sup>1</sup>, C. A. S. Moura<sup>1</sup>, G. Reddy<sup>2</sup>, K. E. Gonsalves<sup>2</sup>, D. E. Weibel<sup>1</sup>

<sup>1</sup> Universidade Federal do Rio Grande do Sul, Departamento de Química, 91501-970, Porto Alegre, Brazil; <sup>2</sup> Indian Institute of Technology Mandi, School of Basic Sciences, 175001, Mandi, India.

danielw@iq.ufrgs.br

Extreme Ultraviolet (EUV) radiation is considered a candidate for the Next-Generation Lithography (NGL) for the fabrication of integrated circuits (ICs) with high density [1]. However, overcoming the 7 nm limit and below it is becoming incredibly critical. Additionally, EUVL photons of 13.5 nm ( $\sim 91.8$  eV) have enough energy to break chemical bonds producing a high yield of secondary electrons that finally affect resolution and cross-section pattern profiles [2]. Therefore, new resist must be synthesized to attend all the stringent requirements of the lithography industry. In the last years, our research group has been investigating the photodynamic of some resists by synchrotron radiation (SR) [3]. Here it is presented the photodynamic study of new resists containing a high EUV absorption center (antimony) in the polymer formulation MAPDSA-MAPDST (see Fig. 1). The excitation wavelength of 12 nm was chosen because is close to the 13.5 nm used in EUVL.

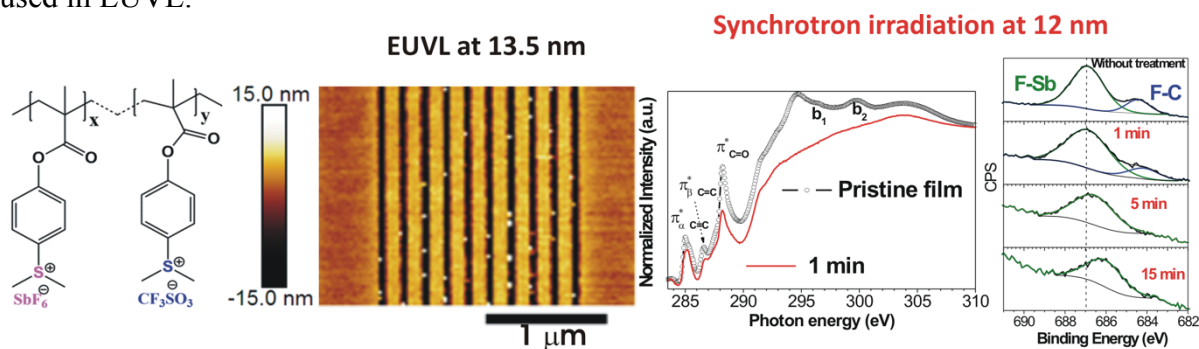


**Figure 1.** From left to right: structure of the 2.15%-MAPDSA-MAPDST resist, AFM image of EUV exposed patterns of the resist, NEXAFS and XPS spectra of the resist before and after irradiation at 12 nm.

The films were prepared by spin coating the resist solution on Si (100) substrates inside a glovebox under argon atmosphere and without UV light. The photofragmentation study of the 2.15 % MAPDSA-MAPDST copolymer resist was carried out following the methodology already used in previous works [3]. The experiments with SR were carried out at the Brazilian Synchrotron Light Source (LNLS), Campinas, Brazil. The PGM beam line (100-1500 eV) for EUV, VUV and soft x-ray spectroscopy was used. Resist thin films were characterized before and after irradiation by Near-edge X-ray absorption fine structure (NEXAFS) and X-ray photoelectron spectroscopy (XPS).

The obtained results showed the fast decomposition rate of the radiation sensitive sulfonium triflate ( $b_1$  and  $b_2$  signals in Fig 1). Sulfur  $L$ -NEXAFS spectra of the copolymer films revealed that after irradiation a transition assigned to a  $\text{CH}_3\text{-S-CH}_3$  group bonded to the phenyl ring merged, confirming the polarity switching mechanism from hydrophilic sulfonium triflates to hydrophobic aromatic sulfides. The inorganic component  $\text{SbF}_6$  included in the resist formulations was particularly illustrative about the

---

photofragmentation process. F 1s and O 1s HR-XPS spectra (see fig. 1) showed that fluorine remains linked to antimony even after 15 min of irradiation. The current mechanistic study work provides a basic initiation of wide readers working on the area of EUVL resist for future technological nodes.

[1] I. Toshiro and T. Kozawa, *Jpn. J. Appl. Phys.*, 52, 1R, 10002, 2013.

[2] V. Skurat, *Nucl. Instruments Methods Phys. Res. Sect. B Beam Interact. with Mater. Atoms*, 208, 1–4, 27–34, 2003.

[3] V. S. V Satyanarayana, F. Kessler, V. Singh, F. R. Scheffer, D. E. Weibel, S. Ghosh, and K. E. Gonsalves, *ACS Appl. Mater. Interfaces*, 6, 6, 4223–4232, 2014.

*Acknowledgements:* The authors would like to thank CNPq, CAPES and LNLS.

# PDF Pharma research team: high-energy X-ray characterization of amorphous solid drugs using synchrotron radiation

Vinicius D. N. Bezzon<sup>1</sup> and Gabriel L. B. de Araujo<sup>1</sup>

<sup>1</sup> Universidade de São Paulo, Departamento de Farmácia, São Paulo - SP, Brazil;  
*gabriel.araujo@usp.br*

The X-ray total scattering (XRTS) and the Pair Distribution Function (PDF) analysis are efficient tools for the characterization of materials with short and medium order, which provide the information of the local structure in the real space [1]. The application of the method to pharmaceutical research has gained prominence because of its large potential to characterize the structure at intra and intermolecular levels of important drug systems such as crystalline, nanocrystalline and amorphous solid dispersions [2]. However, the technique is limited by the energy momentum transfer  $Q_{\max}$  ( $Q=4\pi \sin(\theta)/\lambda$ ) that restricts the spatial resolution of the experiments [3], and therefore, it is necessary to use higher X-ray energy to increase the Q-value. Herein, we present some of the applications and perspectives in pharmaceutical analysis that are being developed by the PDF Pharma Research Team and partners using the PDF method with high-energy synchrotron data. As a first example, we discuss the study of the local structure and crystallization prediction of amorphous solid dispersions of an antitumor drug and polymers [4]. In another application, the identification of interaction mechanisms has been shown between polymeric matrix and drug in controlled-release systems, and its consequences to the stability (Fig. 1)[5]. The goal of the research group is to expand the use of the XRTS and PDF method in amorphous solid drug analysis, spreading the potentialities of the method for the industry and academic area related to drug research and development. The group aims to use the new Sirius synchrotron facilities that will be available (for example the high-energy beamline JATOBÁ) to consolidate and expand the research in this field.

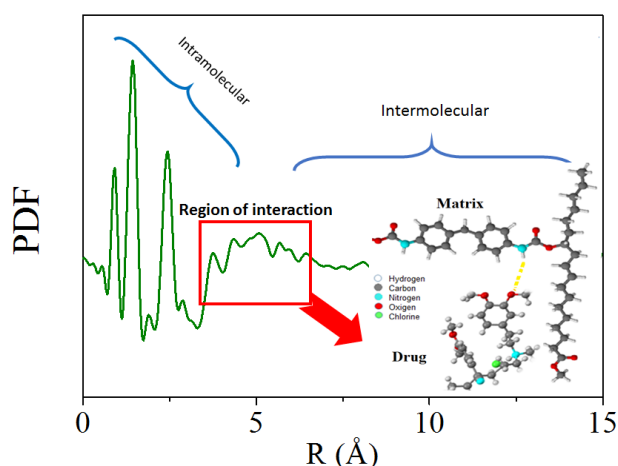


**Figure 1:** Example of result obtained for amorphous solid dispersion drug using PDF method with synchrotron data.

- [1] Billinge, S.J.L *Zeitschrift für Kristallographie - Crystalline Materials* 219, 117-121 (2004).
- [2] Billinge, S.J.L. *et al. CrystEngComm* 12, 1366-1368 (2010).
- [3] Dykhne, T., *et al. Pharm Res* 28, 1041-1048 (2011).
- [4] de Araujo, G.L.B., Benmore, C.J. and Byrn, S.R., 2017. *Scientific Reports* v7, p46367. (2017)
- [5] Bezzon, V.D.N., 2017. *Dispersões sólidas de cloridrato de verapamil em matriz poliuretânica para aplicação em sistema de liberação controlada: caracterização estrutural e aplicação do método PDF.*

---

*Acknowledgements:* The authors would like to thank the financial support of Fapesp, project number 2015/05685-7.

# Study about luminescence in doped CaYAl<sub>3</sub>O<sub>7</sub> using VUV

Giordano F. C. Bispo<sup>1</sup>, Adriano B. Andrade<sup>1</sup>, Verônica C. Teixeira<sup>2</sup>, Suellen M. V. Novais<sup>1</sup>, Zélia S. Macedo<sup>1</sup> and Mário E. G. Valerio<sup>1</sup>

<sup>1</sup> Physics Department, Federal University of Sergipe, 49100-000 São Cristóvão, SE, Brazil; <sup>2</sup> Brazilian Synchrotron Light Laboratory, National Center for Research in Energy and Material, 13083-970, Campinas – SPE

gfredericoc@gmail.com.br

The CaYAl<sub>3</sub>O<sub>7</sub> (CYAM) has been studied as a luminescence host due to its luminescence properties when doped or codoped with rare earth ions [1,2,3]. This compound has been pointed to applications as sensing structural damage, solid-state light source for white LED's and temperature sensors[1,2,3,4]. Recently, the experiments performed out using facilities of the LNLS (Brazilian Synchrotron Light Laboratory) showed undoped CYAM produced via Pechini method as a good candidate for scintillator material [4]. In this work, CYAM doped with Eu<sup>3+</sup>, Tb<sup>3+</sup>, Ce<sup>3+</sup> and Sm<sup>3+</sup> were produced via Pechini method and luminescence properties were studied in the range from near-ultraviolet (NUV) to vacuum ultraviolet (VUV). Photoluminescence (PL) measurements were carried out by exciting samples in a range from 4.2 up to 10.9 eV using the facilities of the Toroidal Grating Monochromator (TGM) beamline[5] (proposals TGM 18991, 20150249). The resulting curves were used to construct the 3D mesh plots of the PL intensity versus excitation energy and versus emission energy to detail the band behaviour under several excitations. This plot allowed a study about changes in band structure caused by doping with different rare earth ions. The results showed a band emission around 2.88 eV(430 nm) for the CYAM:Ce<sup>3+</sup> sample ascribed to 5d→<sup>2</sup>F<sub>7/2,5/2</sub> transitions. The emission spectra of Tb<sup>3+</sup>-doped sample showed the <sup>5</sup>D<sub>4</sub>→<sup>7</sup>F<sub>j</sub> and <sup>5</sup>D<sub>3</sub>→<sup>7</sup>F<sub>j</sub>. and the typical transitions <sup>4</sup>G<sub>j</sub>→<sup>6</sup>H<sub>j</sub> of Sm<sup>3+</sup>-doped sample also were observed. In CYAM:Eu<sup>3+</sup> the <sup>5</sup>D<sub>0</sub>→<sup>7</sup>F<sub>2</sub> emission was more intense than <sup>5</sup>D<sub>0</sub>→<sup>7</sup>F<sub>1</sub> emission due to the low local symmetry in Ca/Y site. A fundamental interband transition around 6.7 eV was showed to the excitation spectra of all samples in accordance with that found in literature [4]. Charge transfer band (CTB) localized in 6.00 eV and 5.10 eV were observed for Sm<sup>3+</sup> and Eu<sup>3+</sup>-doped samples, respectively. The data obtained from the excitation and emission spectra of doped samples supplemented by the exciton and band gap energies allowed to build a diagram with energy position of all 4f<sup>n</sup> and 4f<sup>n-1</sup>5d<sup>1</sup> ground states for divalent and trivalent lanthanides. This model has predicted with reasonable accuracy the 4f-5d<sup>1</sup> transition for lanthanides Tb<sup>3+</sup> and Pr<sup>3+</sup>, besides charge transfer band for Sm<sup>3+</sup>. The energy diagram can be used to interpret luminescence characteristics of CYAM.

[1] H. Zhang, H. Yamada, N. Terasaki, C.-N. Xu, Blue Light, J. Electrochem. Soc. 155, J128. (2008).

[2] S. Unithrattil, K.H. Lee, W.J. Chung, W. Bin Im, J. Lumin. 152, 176, (2014).

[3] V. Singh, V.K. Rai, K. Al-Shamery, J. Nordmann, M. Haase, J. Lumin. 131, 2679, (2011).

[4] G. F. C. Bispo, A. B. Andrade, C. S. Bezerra, V.C. Teixeira, D. Galante, M.E.G. Valerio, Phys. B: Cond. Matt. 507, 119 (2017).

[5] R.L. Cavasso Filho, A.F. Lago, M.G.P. Homem, S. Pilling, A. N. de Brito, J. Electron Spectros. Relat. Phenomena. 156, (2007).

## Acknowledgements

---

This work was supported by CNPq, CAPES, FINEP and FAPITEC-SE. The authors would like to thank Brazilian Synchrotron Laboratory, the Multiuser Center for Nanotechnology of the Federal University of Sergipe and its staff for measurements.

## Modelling the structure of Nafion membranes by using small angle x-ray scattering

S.P. Fernandez Bordín<sup>1</sup>, H. Andrada<sup>1</sup>, A. Carreras<sup>1</sup>, G. Castellano<sup>1</sup>, R. Oliveira<sup>2</sup>, V. Galván<sup>1</sup>

<sup>1</sup>*Instituto de Física Enrique Gaviola, CONICET. M. Allende s/n, Ciudad Universitaria,(5000) Córdoba, Argentina*

<sup>2</sup>*Centro de Investigaciones en Química Biológica de Córdoba, CIQUIBIC, Córdoba, Argentina*

galvan@famaf.unc.edu.ar

Small angle x-ray or neutron scattering (SAXS/SANS) is widely used for characterizing the size, shape and interfacial properties of particles in nanostructure materials. The algorithm introduced by Schmidt-Rohr [1] allows the modelling of the scattering intensity as a function of  $q$ ,  $I(q)$ , by using the Inverse Fourier Transform in a tridimensional electronic or scattering length density map -systems with axial symmetry have a bidimensional density map.

This work studies the channel structure of polymeric membranes Nafion which are used in polymeric electrolyte membrane fuel cell. This structure is still in discussion. In order to improve the models available in the bibliography, we propose a structural model based in hexagonal cluster of cylindrical core-shell water channels and prismatic crystals in the amorphous polymer matrix.

We develop electronic density maps using Monte Carlo simulations to use as input in the algorithm. To correlate the proposed structure with the SAXS experimental data, the model variables were refined. The SAXS measurement were carried out following Nafion dynamic scheme of dehydration at the SAXS-1 beamline at the Brazilian Synchrotron Light Laboratory (LNLS) at Campinas, Brazil.

[1] K. Schmidt-Rohr, "Simulation of small-angle scattering curves by numerical Fourier transformation," *Journal of Applied Crystallography*, 40, 16–25, (2007).

*Acknowledgements:* This work was supported by Consejo Nacional de Investigaciones Científicas y Técnicas

# Sodium Caseinate/Sunflower Oil Nanoemulsion-Based Gels Analyzed by SAXS

V. Borroni<sup>1</sup>, J. M. Montes de Oca-Avalos<sup>2</sup>, R. Candal<sup>2</sup> and M.L. Herrera<sup>1</sup>

<sup>1</sup> Instituto de Tecnología en Polímeros y Nanotecnología (ITPN), UBA/CONICET, Buenos Aires, Argentina; <sup>2</sup> Instituto de Investigación e Ingeniería Ambiental, UNSAM, Buenos Aires, Argentina.

mvirborroni@gmail.com

The structural elements in foods (air cells, crystals, fat globules) play an important role in determining quality and shelf stability. It is this structure that provides the desired rheological properties of the food (hardness, stiffness, snap, etc.) and contributes to organoleptic properties. Protein gels have attracted attention since they allow structuring foods with no trans or saturated fats. In this way, emulsion-based gels are good alternatives to obtain solid foods from liquid raw materials. Therefore, a deep characterization of gel structure is required to determine the feasibility of its application. In this work the effects of protein concentration and sucrose addition on structure of sodium caseinate (NaCas)/sunflower oil nanoemulsion-based gels were studied. Gelation was achieved by homogeneous acidification with glucono-delta-lactone (GDL) (final pH 4.5). Oscillatory rheology demonstrates that nanogels are more rigid than gels based in conventional emulsions since they have a greater  $G'_{\infty}$  value. By using SAXS and synchrotron radiation we can follow gelation process in real time and describe changes in structure with time. SAXS measurements for the nanoemulsion/gel transition shows that NaCas aggregates increased in size with time suggesting that gelation is consequence of the aggregation of the construction units. In addition, values of initial  $q_{\max}$  significantly increased with increasing sucrose concentration ( $p < 0.05$ ) indicating that nanoaggregate sizes were smaller with increasing sucrose concentration. For all samples, values of  $q_{\max}$  versus time showed a linear correlation, because aggregates grew with linear rate. Taking together these data support the hypothesis that polar groups of protein interacted with sucrose and therefore interactions among protein molecules diminished. As a result of weaker interactions, nanoaggregates were smaller. The smaller size of NaCas aggregates led to an even spatial distribution of mass, and therefore, in the macroscale, visual appearance of gels was improved. Nanogels are transparent, display a more homogeneous distribution of oil and they are more stable with respect to syneresis (loss of oil).

*Acknowledgements:* This work was supported by Synchrotron Light National Laboratory (LNLS, Campinas, Brazil) through project D11A-SAXS1-14296.

## Insights into Aminotransferases From The Biosynthesis Pathway of Aminoglycosides Antibiotics

Bury, P.S.<sup>1</sup>, Huang, F.<sup>2</sup>, Sun, Y.<sup>3</sup>, Cerrone, N<sup>1</sup>, Leadlay, P<sup>2</sup>., Dias, M. V. B.<sup>1</sup>  
<sup>1</sup>University of São Paulo, Department of Microbiology, SP, Brazil; <sup>2</sup>Department of Biochemistry – University of Cambridge-UK; <sup>3</sup>Key Laboratory of Combinatorial Biosynthesis and Drug Discovery, Ministry of Education, School of Pharmaceutical Sciences, Wuhan University, P.R.China.

*mvdias@usp.br*

Clinically used gentamicin is a mixture of molecules with different methylation and amination level, while sisomicin is a less functionalized closed related gentamicin antibiotic. Gentamicin biosynthesis has several class III aminotransferases: GenB1 to GenB4, while sisomicin biosynthesis has two: Sis5 and Sis18, which are similar to GenB1 and genB3. The GenB1 and Sis5 perform the transamination of 6-DOX and 6-DOG intermediates to JI-20b and JI-20a, respectively, while GenB2 catalyzes the gentamicin C2 epimerization [1,2,3]. Structurally decipher the catalytic mechanism of aminostransferases from the biosynthesis of gentamicin/sisomicin. Aminotransferase genes were cloned into pET28a and the proteins were overexpressed using BL21(DE3) cells. The proteins were purified and submitted to crystallization trials, data collections were performed at SLS and LNLS, the X-ray data analysis was effected by XDS and the structures were solved using Phaser.Sis5 was crystallized in C2 space group and the structure was determined by SAD. The enzyme form a binary complex with PLP (pyridoxal-5-phosphate) through a Schiff base with Lys-232 (Sis5:PLP). Sis5:PMP (pyridoxamine-5-phosphate) and Sis5:PLP:G418 (G418 is a biosynthesis intermediate) were solved by molecular replacement (MR). GenB2 was crystalized in C222<sub>1</sub> and was determined by MR with Sis5:PLP. Sis5 has a dimer in the asymmetric unit while GenB2 has monomer. Sis5 and GenB2 have similar fold to other class III aminotransferases and the difference of activity should involve different loop conformations in the active site. In both aminotransferases, PLP and PMP are buried in active site and make various hydrogen interaction with the protein. On the other hand, G418 binds in a shallow pocket near of PLP and make few interactions. Although Sis5 and GenB2 are similar, particularities involving loops in the active site might drive the differences of activities [1]. Analyzing these structures will reveal details of the catalytic mechanism and peculiarities and provide further insights into their enzyme versatility.

[1]Guo *et al.* Specificity and promiscuity at the branch point in gentamicin biosynthesis (*Cell press*, 2014) p. 608-618.

[2]Hong, W. R. *et al.* Molecular cloning and sequence analysis of the sisomicin biosynthetic gene cluster from *Mycromonospora inyoensis*. (*Biotechnol Lett*, 2009) p. 449-455.

[3]Kudo, F.; Eguchi, T. Biosynthetic genes for aminoglycoside antibiotics. (*J Antibiot*, 2009) p. 471-481.

## Analysis of sugarcane bagasse particles by X-ray microtomography

Daison M. Y. Caballero<sup>1,2</sup>, Liu Yi Ling<sup>2</sup>, Nathaly L. Archilha<sup>3</sup>, João Eduardo Ferreira<sup>1</sup>,  
Carlos Driemeier<sup>2</sup>

<sup>1</sup> *Institute of Mathematics and Statistics (IME), University of São Paulo (USP), São Paulo, SP, Brazil.*

<sup>2</sup> *Brazilian Bioethanol Science and Technology Laboratory (CTBE), Brazilian Center for Research in Energy and Materials (CNPEM), Campinas, SP, Brazil.*

<sup>2</sup> *Brazilian Synchrotron Light Laboratory (LNLS), Brazilian Center for Research in Energy and Materials (CNPEM), Campinas, SP, Brazil.*  
*daisyancy@gmail.com*

Keywords: x-ray microtomography, mineral particles, sugarcane bagasse, 3D models

### Abstract

Sugarcane bagasse is well-suited for bioethanol production purposes. The use of this biomass as a raw material is highly attractive due to the vast available amounts at the processing site besides its low-cost. A challenge for bagasse valorization is the presence of mineral particles in the biomass, which causes problems such as corrosion, sintering, and vitrification in boilers, gasifiers, and combustors because of the presence of inorganic constituents. In this work, we employed the LNLS IMX beamline to obtain X-ray microtomography images of dry and fresh wet bagasse fibrous particles. Such images were analyzed to quantify 3D morphological features and analyze the cellular structure of the bagasse. Furthermore, the 3D images served as input to construct 3D computational models of the sugarcane bagasse particles, which will have useful applications in future simulations studies of biomass conversion processes. Results show the sizes, shapes and preferred location of mineral particles within the bagasse structure and demonstrate the potential use of the microtomography to support the development of novel biomass technologies to improve ethanol production processes.

**Acknowledgments:** LNLS IMX beamline, CAPES, CNPq, and FAPESP.

# Polymeric precursor based fast-synthesis of lanthanum-doped bismuth ferrite nanoparticles

Igor Charaba Cancellieri<sup>1</sup>, Claudia P. F. Perdomo<sup>2</sup> and Rodolfo Foster Klein-Gunnewiek<sup>1</sup>

<sup>1</sup>Universidade Federal de Alfenas, 37715-400, Campus Avançado de Poços de Caldas, Brazil;

<sup>2</sup>Universidade Federal de São Carlos, 13565-905, Departamento de Engenharia de Materiais, São Carlos, Brazil

igorcharaba@gmail.com

Bismuth ferrite (BiFeO<sub>3</sub>) is a multiferroic ceramic material with magnetoelectric properties, i.e. when the material undergoes an electrical stimulus for a magnetic response, or when magnetically stimulated for an electric response. Its properties are of great value in the production of sensors and actuators, in both bulks and thin films. In the present work, pure and lanthanum doped nanostructured bismuth ferrite (0.1% and 0.5%-mol) was synthesized by a fast-polymeric based method [1]. The cations and the water-soluble polymer were dissolved in water and dried to obtain a porous precursor, and calcined at 400, 450, 500 and 550°C, with a heating rate of 5°C / min and soaking time of 120 minutes. The as-synthesized powders were characterized by X-ray diffraction at XRD1 beamline (LNLS), the stoichiometry by X-ray fluorescence (XRF beamline at LNLS), infrared spectroscopy (FTIR) and microstructural analysis by scanning electron microscopy. The stoichiometry of the synthesized powders (doped and undoped) followed the theoretical, observed in XRF analysis. It is possible to observe the presence of well crystallized nanoparticles of around 50 nm, depending the doping level and calcination temperature, calculated by Scherrer's equation. Although the major phase is the BiFeO<sub>3</sub>, secondary phases were also observed in the diffractograms, even in the doped powders. The presence of a secondary phase maybe is due the inadequate calcination temperature.

[1] R. F. K. Gunnewiek, C. F. Mendes, R. H. G. A. Kiminami, *Advanced Powder Technology*. 27, (2016) 1056-1061.

*Acknowledgements:* This work was supported by CNPEN LNLS (proposals number 20160362 (FRX) and 20160680 (XRD1)), CAPES and FAPEMIG and the authors would like to thank the CNPEN LNLS beamline coordinators Carlos A. Pérez and Alexandre M. G. Carvalho.

## Structural Characterization of Sodium Caseinate Aerogels

R.J. Candal<sup>1</sup>, J.M. Montes de Oca Ávalos<sup>2</sup>, M.V. Borroni<sup>2</sup> and M.L. Herrera<sup>2</sup>

<sup>1</sup> *Instituto de Investigación e Ingeniería Ambiental, CONICET, University of San Martín , 1650 San Martín, Provincia de Buenos Aires, Argentina;* <sup>2</sup> *Institute of Polymer Technology and Nanotechnology (ITPN), University of Buenos Aires-CONICET, 1127, Buenos Aires, Argentina*

rjcandal@gmail.com

Gelation of caseinate emulsions by homogeneous acidification produce hydro-gels containing oil drops, that can be used in different food and medical applications. The hydrogels find also applications in the preparation of plastic films with potential application in food packaging or drug delivery. The rheological and mechanical properties of the materials (hydrogels or films) determine its further applications in the different fields. These properties are very dependent on the micro and nanostructure of the material, which are very much influenced by formulation. The presence of sucrose as a soluble additive in the emulsion, affects the gelation process and very likely the microstructure of the resulting hydrogel. Among other properties, the retention of oil inside the hydrogel and the macroscopic aspect are also affected by sucrose. Hydrogels containing sucrose can retain the oil, while without sucrose the oil is expelled from the hydrogel. It is possible that the framework of the hydro-gels is determined by the connectivity of the construction units, which are aggregates of sodium caseinate or micelles [1]. Previous studies by SAXS demonstrated that during gelation the size of the aggregates increases indicating that gelation is consequence of the aggregation of the construction units. In the presence of sucrose, the size of the construction units is notably smaller [1]. When the units are in the nanometric scale, the interactions between the caseinate molecules that lead to gelation are different from the ones of microemulsions. The gel framework (and rheological properties) should also be different. Preliminary results from our group indicate that nano-hydrogels displayed a more homogeneous distribution of oil. Nanosystems are more stable with respect to syneresis (loss of oil) and more transparent. Synchrotron X-ray imaging is a powerful technique that provides direct information about the distribution of pores and/or particles in a continuous matrix [2]. In the particular case of hydrogels, where water is distributed in a framework formed by a polymer or particle net, the elimination of water by lyophilization allows determining the microstructure of the solid network (aerogel). The aim of this project was to describe the porosity of aerogels formulated with different concentrations of sodium caseinate and sucrose. Micro and nano gels were prepared stabilizing emulsions or nanoemulsions with 3 or 4 wt.% sodium caseinate. The effect of sucrose was checked on the 4 wt.% micro and nanoemulsions. Selected concentrations were: 2, 4, 6 and 8. The results showed that porosity diminished when protein or sucrose concentration increased. Images of gels with 3 wt.% of sodium caseinate (less amount of protein) showed more voids than gels with 4 wt.% of sodium caseinate. No sucrose crystals were present in images indicating that sugar form part of protein structure. Protein network looked thicker with 6 or 8 wt.% sucrose concentrations, more likely because sucrose interacted with sodium caseinate and formed part of connectivity units. The experiments performed added evidence to confirm the effect of sucrose and droplets size on the microstructure of the gels. A better understanding of the relationship between the microstructure and the mechanical and

---

rheological properties of these materials was obtained. This knowledge will allow a better fitting to the applications for which they were developed.

[1] J.M. Montes de Oca-Ávalos, C. Huck Iriart, R.J. Candal and M.L. Herrera, Food Bioprocess Technol. 9, 981 (2016).

[2] D. Wildenschild and A.P. Sheppard, Advances in Water Resources 51, 217 (2013).

*Acknowledgements:* This work was supported by the National Agency for the Promotion of Science and Technology (ANPCyT) through project PICT 2013-0897 and the Synchrotron Light National Laboratory (LNLS, Campinas, Brazil) through project IMX-20160535.

## Microwave induced mineralogical transformation in copper ore

André L. F. Cardoso<sup>1</sup>, Tiago A. Magalhães Filho<sup>1</sup>, Claudia P. F. Perdomo<sup>2</sup>, Ruth. H. G. A. Kiminami<sup>2</sup>, Rodolfo F. K. Gunnewiek<sup>1</sup>

<sup>1</sup> Universidade Federal de Alfenas, Instituto de Ciência e Tecnologia, PPGCEM, -000, Poços de Caldas, Brazil; <sup>2</sup> Universidade Federal de São Carlos, Departamento de Engenharia de Materiais, PPGCEM, -000, São Carlos, Brazil.

Email: rodolfo.foster@unifal-mg.edu.br

The searching for effective, low cost and environmental-friendly methods to treat low-grade ores are imperative, since high grade are rare and economically impracticable. In this context, an alternative is to use microwave radiation to promote many processes in the ore, which can help the mineral extraction. Microwave can heat fast the entire ore or promote selective heating, which promotes thermomechanical tension and reduces the fracture energy, enhancing the comminution [1] or even detach some of the minerals present in the ore. The most interesting feature of microwave radiation in ores is the mineralogical transformation due the heating and/or the incidence of electromagnetic field [2-3]. The mineralogical transformation can enhance the extraction of the interest element, such the transformation of sulfides minerals to oxides or even the melting of rocks. The aim of this work is to study the mineralogical changes after microwave treatment in low grade copper ore, containing chalcopyrite as main copper source. The ore was microwave treated in several conditions and the phases were analyzed by X-ray diffraction at XRD1 beamline, at wavelength of 1.033 nm and the microstructural changes were observed both in optical and scanning electron microscopes. During the microwave treatment, a pale-yellow gas was observed, since the samples were treated in normal atmosphere, characterizing possible oxidation and sulfur evolution. Visually, the ore has changed the color and, by optical microscope, it was possible to find more violet-dark crystals instead yellow, which corresponds to bornite and chalcopyrite respectively.

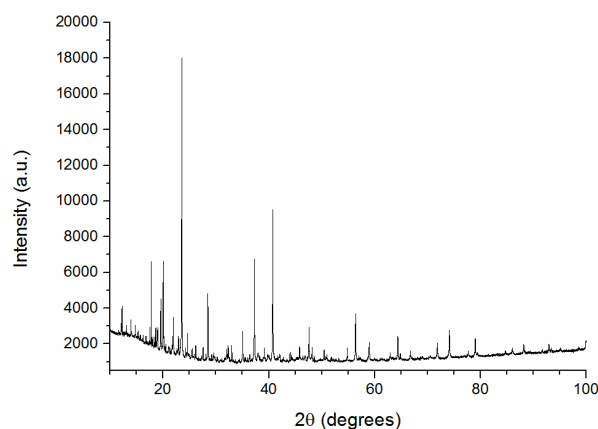


Figure 1 – X-ray diffractogram of a non-treated copper ore.

- 
- [1] Jones, D. A., Kingman, S. W., Whittles, D. N., and Lowndes, I. S., *Minerals Eng*, 18, 659 (2005)  
[2] Waters, K. E., Rowson, N. A., Greenwood, R. W., and Williams, A. J., *Minerals Eng*, 21, 679 (2008).  
[3] Chen, J., Li, L., Chen, G., Peng, J., and Srinivasakannan, C., *J. J Alloys Compd*, 699, 430 (2017).

Acknowledgements: This work was supported by FAPEMIG (proc. TEC - APQ-03636-16), FAPESP (proc. 2008/0425-0) and CNPq (proc. 142911/2009-7). The authors would like to thank Dr Alexandre Magnus Gomes Carvalho (CNPEM-LNLS XRD1 beam line, proposal 20160680) for the technical support.

# A versatile setup in reflection mode for *in situ* diffraction patterns acquisition from flat polycrystalline specimens bathed in a liquid medium

G.L. Carezzato<sup>1</sup>, C.P. Couto<sup>1</sup>, J.L. Rossi<sup>1</sup>, L.G. Martinez<sup>1</sup>, and X. Turrillas<sup>2</sup>

<sup>1</sup>Instituto de Pesquisas Energéticas e Nucleares, IPEN-CNEN/SP, 05508-000, São Paulo, Brazil

<sup>2</sup>Institut de Ciència de Materials de Barcelona, ICMAB/ CSIC, 08193 Bellaterra, Spain  
xturrillas@icmab.cat

A cell to perform *in situ* diffraction measurements of specimens regularly immersed in a liquid medium has been developed. The assembly (see Fig. 1) has been adapted to work in beamline XRD2 in reflection mode. Basically consists of a polypropylene box with two windows made of polyimide to allow the passage of X-rays (incident and diffracted) at lower angles. The flat sample is placed in the middle of the box that is on top of the goniometer head. For safety reasons the central box is positioned over a tray to avoid spillage of liquid. On the bottom of the cell there is a connection to the pipe linked to the syringe. The syringe is driven by a beamline stepping motor. This way it is easy to synchronise the filling and evacuation of liquid from the cell with the actual data acquisition of diffraction patterns. The idea is to soak the flat specimen with the liquid and then remove it to acquire the diffraction data. This can be done in a sequential way for several hours to monitor the crystalline phases present on the surface (or rather a few microns deep) of the flat specimen. Various reactions can be investigated this way, provided that the sample is flat. Ceramics, metals, and polymers in contact with liquids could be studied. Preliminary tests have been performed in two theta – theta geometry on metal plates in contact with acid solutions to simulate accelerated corrosion. However a large variety of experiments with other geometries, (grazing incidence) could be carried out and of course this assembly could be used on SIRIUS with better time resolution.

*Acknowledgements:* This work was supported by a CNPq grant no. PVE 314000/2014-3

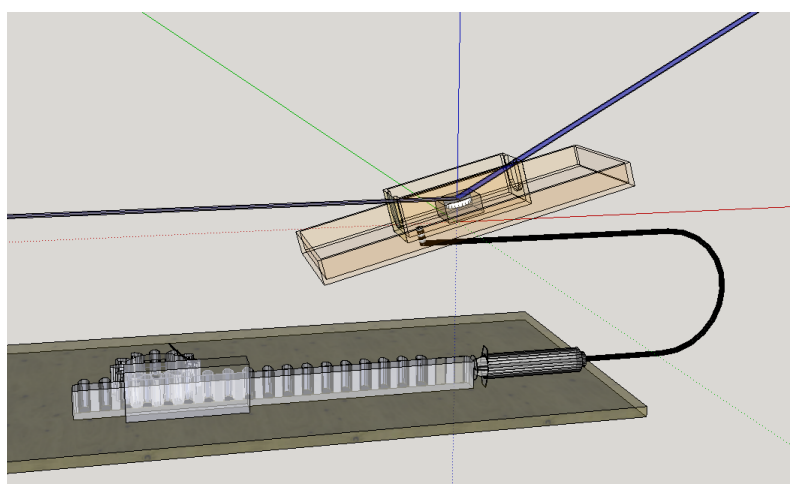


Figure 1. Schematic setup of the assembly showing the cell placed on the goniometer head (omitted for clarity) irradiated by the beam and linked to the automated syringe.

# Magnetic and structural behavior of $\text{Ca}_2\text{MnReO}_6$ under pressure

A. S. Cavichini<sup>1</sup>, M. T. D. Orlando<sup>1</sup>, J. B. Depianti<sup>1</sup>, J. L. Passamai Jr.<sup>1</sup>, Eduardo Granado<sup>2</sup>

<sup>1</sup> Universidade Federal do Espírito Santo, Pós-graduação em Física, 29075-910, Vitória, Brazil;

<sup>2</sup> Universidade de Campinas

cavichiniart@gmail.com

Double perovskites have been widely studied in the last years because some of them present great potential on spintronic devices. One of these materials is the double perovskite  $\text{Ca}_2\text{MnReO}_6$ . This compound was firstly studied in 2004 by Kato et al.[1] and shows monoclinic structure with insulating and weak ferromagnetic macroscopic behavior. Since then, only a few works were published about this compound [2-4], but none of them explained clearly the magnetic ordering. In order to study the magnetic ordering and structure of  $\text{Ca}_2\text{MnReO}_6$ , Neutron Diffraction (ND), Synchrotron X-ray Diffraction (XRD) under pressure and Synchrotron X-ray Absorption (XAS) under pressure were performed. Neutron diffraction measurements were performed as a function of temperature (1.7 K- 300 K) in the G4-1 cold neutron two-axis diffractometer of Laboratoire Léon Brillouin (LLB), France. The measures were analyzed by Rietveld refinement with FullProf [5]. XRD and XAS were performed under pressure (0.0-0.9 GPa) using a B4C anvil-cell [6]. The measurements were performed in DRX1 and DXAS beamline in Brazilian Synchrotron Light Laboratory (LNLS). Magnetic AC susceptibility ( $\chi_{ac}$ ) under pressure (0.0-0.9 GPa) were performed using a homemade B4C anvil-cell [6].

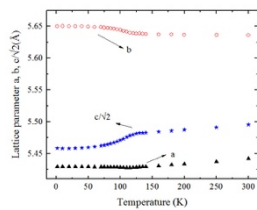


Fig. 1

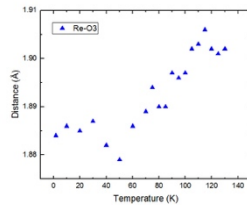


Fig. 2

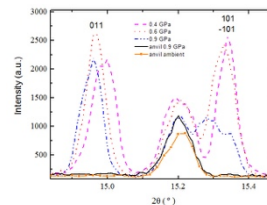
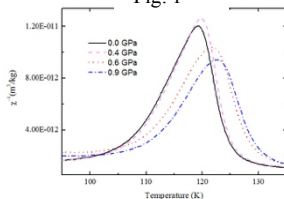


Fig. 3

Fig. 4



Analysis of Neutron Diffraction patterns as a function of temperature had shown no structural phase transition in the range temperature (1.7K – 300 K). Rietveld analysis revealed an anomaly (Fig. 2) in the lattice parameter  $b$  between 75 K- 120K, which increases with decrease of temperature. It is also observed that axial Re-O3 bonds length decreases with temperature, which increases the Jahn-Teller distortion of ReO6 octahedral provoked by  $\text{Re}^{+6} d^1$  state [3-4]. XAS in Re  $L_{III}$  edge shown a change in the absorption white line leading the valence from +5.8 [3-4] to established +6.0 with pressure. Synchrotron X-ray diffraction under pressure (Fig. 3) shown a dislocation of some peaks centers to the left, which is related to an expanse of a lattice parameters. Assuming the decrease of temperature as hydrostatic pressure, then the observed expanse is related to

lattice parameter  $b$  (Fig.2). Magnetic AC susceptibility ( $\chi_{ac}$ ) under pressure (Fig. 4) shows an increase of ordering temperature with pressure. As considering this scenario, new measurements are going on in order to verify whether Re-O bonds length plays an important role in the  $\text{Ca}_2\text{MnReO}_6$  magnetic ordering.

- [1] H. Kato et al., Physical Review B 69, 184412 (2004).
- [2] B. Fisher et al., J. of Appl. Physics 104, 033716 (2008).
- [3] Côrrea et al., Cerâmica 56, 193 (2010).
- [4] Depianti et al., Cerâmica 59, 262, (2013).
- [5] J. Rodriguez-Carvajal, Physica B. 192, 55 (1993).
- [6] F. F. Ferreira et al. J. Synchrotron Rad. 16, 48, (2009).

*Acknowledgements:* The authors would like to thank CNPq, CAPES, the Brazilian Synchrotron Light Laboratory – LNLS (XRD1 – 8571, DXAS - 8076 , XAFS1 – 14567) and Laboratoire Léon Brillouin – LLB.

# Production and initial crystallographic studies of 2,5-furandicarboxylic acid decarboxylase 1 enzyme from *Paraburkholderia xenovorans* LB400

Brisa Caroline Alves Chagas<sup>1</sup>, Raquel Rocha<sup>1</sup>, Mariana Amália Figueiredo Costa<sup>1</sup>,  
Fernandes Tenório Gomes Rodrigues<sup>1</sup> and Ronaldo Alves Pinto Nagem<sup>1</sup>

<sup>1</sup> Universidade Federal de Minas Gerais, Instituto de Ciências Biológicas, Departamento de Bioquímica e Imunologia, Belo Horizonte, Minas Gerais, Brazil.

Email\_corresponding\_author: [brisachagas@gmail.com](mailto:brisachagas@gmail.com) & [nagem@icb.ufmg.br](mailto:nagem@icb.ufmg.br)

Furanic derivatives such as furfural and hydroxymethylfurfural (HMF) are considered toxic compounds resulted from lignocellulosic pretreatment [1,2]. Nevertheless, furanic degradation pathway produces multiple byproducts with relevant industrial applications. Furandicarboxylic acid (FDCA) for instance is commonly used as a precursor in polymer production [3]. Through oxidation and reduction reactions, furfural is converted to 2-furoic acid intermediate and finally into 2-oxoglutarate. HMF is also converted to 2-furoic acid via 2,5-furandicarboxylic acid (FDCA). In HMF pathway, 2,5-furandicarboxylic acid decarboxylase 1 enzyme (HmfF) is responsible for the conversion of FDCA to 2-furoic acid. The study of HmfF structure would provide more information about its mechanism in HMF pathway. In this work, HmfF enzyme from *Paraburkholderia xenovorans* LB400 was recombinantly produced for structural studies. HmfF protein was chosen by solubility and crystallization criteria. hmfF gene was optimized for expression in *E. coli*, synthesized and cloned in pET28a(+)TEV vector. Recombinant protein HmfF was expressed in Arctic Express bacteria at 12°C and purified by nickel affinity chromatography with 55 kDa. HmfF was obtained as a hexamer after size exclusion chromatography. Dynamic light scattering experiments showed that HmfF is monodisperse in solution (10.2% Pd) with an average radius of 5.8 nm. Circular dichroism assay suggests that HmfF possesses  $\alpha$ -helices (26.2%) and  $\beta$ -sheet structures (27.8%) in similar proportions. Initial crystallization trials were performed for recombinant HmfF by hanging drop technique. A single HmfF crystal diffracted to a resolution of 3.0 Å. The crystals belong to space group I23, a cubic group. Matthews coefficient indicates the presence of two molecules present in asymmetric unit of the crystal ( $V_m = 1.94 \text{ \AA}^3 \cdot \text{Da}^{-1}$ ), suggesting a solvent content of 36.8%. In conclusion, recombinant HmfF was expressed in the soluble fraction in a monodisperse state and could be crystallized. The study of HmfF recombinant enzyme structure would provide a better understanding of its role in the hydroxymethylfurfural degradation pathway.

[1] Koopman, F.; Wierckx, N.; de Winde, J. H.; Ruijsenaars, H. J. Identification and characterization of the furfural and 5-(hydroxymethyl)furfural degradation pathways of *Cupriavidus basilensis* HMF14. PNAS, pg 1-6 (2010).

[2] Wierckx, N.; Koopman, F.; Ruijsenaars, H. J.; de Winde, J. H. Microbial degradation of furanic compounds: biochemistry, genetics, and impact. Applied Microbiology Biotechnology, vol 92, pg 1095–1105 (2011).

[3] Dijkman, W.P.; Binda, C.; Fraaije, M.W.; Mattevi, A. Structure-based enzyme tailoring of 5-hydroxymethylfurfural oxidase. ACS Catalysis. Vol 5, pg 1833-1839, 2015.

---

*Acknowledgements:* This work was supported by CNPq, FAPEMIG and CAPES. The authors would like to thank the Laboratório Nacional de Luz Síncrotron (CNPEM, Campinas, Brazil) for provision of synchrotron-radiation facilities.

# Internal structures of *Thoropa miliaris* tadpole using phase-contrast synchrotron microtomography

M.V. Colaço<sup>1</sup>, G. Fidalgo<sup>2</sup>, D. Braz<sup>2</sup>, L.P. Nogueira<sup>1</sup>, G. Colaço<sup>3</sup>, H.R. Silva<sup>3</sup>, R.C. Barroso<sup>1</sup>

<sup>1</sup> Laboratory of Applied Physics to Biomedical Science /Physics Institute/State University of Rio de Janeiro, Brazil

<sup>2</sup> Nuclear Engineering Program/COPPE/Federal University of Rio de Janeiro, Brazil

<sup>3</sup> Laboratory of Herpetology/Biological Sciences and Health Institute/Federal Rural University of Rio de Janeiro, Brazil.

mvcolaco@gmail.com

Amphibians are used extensively in physiological studies aimed at generating new insights in evolutionary biology, especially in the investigation of the evolution of air breathing and terrestriality [1]. The approximately 5770 living species of amphibians are grouped into three orders—Gymnophiona (caecilians), Caudata (salamanders), and Anura (frogs and toads). The latter is the largest, including more than 5065 species currently recognized [2]. Anurans present a variety of reproductive modes, most species are direct developers and lay eggs on water and a tadpole hatches and swim in bodies of water till completion of metamorphosis, with a small froglet that abandons the aquatic life [3]. The species *Thoropa miliaris* present morphological conditions that differentiate it from other species. Tadpoles live in the film of water on rock surfaces at the wet borders of waterfalls in rain-forest areas, and in rock fields of mountain ranges of southeastern Brazil [3].

Although most species in the genus are common and well sampled in collections of natural history museum, little is known of the group's morphology. Application of microtomography ( $\mu$ CT) for the study of frogs is quite recent [4, 5]. Here, we present the first results of the high-resolution non-invasive investigation of external morphology and internal structures *Thoropa miliaris* tadpoles. Microtomographic images were obtained at the imaging beamline (IMX) at Brazilian Synchrotron Light Laboratory (LNLS). The synchrotron light source is a 1.67T bending magnet of critical energy of 1.7keV; providing monochromatic beam spectrum of 4keV to 25keV and useful photons of up to 25keV in white beam mode.

A detailed knowledge of the interior of biological structures and organisms is crucial for a better understanding of their function and evolution. In this work, whole-specimens of *Thoropa miliaris* in three different larval stages of development were imaged. Phase retrieval algorithm was implemented together with the conventional filtered backprojection reconstruction algorithm using the PYRAFT software developed by the LNLS team. The resulting voxel data sets were visualized with Avizo 8.0. The contrast between the different tissues in the  $\mu$ CT images was sufficient to be able to distinguish complex internal structures, such as liver, notochord, cerebral, crystalline and bone formation.

[1] W.W. Burggren, S. Warburton, ILAR J 48(3), 2007, 260-269.

[2] AmphibiaWeb: Information on Amphibian Biology and Conservation. Berkeley (CA): AmphibiaWeb. (20 January 2005; <http://amphibiaweb.org/>).

- 
- [3] R.B Cocroft, W.R. Heyer, Proc. Biol. Soc. of Washington 101, 1988, 209–220.  
[4] A. Haas et al, Zoomorphology, 133, 2014, 321–342.  
[5] E. Descamps et al., Belg. J. Zool. 144(1), 2014, 20-40.

*Acknowledgements:* This work was supported by SAU-LNLS and CNPQ.

# XAS and XPS studies of Zn<sub>1-x</sub>Co<sub>x</sub>O thin films applied as gas sensors

Nathaly Colmenares<sup>1</sup>, Wagner Correr<sup>1</sup> and Valmor Roberto Mastelaro<sup>1</sup>

<sup>1</sup> *São Carlos Institute of Physics, University of São Paulo, P.O. Box 369, 13560-970 São Carlos, Brazil;*

valmor@ifsc.usp.br

In the past few years, metal oxide semiconductor films used as gas sensing devices has become an important subject in material science [1]. Numerous experimental studies conclude that the sensing properties, sensitivity and selectivity of the film depend upon the type of semiconductor material, the presence of doping elements and the synthesis method [2]. Despite the irrefutable importance of morphology in controlling operating characteristics of solid-state gas sensor, reported studies of zinc oxide materials synthesis picture the complexity of finely controlling microstructural features in thin film growth [3], hindering the study of ZnO morphology influence in the gas sensing properties. In this work, we study the Zinc Oxide (ZnO) thin film morphology and its relationship with gas sensing properties towards ozone detection. Radio Frequency (RF) sputtering is used to deposit Zinc films; this technique is one of the best-known physical deposition methods, allowing a highly controllable and stable deposition process for the formation of porous and uniform films [4], with great reproducibility and specific gas sensing properties. Zinc oxide films were obtained by sputtering of metallic zinc and subsequent thermal oxidation. The films were deposited on silicon substrates in a RF-magnetron sputtering system with a working pressure of  $2 \times 10^{-2}$  mbar of argon and radio frequency at 13.5 MHz. To understand the influence of the argon atoms energy, depositions were made using powers between 30 and 250 W. Thermal oxidation was achieved by treatment of zinc films into a furnace at 530 °C during one hour in air atmosphere. In order to elucidate and study the surface interactions responsible for sensing mechanism, XPS and XAS measurements were performed. The XPS spectra were obtained at the beamline station SXS in the Brazilian synchrotron light laboratory (LNLS) using the line x-ray source in 1840eV and a *SPECS PHOIBOS 150* spectrometer analyzer in a constant pass energy mode in 40eV. The XPS spectra were recorded in samples before and after exposure to N<sub>2</sub>O in room temperature and at 250°C. The structural and electronic configuration of cobalt in cobalt-doped zinc oxide films were studied by X-ray absorption near edge spectroscopy (XANES) which measurements were performed at the Brazilian synchrotron light laboratory (LNLS) at the XAFS2 beamline. The XANES spectra were recorded with energy steps of 0.5 eV around the Co K-edge between 7620 and 7800 eV using a fluorescent mode and at room temperature. The XPS and XANES data are being analyzed and a possible correlation between structure and gas sensing properties will be presented.

- [1] Comini, E. Metal oxide nanowire chemical sensors: Innovation and quality of life. *Mater. Today* **2016**, *19*, 559–567.
- [2] Wang, C.; Yin, L.; Zhang, L.; Xiang, D.; Gao, R. Metal Oxide Gas Sensors: Sensitivity and Influencing Factors. *Sensors* **2010**, *10*, 2088–2106
- [3] Ji, S.; Ye, C. Synthesis, Growth Mechanism, and Applications of Zinc Oxide Nanomaterials. *J. Mater. Sci. Technol.* **2008**, *21*, 457–472.
- [4] Li, Z.; Gao, W. ZnO thin films with DC and RF reactive sputtering. *Mater. Lett.* **2004**, *58*, 1363–1370.

---

Acknowledgements: This work has been supported by the Brazilian research financing institutions FAPESP/CEPID (grant nos. [2013/09573-3](#), [2013/07296-2](#), [2015/20124-1](#), and [2012/15170-6](#)) and CNPq. The research was partially performed at the Brazilian Nanotechnology National Laboratory (LNNano), Microfabrication laboratory (Project LMF-18580) and Brazilian Synchrotron Light Laboratory (LNLS - Proposal 20170309), Campinas, SP, Brazil. The authors also would like to thanks the Electron Microscopy Laboratory from the Center for Technology of Hybrid Materials for the electron microscopy analysis (CTMH-USP).

# Magnetic Field Induces Nanoparticles Structuring. A SAXS Application: Instrumental Development at LNLS and Data Analysis

D.F. Coral<sup>1,2</sup>, P. Mendoza Zélis<sup>1</sup>, J. M. Polli<sup>3</sup> and M.B. Fernández van Raap<sup>1</sup>

<sup>1</sup> Instituto de Física La Plata, UNLP, CONICET, Facultad de Ciencias Exactas, 49 y 115, La Plata, Argentina; <sup>2</sup> *Institución Universitaria CESMAG, Pasto-Colombia*; <sup>3</sup> Laboratorio Nacional de Luz Sincrotrón, CNPEM, Campinas-Brazil.

dfcoral@fisica.unlp.edu.ar

Small Angle X-ray scattering is a useful technique to characterize magnetic nanoparticles (MNP) structuring in suspension. Usually, the inter-particle interactions as steric, electrostatic or dipolar magnetic, induce the structuring of the even coated MNP resulting in fractal [1] or more compact structures [2]. The MNP response to external magnetic field is an important parameter for several MNP applications, this response can be affected by the structuring of the single particles in the suspension, and most important, the applied magnetic field can modify the MNP structuring. One example is the magnetic hyperthermia therapy, in this application, magnetic nanoparticles absorb energy from an alternating magnetic field when they are subjected to it, and release this energy as heat resulting in an increase of the MNP-suspension temperature. This temperature elevation is highly influenced by the dipolar interactions among particles, in this way, a modification of the MNP structuring results in a modification of the dipolar interactions and consequently in a modification of the temperature rise [3]. For these reasons, the analysis of the structuring evolution under applied field is of importance and can be achieved measuring SAXS under applied static fields.

In this work, a modification of the liquid sample holder for constant magnetic field application in the SAXS beamline is presented. The magnetic field is applied perpendicular to x-ray beam using constant NdFeB ring shapes magnets. The sample holder allows magnetic field strength, between 0 and 90 kA/m varying the sample-magnet distance. This field strength range is the same used in magnetic hyperthermia experiments. Scattering patterns obtained from this set-up are anisotropic. An anisotropic model, based on the second order Legendre polynomials, is applied to analyze the azimuthal scattering SAXS pattern, and used to determine the anisotropy degree ( $A$ ) as function of field strength. This model allows to differentiate between individual or collective structuring of MNP in magnetic fields, in this way the scattering  $q$ -value vector at which  $A = 0$  corresponds to the size  $d = 2\pi/q$  of the smallest anisotropic structure. Information about the structure factor is derived from the azimuthal integration of the 2D field-applied-pattern, keeping constant the form factor deduced from non-field scattering patterns. Results show that the structure factor change from fractal to hard sticky when magnetic field is applied, and that the anisotropy degree is reduced when the interparticle distance is increased by diluting the suspension.

- 
- [1] M.B. Fernández van Raap, P. Mendoza Zélis, D.F. Coral, T.E. Torres, C. Marquina, G.F. Goya, F.H. Sánchez, *Journal of Nanoparticle Research*, Vol. 14, p. 1072, (2012).
- [2] J.M. Orozco-Henao, D.F. Coral, D. Muraca, O. Moscoso-Londoño, P. Mendoza Zélis, M.B. Fernández van Raap, S.K. Sharma, K.R. Pirota, M. Knobel, *Journal of Physical Chemistry C*, Vol. 120, p. 12796-12809, (2016).
- [3] D.F. Coral, P. Mendoza Zélis, M. Marciello, M.P. Morales, A. Craevich, F.H. Sánchez, M.B. Fernandez van Raap, *Langmuir*, vol. 32, p. 1201-1213, (2016).

*Acknowledgements:* This work was supported by Laboratorio Nacional de Luz Sincrotrón (SAXS D02A and D01B Beamlines), Campinas-Brazil, Universidad Nacional de La Plata-Argentina, and CONICET-Argentina.

# STRUCTURING OF MAGNETIC NANOPARTICLES IN LIVING CELLS

D.F. Coral<sup>1,2</sup>, P. Soto<sup>3</sup>, G.A. Muñoz<sup>1</sup>, P. Setton<sup>3</sup>, F. H. Sánchez and M.B. Fernández van Raap<sup>1</sup>

<sup>1</sup> Instituto de Física La Plata, UNLP, CONICET, Facultad de Ciencias Exactas, 49 y 115, La Plata, Argentina; <sup>2</sup> *Institución Universitaria CESMAG, Pasto-Colombia*; <sup>3</sup> Instituto De Química y Físico-Química Biológicas "Prof. Alejandro C. Paladini", UBA, CONICET, Buenos Aires-Argentina .

guillermoamm19@fisica.unlp.edu.ar

The use of iron oxide magnetic nanoparticles (MNP) in the treatment of cancer by magnetic hyperthermia (MH) has been extensively studied. The success of the therapy lies in the optimization of the magnetic response of MNPs to radiofrequency fields (RF) [1]. Experiments are more often carried out on MNP suspensions, where particles-structuring is governed by the competition of the steric, electrostatic and magnetic interactions [2]. A second stage in MH investigations corresponds to study the MNP internalization by in-vitro cultured living cells. In these experiments, the MNP are loaded in endosomes inside the cell cytoplasm, where particles aggregation is observed. This effect produces compact structures composed by several MNP, different to structures observed in MNP suspensions. In these structures, the magnetic dipolar interaction is dominant and the MNP properties are affected, especially those related with their MH efficiency [3]. Small Angle X-ray scattering technique is a useful to characterize MNP structuring in suspension and in living cells, allowing structure comparison between both cases. In this work, the SAXS patterns of MNP in suspensions and internalized by A549 (human pulmonary carcinoma cells) and B16 (murine melanoma tumor) line cells, and ASC stem cells (Wistar Rat Adipose-derived Mesenchymal Stem Cells), cultured *in vitro*, are presented. In order to analyze the effects of size and coating in MNP structuring inside endosomes, iron oxide core MNP, and coated with different surfactants (DMSA, citric acid and sodium citrate) were used. A core/shell structure composed by iron/iron oxide coated with sodium citrate, and other system composed by iron oxide nanoflowers-like structures coated with sodium citrate were used. Results reveals that, for patterns analyzed with fractal-like structure factor, the fractal exponent increases indicating structures that are more compact. This result is confirmed by TEM images where ring-shape structures are observed inside cell endosomes. We are reporting for the first time the observation of structuring of MNP in cells with SAXS, no reports concerning with this issue has been published yet.

[1] M.E. de Sousa, M.B Fernández van Raap, P.C. Rivas, P. Mendoza Zélis, P. Girardin, G. Pasquevich, J.L. Alessandrini, D. Muraca, F.H. Sánchez. *Journal of Physical Chemistry C*, Vol. 117, p. 5436–5445, (2013).

[2] M.B. Fernández van Raap, P. Mendoza Zélis, D.F. Coral, T.E. Torres, C. Marquina, G.F. Goya, F.H. Sánchez, *Journal of Nanoparticle Research*, Vol. 14, p. 1072, (2012).

[3] D.F. Coral, P. Mendoza Zélis, M. Marciello, M.P. Morales, A. Craevich, F.H. Sánchez, M.B. Fernandez van Raap, *Langmuir*, vol. 32, p. 1201-1213, (2016).

*Acknowledgements:* This work was supported by Brazilian Synchrotron Light Laboratory (Proposals: SAXS1-14429, SAXS2-22014, SAXS1-20160237), Brazilian Nanotechnology National Laboratory (Proposal: 16901), Campinas-Brazil, Universidad Nacional de La Plata-Argentina, and CONICET-Argentina.

# Study of the partial substitution of Ni by Nb in perovskite based catalysts applied on partial oxidation of methane using XPD line

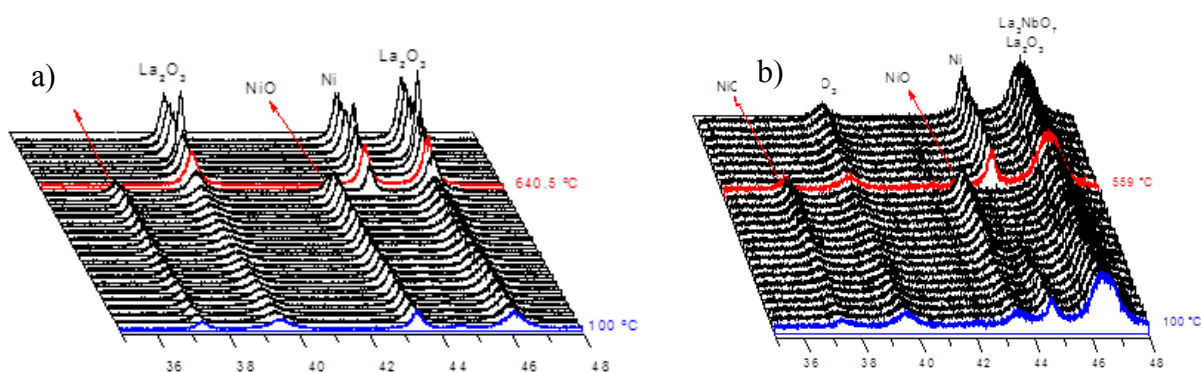
Costa, D. S.<sup>1</sup>, Rodella, C. B.<sup>2</sup>, Gomes, R. S.<sup>1</sup> and Brandão, S. T.<sup>1</sup>

<sup>1</sup> Universidade Federal da Bahia, Departamento de Química Geral e Inorgânica, 40170-115, Salvador, Brazil

<sup>2</sup> Centro Nacional de Pesquisa em Energia e Materiais, Laboratório Nacional de Luz Síncrotron, 13084-971, Campinas, SP – Brazil

denilson\_costa19@hotmail.com

In this work perovskite  $\text{LaNiO}_3$  and  $\text{LaNi}_{0.5}\text{Nb}_{0.5}\text{O}_3$  were investigated as catalyst precursors in the partial oxidation of methane (POM). The objective was investigating the influence of the partial substitution of Ni by Nb in the catalytic performance. The catalysts were obtained by reduction of the perovskite precursors under  $\text{H}_2$  flow (30mL/min) at 800 °C. Analysis of the post reduction x-ray diffraction (XRD in situ) indicated the presence of Ni and  $\text{La}_2\text{O}_3$  for the catalyst obtained from  $\text{LaNiO}_3$  and Ni,  $\text{La}_2\text{O}_3$  and  $\text{La}_3\text{NbO}_7$  for that derived from  $\text{LaNi}_{0.5}\text{Nb}_{0.5}\text{O}_3$ . The catalysts were characterized by experiments XRD in situ performed at XPD line (LNLS) at high temperatures and under  $\text{CH}_4$  and  $\text{O}_2$  flows (2:1  $\text{CH}_4/\text{O}_2$  ratio). The diffractograms (Figure 1) indicated that is more difficult to oxidize Ni. Moreover nickel is regenerated at lower temperature in the catalyst containing Nb which was attributed to the presence of  $\text{La}_3\text{NbO}_7$ . Metal oxides such as NiO promote total oxidation of methane instead of partial oxidation producing  $\text{CO}_2$  and  $\text{H}_2\text{O}$  [1]. Thus the lower susceptibility to Ni oxidation in the niobium-containing catalyst is quite relevant in the partial oxidation of methane. Tests performed with catalysts obtained from  $\text{LaNi}_{0.5}\text{Nb}_{0.5}\text{O}_3$  during 20h at 750 °C and  $\text{CH}_4/\text{O}_2$  2:1, even containing approximately half amount of Ni than the catalyst derived from  $\text{LaNiO}_3$ , exhibited  $\text{CH}_4$  conversion just 15% lower and ratio  $\text{H}_2/\text{CO}$  close to the



stoichiometric to POM. Based on these results it can be proposed that the partial substitution of Ni by Nb lead to a better resistance to oxidation of the Ni sites and which makes possible a  $\text{H}_2/\text{CO}$  ratio close to the stoichiometric in POM, which can be attributed to the presence of  $\text{La}_3\text{NbO}_7$  phase.

---

[1] R. JIN et al. *Applied Catalysis A: General* 201, 71–80 (2000).

*Acknowledgements:* This work was supported by CNPq. The authors acknowledge the support of the LNLS/CNPEM for beamline time.

# ***In vivo* XANES for determination of the chemical environment of Zn in the stem of kidney beans treated with ZnO nanoparticles**

T. N. M. da Cruz<sup>1</sup>, S. M. Savassa<sup>1</sup>, C. D. Picolla<sup>1</sup> and H. W. P. de Carvalho<sup>1</sup>

<sup>1</sup> University of São Paulo, Laboratory of Nuclear Instrumentation, 13416-000, Piracicaba, Brazil.

tatiana.nishida@gmail.com

Seeking for a better understand about how Zn is absorbed and transported when it is provided by ZnO nanoparticles (NPs), this study aims to verify how is the chemical environmentl of it inside plant tissues. So, it was employed 3 different sizes of ZnO nanoparticles acquired as dispersions in water with surfactants. They had 40 (Nanophase, USA), 60 (Nanophase, USA) and 300 nm (Agrichem, Company, Brazil), and were used to prepare 1,000 mg L<sup>-1</sup> of Zn aqueous dispersion.

The *Phaseolus vulgaris* plants, at its first leaflet totally expanded stage, had their roots immersed in the 1,000 mg L<sup>-1</sup> ZnO nanoparticles dispersions, and after 48 hours of exposure, the stem and leaves of these plants were analyzed at XAFS2 beamline of LNLS (Campinas, Brazil). The measurements were performed in fluorescence mode, 3 times per sample, and the spectra were merged, energy calibrated and normalized using Athena program within the IFEFFIT package. Besides the treated plants, we also recorded spectra for Zn-malate, Zn-citrate, Zn-phosphate, Zn-cysteine, Zn-succinate and Zn-histidine reference compounds synthetized in our laboratory according to the reference<sup>2</sup> and the pristine ZnO nanomaterials. These references compounds were made mixing the material cited above with cellulose and pelletized. At this analysis, it was not detected any spectra changes for subsequent spectra recorded in the same sample, so there was no induced chemical changes on it.

The present analysis observed that for all different sizes of ZnO NPs used, it was not found any evidence of the uptake, transport or accumulation of entire ZnO NPs. And it was also observed that, in the stems, the Zn was associated mostly with malate and citrate,

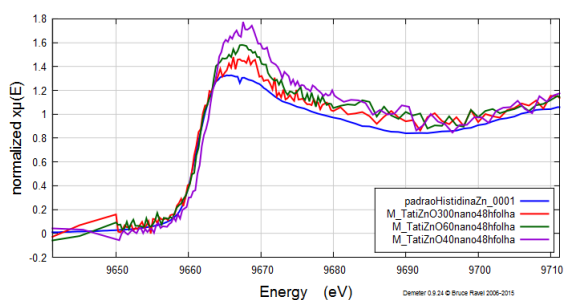


Figure1, Zn-K edge XAS spectra at the leaves of kidney beans.

and in the leaves, the Zn was mostly found associated with histidine (Figure 1). These results are congruent with a study done with cowpea plants, where it was not detected any upward translocation of ZnO NPs, but it was observed in stem and leaves Zn combined with citrate, histidine and phytate<sup>3</sup>. So, it is possible that ZnO NPs can be transformed in Zn<sup>+</sup> ions at the rhizosphere before being uptake by roots, or it is transformed right after being absorbed. In addition to these results, we

also find in some stems the presence of ZnO, but after analyzing the roots of its plants on a magnifying glass, we concluded that only plants with damages on its roots could uptake the entire NPs. Nonetheless, it is also reported that researches found ZnO NPs in the shoot system<sup>4</sup>, and it may be a consequence of the reconstitution of it inside the vacuole. It is not yet well understood how the ZnO NPs are transformed, and it is possible that each species has a different response on its absorption.

- 
- [1] F. Han, X. Q. Shan, J. Zhang, Y. N. Xie, Z. G. Pei, S. Z. Zhang, Y. G. Zhu and B. Wen, *New Phytologist*, 165, 481-492 (2005)
- [2] P. Wang, N. W. Menzies, E. Lombi, B. A. McKenna, B. Johannessen, C. J. Glover, P. Kappen, P. M. Kopittke. *Environ Sci Technol.* 47, 13822–13830 (2013)
- [3] S. Bandyopadhyay, G. Plascencia-Villa, A. Mukherjee, C. M. Rico, M. Jose-Yacaman, J. R. Peralta-Videa and J. L. Gardea-Torresdey, *Science of the Total Environment*, 515, 60-69 (2015)

*Acknowledgements:* This work was supported by FAPESP, project 2016/04611-2. The authors would like to thank the LNLS for beamtime at XAFS2 beamline, and EMBRAPA for supplying seeds of BRS Cometa variety.

## Structure and Properties of Siloxane-Polyether Hybrid Organic-Inorganic Materials for Drug Delivery of Salicylic Acid

Karim Dahmouche<sup>1,2</sup>, Erika Imada Barcelos<sup>2</sup> and Ailton de Souza Gomes<sup>2</sup>

<sup>1</sup> Universidade Federal do Rio de Janeiro (UFRJ), Campus de Xerém, 25245-390, Duque de Caxias-RJ, Brazil;

<sup>2</sup> Universidade Federal do Rio de Janeiro (UFRJ), Instituto de Macromoléculas(IMA), 21941-598, Rio de Janeiro-RJ, Brazil

karim@xerem.ufrj.br

Organic - inorganic hybrids represent a class of promising materials in biomedical applications [1], especially in the field of controlled drug delivery. In this work, hybrid matrices in which siloxanes nanoparticles are crosslinked by polyethylene oxide (PEO - hydrophilic) and / or polypropylene oxide (PPO - hydrophobic) chains were synthesized by the sol-gel process [2]. The effect of different proportions of PEO and PPO on the release mechanisms of salicylic acid was investigated. Chemical, structural, thermal and biological characterizations of the material were also performed. The drug release mechanism changes from swelling / relaxation of the polymer chains to Fick diffusion by increasing PPO content. For intermediate compositions, a mixed mechanism of diffusion and swelling was observed. These results are consistent with those obtained by Small Angle X-ray Scattering (SAXS) analysis, which reveal an increase of the interparticle distance by increasing PEO content in the material. Fourier-Transform Infrared Spectroscopy (FTIR) and Thermogravimetric Analysis (TGA) suggest a preferential interaction between drug molecules and polymer chains when PEO is present in the formulation, while for pure PPO the drug essentially interacts with amide groups located close to siloxane particles surface. The amorphous character of these materials is demonstrated by Differential Scanning Calorimetry (DSC) analysis. X-Ray Diffraction (DRX) reveals an excellent dispersion of the drug in all hybrid matrixes. Furthermore, a lamellar structure formed by ordered polymer chains was detected in the PPO-free sample in which salicylic acid was incorporated. Such structure progressively disappeared as PPO content increased. For hybrid films, the more suitable composition for potential application in controlled release was 70% wt PPO and 30% wt PEO, in which the release time was about 12 hours. In-situ SAXS measurements performed during drug release in this sample revealed the existence of a hierarchical structure formed by the primary siloxane particles and hybrid secondary aggregates. Such structure is affected by the drug release process.

[1] C.Sanchez, L. Rozes, F. Ribot, C. Laberty-Robert, D. Grosso, C. Sassoie, C. Boissière and L. Nicole, C.R Chimie, 13 (2010) 3-39

[2] K. Dahmouche, M. Atik, N.C Mello, T.J Bonagamba, H. Panepucci, M.A Aegerter and P. Judeinstein, Journal of Sol-Gel Science and Technology, 8 (1997) 711

*Acknowledgements:* This work was supported by FAPERJ and CAPES. We acknowledge the LNLS for opportunity of SAXS measurements.

---

## **Catalytic Nanoparticles sitting on top of Graphene: The heterojunction interaction with H<sub>2</sub> gas followed by in-situ GISAXS Experiments**

Dalfovo, M.C., Huck Iriart, C., Giovanetti, L. J., and Ibañez, F.J.

There is a great interest in better understanding the phenomena that occurs at the nanoscale between metallic/catalytic nanoparticles and hydrogen gas. This has implications not only in fundamental aspects but also in some applications such as in hydrogen sensing and catalysis. We chemically synthesize Pd, Pt, and Pd/Pt alloy nanoparticles (NPs) protected with organic ligands which are later assembled on graphene (obtained by CVD). The film of NPs is simply formed by incubating graphene in the NPs solution for some time. Once the heterojunction is formed, it is placed in an ad-hoc chamber and exposed to alternating flows of pure He and H<sub>2</sub> (at 5%) during in-situ GISAXS experiments. First, I will show the differences in NPs assembly when using Si vs. graphene as substrates. I will also show how the film restructures upon the presence of H<sub>2</sub> gas and the importance of the metal composition. Finally, I will demonstrate that this heterostructures can be used for detecting H<sub>2</sub> at low concentrations and for reducing molecules such as methylene blue.

# BI-REFORMING OF BIOGAS FOR HYDROGEN PRODUCTION USING $\text{LaNiO}_3/\text{Ce}_x\text{Zr}_{1-x}\text{O}_2$ ( $x = 1; 0.75; 0.5$ ) AS PRECURSOR MATERIAL

D.B.L. dos Santos<sup>1</sup>, F. B. Noronha<sup>2</sup>, C. E. Hori<sup>1</sup>

<sup>1</sup> Universidade Federal de Uberlândia, School of Chemical Engineering, Av. João Naves de Ávila, 2121, Bloco 1K, 38408-144, Uberlândia – MG, Brazil.

<sup>2</sup> National Institute of Technology, Division of Catalysis and Chemical Processes, Av. Venezuela, 82, Centro, 20081-312, Rio de Janeiro – RJ, Brazil.  
cehori@ufu.br

The oxidative state of the nickel and cerium in  $\text{LaNiO}_3/\text{Ce}_x\text{Zr}_{1-x}\text{O}_2$  ( $x=1; 0.75; 0.5$ ) catalysts during hydrogen reduction and bi-reforming of biogas reaction were investigated by *in situ* X-ray diffraction (XRD) and X-ray Absorption Near Edge Structure Spectroscopy (XANES). The ceria-zirconia mixed oxides and perovskites were prepared by precipitation and sol-gel methods, respectively. *In situ* XRD reduction results showed the destruction of perovskite phase between 573 and 673 K, and the diffraction lines relative to metallic nickel phase appeared around 773 K. These results are in agreement with the literature [1]. *in situ* XAS analysis at Ni-K edge during reduction procedure exhibited the complete reduction of nickel below 973 K for all catalysts, which is in accordance with TPR data. For the catalysts supported on ceria-zirconia mixed oxides, XAS measurements on Ce-L3 edge revealed that under reduction conditions (at 973 K) some cerium changed the oxidative state from  $\text{Ce}^{+4}$  to  $\text{Ce}^{+3}$ . The following order was observed for the reducibility degree of Ce:  $\text{LaNiO}_3/\text{Ce}_{0.5}\text{Zr}_{0.5}\text{O}_2 > \text{LaNiO}_3/\text{Ce}_{0.75}\text{Zr}_{0.25}\text{O}_2 > \text{LaNiO}_3/\text{CeO}_2$ , which is in agreement with TPR data. During catalytic tests, all the samples presented a slight deactivation in the first hours of reaction, probably due some initial oxidation of the metallic phase. After a couple of hours, the activity and  $\text{H}_2$  formation slowly increased during 24 hours of reaction. The best catalytic performance was obtained for the sample  $\text{LaNiO}_3/\text{Ce}_{0.75}\text{Zr}_{0.25}\text{O}_2$ , which was correlated to high degree of reduction of both Ce and Ni.

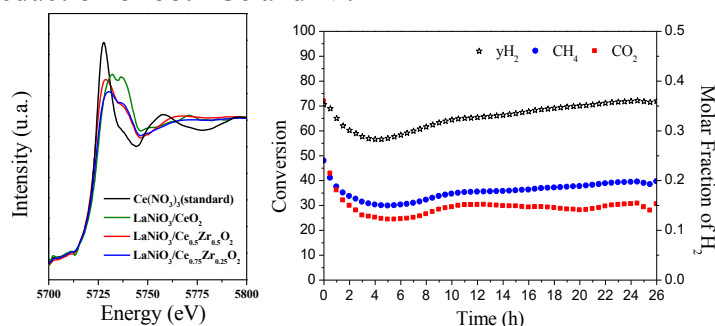


Figure 1: Spectra in the XANES region on the L<sub>3</sub> edge of the Ce at the end of reduction process and conversions and molar fraction of  $\text{H}_2$  in bi-reforming of biogas for the catalyst  $\text{LaNiO}_3/\text{Ce}_{0.75}\text{Zr}_{0.25}\text{O}_2$

[1] A. L. A. Marinho, R. C. Rabelo-Neto, F.B Noronha, L.V. Mattos, Applied Catalysis A: General 520 (2016) 53-64.

*Acknowledgements:* The authors wish to acknowledge the financial support of CAPES, FAPEMIG and CNPq. We also thank LNLs for the use of XPD, DXAS and XAFS2 beamlines.

## Complex structural arrangements of ceramide lipids is produced by asymmetric molecular shape

Dupuy, Fernando<sup>1</sup>; Pérez Bordín, Santiago<sup>2</sup>; Pusterla Julio<sup>2</sup>; Gasperini Antonio<sup>3</sup>; Maggio, Bruno<sup>2</sup>; Oliveira Rafael<sup>2</sup>

<sup>1</sup>.INSIBIO-CONICET/Universidad Nacional de Tucumán, Chacabuco 461,4000 San Miguel de Tucumán;

<sup>2</sup>.CIQUIBIC-CONICET/Universidad Nacional de Córdoba, Haya de la Torre S/N, 5000. Córdoba.

Argentina. <sup>3</sup>Brazilian Synchrotron Light Laboratory - LNLS, CNPEM, Rua Giuseppe Maximo Scolfaro, 10000, Campinas, SP 13083-070, Brazil

fdupuy@fbqf.unt.edu.ar

Ceramide is an important class of sphingolipids, which can be found in minor amounts in cell membranes but participating in transmembrane signaling and in larger amounts in skin and epithelia, providing structural support. Sphingolipids endow a large chemical variability both in head group and in acyl chains, which give rise to a rich mesomorphic behavior. In this project we are studying the effect of the length of the fatty acid chain that is N-bonded to sphingosine in ceramides on the structure and thermodynamic properties of fully hydrated dispersions by means of X-ray techniques, infrared spectroscopy and differential scanning calorimetry. Our previous results showed that a short chain, asymmetric C10:0 ceramide form an inverted HII phase with ordered chains, the latter been not previously reported before [1]. Now we are investigating longer and shorter N-acyl chains lipids, which also show non-bilayer structures provided molecular asymmetry is maintained. Symmetrical shaped ceramides with intermediate chain length prefer to adopt flat bilayer like structures. WAXS shows several small peaks beyond the characteristic peak of hexagonal acyl chain packing. The grazing incidence X-Ray diffraction pattern from Langmuir monolayers at the air/water interface appears comparatively simple. Thickness of the Langmuir mono- and sub-layers is measured by Bragg rod at the Bragg peaks and grazing Incidence X-Ray Off Specular Scattering and compared to the ones measured by light reflectivity.

[1] Dupuy, F.G., Fernández Bordín, S.P., Maggio, B., Oliveira, R.G., *Colloids and Surfaces B: Biointerfaces*. 149, 89 (2017).

*Acknowledgements:* This work was supported by CONICET

## **$\mu$ -XANES and X-ray tomography uncovering the effects of nanoparticles on *Phaseolus vulgaris* seeds**

Duran, N. M.; Costa Júnior, G. T.; Santos, J. R. P. and Carvalho, H. W. P.

University of São Paulo (USP), *Center of Nuclear Energy in Agriculture (CENA), Laboratory of Nuclear Instrumentation (LIN)*, 13416-000, Piracicaba, Brazil

*nadia.duran@usp.br*

Nanoparticles present different properties of their usual bulk counterparts. Properties such as solubility, tunable surface charges and singular reactivity might be explored to improve the performance of fertilizers. Nevertheless, these unique properties may also bring risks to the environment as long as the interaction between nanoparticles and living beings is poorly understood. Seed priming is an attractive way for micronutrient delivery, it has the potential to improve seedling growth and crop productivity [1]. In the present study we investigated the chemical environment of Cu in *Phaseolus vulgaris* L. (common bean) seeds treated with CuO nanoparticles (nCuO) in three different sizes: 25, 40 and <80 nm. The speciation was accomplished using micro-X-ray absorption near-edge structure ( $\mu$ -XANES) at the D09B-XRF beamline at the 1.37 GeV Brazilian Synchrotron Light Laboratory (LNLS, Campinas, Brazil). Prior to the beamtime, we employed a benchtop micro-X-ray fluorescence spectroscopy ( $\mu$ -XRF) system to map the Cu distribution along the seed after nanoparticle exposure. The 2D maps show us three different regions for speciation studies: outside seed coat, within seed coat and cotyledon near seed coat. Figure 5 shows that the chemical neighborhood of Cu incorporated by the seed tissues treated with 25 nm and 80 nm nCuO did not change and remained as CuO. However, Cu located in the embryo of the seed primed with 40 nm nCuO presented redox behavior (Figure 1(c)).

Common beans have a hilum associated to the seed coat, just below the hilum there is the micropyle, a small pore that allows water uptake into the seed. In addition to the above analysis, common bean seeds were also treated with Fe<sub>3</sub>O<sub>4</sub> nanoparticles to verify the 3D distribution of Fe in the hilum region using X-ray tomography at the LNLS X-Ray Imaging beamline (IMX). Figure 2 reveals the internal structure of the hilum and the Fe distribution along this tissue (green spots).

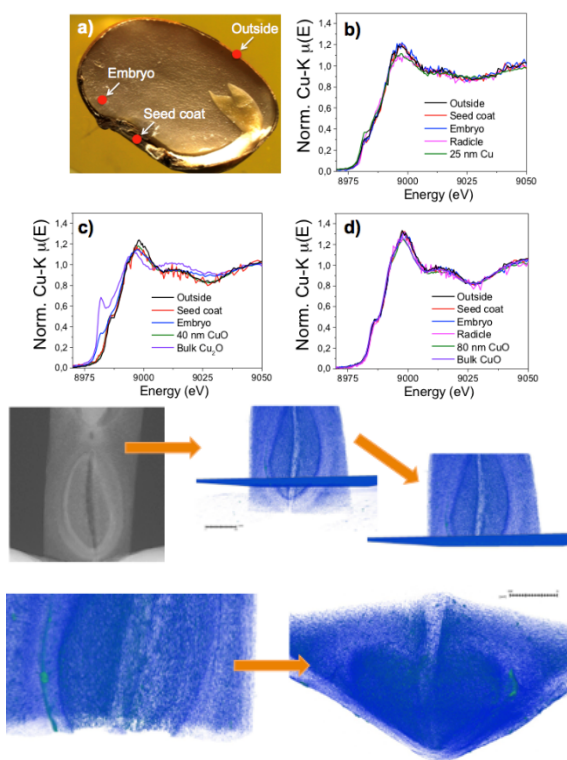


**Figure 1.** Cu-K edge XAS spectra recorded in different regions of *P. vulgaris* seeds treated with 1,000 mg Cu L<sup>-1</sup> dispersions of CuO nanoparticles. (a) Picture of a bean seed pointing out the three regions measured; Spectra recorded of the treatment: (b) 25 nm nCuO (c) 40 nm nCuO and (d) 80 nm nCuO.

**Figure 2.** X-ray tomography imaging of the hilum of a *P. vulgaris* seed treated with 1,000 mg Fe L<sup>-1</sup> dispersion of Fe<sub>3</sub>O<sub>4</sub> nanoparticles. The green spots indicate the Fe 3D distribution.

---

[1] M. Farooq, A. Wahid and K. H. M. Siddique, Micronutrient application through seed treatments - a review (J. Soil Sci. Plant Nut., 2012), 12 (1), 125-142.

*Acknowledgements:* The authors would like to thank LNLS for beamtime at XRF and IMX beamlines and the beamlines scientists, Dr. Carlos A. Perez and Dr. Douglas Galante, for their support during the XAS measurements.

# Synthesis and structural characterization of new ion-conducting PVA/Clay/ionic liquid nanocomposite membranes

J. C. Dutra Filho<sup>1</sup>, K. Dahmouche<sup>2</sup> and A. S. Gomes<sup>1</sup>

<sup>1</sup> IMA, Universidade Federal do Rio de Janeiro, Rio de Janeiro, Brazil;

<sup>2</sup> Campus de Xerém, Universidade Federal do Rio de Janeiro, Duque de Caxias, Brazil.

josecarlosdutra@ima.ufrj.br

A set of ionic conducting nanocomposite membranes containing PVA, organically modified Montmorillonite (MMT) and diethylmethylammonium trifluoromethanesulfonate as a protic ionic liquid (PIL) was synthesized[1]. Their structure at both local and nanometer scale was investigated by X-Ray Diffraction (XRD) and Small Angle X-ray Scattering (SAXS), whereas their thermal stability and ionic conductivity were studied by thermogravimetric analysis (TGA) and electrochemical impedance spectroscopy (EIS), respectively. XRD and SAXS patterns reveal the presence of a large fraction of spatially correlated small clay species surrounded by PIL molecules in all samples and an increase of the lower fraction of clay tactoids and aggregates of larger size by adding more clay. The membrane prepared with the largest amounts of clay and PIL is the only one which contains a particular family of clay aggregates, in which a larger number of PVA chains are intercalated and PIL molecules inserted between clay lamellas, attested by XRD, SAXS and TGA measurements. The presence of these aggregates which probably forms conducting channels in the polymer matrix is responsible for the conductivity of this membrane ( $6.6 \times 10^{-1} \text{ mS.cm}^{-1}$ ), which is the highest of all composites. This property, combined with the more effective PIL-clay support and higher degradation temperatures at 5 and 10% of weight loss compared to samples with lower MMT amount, shows that addition of significant clay and PIL contents should be a promising way to obtain highly conducting and thermally resistant membranes under anhydrous conditions in a next future.

[1] J. J. R. Arias, J. C. Dutra Filho and A. S. Gomes, Hybrid membranes of sulfonated poly ether ether ketone, ionic liquid and organically modified montmorillonite for proton exchange membranes with enhanced ionic conductivity and ionic liquid lixiviation protection. *Journal of Membrane Science* 537, 353 (2017).

*Acknowledgements:* This work was supported by National Council for Scientific and Technological Research (CNPq). The authors would like to thank the National Synchrotron Light Laboratory (LNLS, Campinas, Brazil) for the opportunity to perform the SAXS experiments.

## ***In-situ* x-ray absorption and diffraction studies of formation and phase transition of (Y,RT)CrO<sub>3,4</sub> compounds**

Fernanda A. Fabian<sup>1</sup>, C. C. S. Barbosa<sup>2</sup>, J. G. Santos<sup>1</sup>, J. G. S. Duque<sup>2</sup> and C. T. Meneses<sup>2</sup>

<sup>1</sup> Universidade Federal de Rondônia, Departamento de Física, 76801-059, Porto Velho-Rondônia, Brazil;

<sup>2</sup> Universidade Federal de Sergipe, Departamento de Física, 4950-000, Itabaiana-Sergipe, Brasil.

fernandafabianro@gmail.com

Perovskites and Zircon-type compounds stoichiometry ABO<sub>4</sub> and ABO<sub>3</sub> (where A is a rare-earth element and B includes variety of ions) have been very studied to understand the structural, magnetic and transport properties of mixed transition metal exhibits [1,2]. In this work were obtain (Y,RT)CrO<sub>3,4</sub> (RT = Dy, Gd and Nd) samples using the coprecipitation method [3]. The precursor materials obtained in the synthesis was subjected to measurements of thermogravimetry (TG), differential exploration calorimetry (DSC), *In-situ* x-ray absorption and diffraction for study of the formation process and transition phase. X-ray diffraction measurements was collected at the D10B-XPD beamline (proposal XPD-19040) and X-ray absorption measurements (XANES region) on K-edge of Cr (5989 eV) in transmission mode at the D04B-XAFS1 and D06A-DXAS beamlines (proposal DXAS-19036) at National Synchrotron Light Laboratory (LNLS). *In-situ* X-ray diffraction measurements in the precursors materials showed the single phase formation of the YCrO<sub>4</sub>, DyCrO<sub>4</sub>, GdCrO<sub>4</sub> and NdCrO<sub>4</sub> compounds (tetragonal structure and *I41/amd* space group) follow of a transition to YCrO<sub>3</sub>, DyCrO<sub>3</sub>, GdCrO<sub>3</sub> and NdCrO<sub>3</sub> (orthorhombic structure and *Pbnm* space group), respectively. *In situ* XANES measurements as a function of the temperature in Cr K-edge. In these results, was possible to observe a significant change in the XANES profile, as well as edge displacements due to the change of Cr<sup>5+</sup> to Cr<sup>3+</sup> oxidation state. These results also showed that the compounds formation temperature and phase transition change with ion, that results were also observed by TG and DSC analysis. Magnetization measurements as a function of magnetic field and temperature was performed indicate a ferromagnetic behavior for (Y,Dy,Gd)CrO<sub>4</sub> samples with T<sub>C</sub> estimated in 8.5, 22 and 19 K, respectively. For NdCrO<sub>4</sub> and (Y,Dy,Gd,Nd)CrO<sub>3</sub> samples was observed a predominant antiferromagnetic arrangement and (Dy,Gd,Nd)CrO<sub>3</sub> samples presents two transitions temperature: the first in high temperature was associated to Cr-Cr interaction type and the second more less temperature to RT-Cr, both temperature depend heavily of the rare earth element.

[1] A. Midya, N. Khan, D. Bhoi and P. Mandal, Appl. Phys. Lett. 103, 092402 (2013).

[2] S. Wang, K. Huang, C. Hou, L. Yuan, X. Wub and D. Lu, Dalton Trans. 44, 17201 (2015).

[3] C.T. Meneses, J.G.S. Duque, L.G. Vivas, M. Knobel, J. Non. Cryst. Solids. 354, 4830 (2008).

*Acknowledgements:* This work was supported by Brazilian Federal agency (CAPES), National Council for Scientific Technological (CNPq - DCR) and Foundation for Support to the Development of Scientific and Technological Actions and Research of the Rondônia State (FAPERO). The authors would like to thank for facilites and supported of National Synchrotron Light Laboratory in Brazil (LNLS).

# Study of structural properties of Heavy Fermion compound $\text{YbFe}_2\text{Zn}_{20}$ doped with Cd.

A.L. Fahl<sup>1</sup>, M. Cabrera-Baez<sup>2</sup>, M. A. Avila<sup>2</sup>, C. Adriano<sup>3</sup>, C. Giles<sup>1</sup>, D.R.G.Silva<sup>3</sup>, E. Granada<sup>3</sup>

<sup>1</sup> University of Campinas – UNICAMP, Department of Condensed Matter Physics, "Gleb Wataghin" Institute of Physics, 13083-859, Campinas, SP, Brazil; <sup>2</sup> Universidade Federal do ABC – UFABC, CCNH, 09210-580, Santo André, SP, Brazil; <sup>3</sup> University of Campinas – UNICAMP, Department of Quantum Electronic, "Gleb Wataghin" Institute of Physics, 13083-859, Campinas, SP, Brazil.

fahl@ifi.unicamp.br

The Heavy Fermion compound  $\text{YbFe}_2\text{Zn}_{20}$  was doped with Cd atoms. This compound adopts the complex cubic  $\text{CeCr}_2\text{Al}_{20}$  type of structure with space group  $Fd\bar{3}m$ . In this structure atoms of Yb and Fe occupy a specific crystallographic site (Wyckoff position  $8a$  and  $16d$ , respectively), while the atoms of Zn occupy three different crystallographic sites ( $16c$ ,  $48f$  and  $96g$ ). The introduction of Cd atoms disturbs the system and an increase of the lattice parameter is observed. Refinement of crystalline structure of  $\text{YbFe}_2\text{Zn}_{20}$  and  $\text{YbFe}_2\text{Zn}_{18.6}\text{Cd}_{1.4}$  using single crystal x-ray diffraction data was performed to determine which crystallographic site Cd atoms occupy. The results of refinements show us that Cd substitute only Zn atoms that occupy specifically the  $16c$  crystallographic site. This results also shows a decrease in the Debye-Waller factor for the crystallographic site  $16c$  that are occupied by Cd and Zn atoms in the compound  $\text{YbFe}_2\text{Zn}_{18.6}\text{Cd}_{1.4}$  and an increase of this factor for the other. In order to study the valence shift of Yb atoms in this compound due to Cd doping, we performed x-ray absorption near the edge spectroscopy (XANES) measurements for  $\text{YbFe}_2\text{Zn}_{20}$ ,  $\text{YbFe}_2\text{Zn}_{19}\text{Cd}$ ,  $\text{YbFe}_2\text{Zn}_{18.7}\text{Cd}_{1.3}$  and  $\text{YbFe}_2\text{Zn}_{18.6}\text{Cd}_{1.4}$ . These measurements indicate that the Yb valence is very close to  $\text{Yb}^{3+}$  for the pure and doped materials.

[1] M. Cabrera-baez, R.A. Ribeiro and MA. Avila, J. Phys.:Cond Matt. 28, 375601 (2016).

*Acknowledgements:* This work was supported by CAPES, UNICAMP, IFGW.

## Mixed NiMo, NiW and NiMoW Sulfides Obtained from LDHs

A. C. Faro Jr.<sup>1</sup>, S. Arias<sup>1,2</sup>, Y. Licea<sup>2,3</sup>, J. G. Eon<sup>1</sup>, and L. Palacio<sup>2</sup>

<sup>1</sup>Instituto de Química, Universidade Federal do Rio de Janeiro, Ilha do Fundão, CT bloco A, Rio de Janeiro, Brazil. <sup>2</sup>Instituto de Química, Universidade do Estado do Rio de Janeiro, Rua São Francisco Xavier, 524, Rio de Janeiro, Brazil. <sup>3</sup>CENANO-DCAP, Instituto Nacional de Tecnologia, Av. Venezuela 82, Rio de Janeiro- RJ-Brazil.;

farojr@gmail.com

NiMoAl, NiWAl and NiMoWAl hydrotreating catalysts were prepared from NiAl-terephthalate layered double hydroxides (LDHs), by ion exchange of the terephthalate anion by heptamolybdate ( $\text{Mo}_7\text{O}_{24}^{6-}$ ) and/or metatungstate ( $\text{H}_2\text{W}_{12}\text{O}_{40}^{6-}$ ). The Mo- and/or W-containing LDHs were sulfided, either by direct sulfidation (DS route) or after previous calcination (PC route). The sulfide catalysts were tested in the simultaneous hydrodesulfurization (HDS) of dibenzothiophene (DBT) and hydrogenation (HDA) of tetrahydronaphthalene (THN) in a high-pressure batch reactor at 613 K and 70 bar. The catalysts were characterized by methods such as XRD, TEM, XANES, EXAFS and  $\text{N}_2$  physisorption.

The X-ray absorption spectra of the catalysts at the Ni K-, Mo K- and W  $L_3$ -edges were obtained at the XAFS1 line at the Laboratório Nacional de Luz Síncrotron – LNLS, Campinas, (Brazil). The sulfides recovered from the catalytic tests were washed with n-hexadecane, and kept under this hydrocarbon until shortly before the analyses. The n-hexadecane-soaked samples were then suspended in isopropanol, deposited as a thin layer on filter paper to produce membranes, which were covered with Kapton. Least square fittings to the curves were made, using linear combinations of the XANES spectra of the calcined materials and the standard sulfide patterns ( $\text{Ni}_3\text{S}_2$ ,  $\text{MoS}_2$  or  $\text{WS}_2$ ), with the aim of estimating degree of sulfidation of the active elements in all catalysts.

The results indicated that in the case of the Mo-containing sulfides, all the materials have spectra similar to that of molybdenum disulfide at the Mo-K absorption edge. The first-derivative spectra strengthen the similarity between the spectra of the Mo-containing sulfides and that of molybdenum disulfide, indicating a high degree of sulfidation for all materials. This same similarity between the W-containing sulfides and tungsten disulfide is evident in the W  $L_3$ -edge XANES spectra. The least-square fitting curves showed the good agreement between the experimental curves and the ones calculated from the regressions.

In all materials, nickel has a lower degree of sulfidation than either molybdenum or tungsten. The results confirm the qualitative observation that the degree of nickel sulfidation was higher in catalysts containing both group 6 elements than in those containing only one of them. Furthermore, in molybdenum-containing materials, the degree of sulfidation was higher in the catalysts obtained by DS route than in the PC route. In contrast, the degree of sulfidation was not affected by previous calcination of the LDH containing only tungsten.

It was concluded that the catalysts prepared from LDHs had higher mass-specific activity for the HDA reaction and a higher selectivity for the previous ring hydrogenation (HYD) route in the HDS reaction than an alumina-supported NiMo catalyst. Catalysts prepared by the DS route, especially those containing Mo, were more active and more hydrogenating than corresponding ones prepared by the PC route.

---

From the XANES results, it was possible to conclude that the catalysts with the largest activities and hydrogenation selectivities were the ones with the highest degree of sulfidation of the active elements.

*Acknowledgements:* The authors would like to thank to Laboratório Nacional de Luz Sincrotron (LNLS) by the XAS measurements by means of the XAFS1-17762 project. To PETROBRAS and CNPq (Universal grant nbr. 460424/2014-9) for financial support to the project. S. Arias thanks PRH01-ANP-Petrobras program for a doctorate scholarship. A. C. Faro Jr, and J. G. Eon thank CNPq for research productivity scholarships.

# **[1]Benzothieno[3,2-b]benzothiophenes derivatives : influence in the molecular orientations and charge delocalization process**

*Ana Buzzi Fernández<sup>1</sup>, Amanda Garcez da Veiga<sup>1a</sup>, Almaz Aliev<sup>2</sup>, Yves H. Geerts<sup>2</sup>, and Maria Luiza Rocco<sup>1b</sup>*

*<sup>1</sup>Institute of Chemistry, Federal University of Rio de Janeiro, Rio de Janeiro 21941-909, Brazil  
<sup>2</sup>Laboratoire de Chimie des Polymères, Faculté des Sciences, Université Libre de Bruxelles (ULB), CP 206/1 Boulevard du Triomphe, 1050 Bruxelles, Belgium.*

*91buzzi@gmail.com*

The electronic structure, molecular orientation and charge transfer dynamics of 2,7-diisopropyl[1]benzothieno[3,2-b]benzothiophene (di-iPr), 2,7-di-tert-butyl[1]benzothieno[3,2-b]benzothiophene (di-tBu) and 2,7-di-tert-pentyl[1]benzothieno[3,2-b]benzothiophene (di-(Me)<sub>2</sub>Pr) films were investigated using Near-edge X-ray absorption fine structure (NEXAFS) and Auger decay spectroscopies. Angular dependence at the sulfur 1s NEXAFS spectra for di-iPr and di-tBu films points to a preferred molecular orientation. For these oligomers, the molecules are lying down (molecular plane parallel to substrate surface), while for the di-(Me)<sub>2</sub>Pr film little variation is seen, indicating an essentially disordered film. The delocalization dynamics of excited electrons over empty molecular orbitals were studied by the branching ratio of the competing core-hole decay channels. We find evidence of ultrafast charge transfer in the femtosecond time scale to specific orbitals (LUMO+1) and increased coupling in di-tBu film, corresponding to the better organized film.

# Structural characterization of Sb-based type II superlattices

S. O. Ferreira<sup>1</sup>, C. Deneke<sup>2</sup>, M. Zamiri<sup>3</sup> and F. Cavallo<sup>3</sup>

<sup>1</sup> Universidade Federal de Viçosa, Departamento de Física, 36570-000, Viçosa, Brazil; <sup>2</sup> Universidade Estadual de Campinas, Departamento de Física Aplicada, Campinas, Brasil, <sup>3</sup> University of New Mexico, Department of Electrical and Computer Engineering, 87106, Albuquerque, USA.

sukarno@ufv.br

Type-II heterostructures of Sb-based III-V compounds have been investigated in recent years for application as high performance infrared detectors and focal plane arrays. [1] In this work, we have used co-planar and grazing incidence x-ray diffraction to investigate the strain state of InAs/GaSb/InSb and InAs/InAsSb multilayers grown by molecular beam epitaxy on GaSb substrates. A AlGaSb sacrificial layer between the multilayer and the substrate was used to allow the release of the whole structure and its transfer to a new host substrate. The x-ray characterization was performed before and after the transfer process. The measurements were carried out at the XDR2 beam line of the Brazilian Synchrotron Light Facility (LNLS) using a beam energy of ca. 10 keV. The beam line is equipped with a 6-circle diffractometer and we used an area Si detector ca. 1 m after the sample. Co-planar measurements, around the GaSb (004) reflection, were used to determine the superlattice layer structure. The GI-XRD measurements at the (220) reflection, carried out with a grazing-incident angle of  $0.2^\circ$ , allowed the determination of the in-plane lattice parameter. To compare the as-grown and released T2SLs samples, diffraction patterns of the co-planar measurements were fitted by a commercial software package and compared to the thicknesses data of the initial growth receipt. The measurements demonstrate that the as-grown multilayers structures were pseudomorphic to the GaSb substrate having high structural quality and showed additional satellite peaks in the experimental data that were ascribed to multi-diffraction effects that cannot be fitted by the used software package. Measurement of the released structures showed that the transfer process caused almost no degradation of the crystalline quality, but only a small relaxation of the whole structure. The released InAs/GaSb/InSb multilayer showed a in-plane lattice parameter 0.096% bigger than the as-grown, while for the InAs/InGaSb structure, it is 0.054% smaller compared to the initial structure. Further confirmation of the transfer process success was given by photoluminescence measurements and characterization of an IR detector fabricated with a transferred InAs/InAsSb membrane. [2]

[1] Kim, HS, et al. Appl Phys Lett 101(16):161114 (2012)

[2] Zamiri, M, et al. PNAS 1615645114 (2017)

*Acknowledgements:* This work was supported by the funding agencies CAPES, CNPq, FAPEMIG and FAPESP.

# Physicochemical properties of nanostructured Pd/lanthanide-doped ceria spheres with high catalytic activity for CH<sub>4</sub> combustion

Rodolfo O. Fuentes,<sup>1,2</sup> Leandro M. Acuña,<sup>2,3</sup> A. Gabriela Leyva,<sup>1,4</sup> Richard T. Baker,<sup>5</sup> Huiyan Pan,<sup>6</sup> Xiaowei Chen<sup>6</sup> and Juan J. Delgado-Jaén<sup>6</sup>

<sup>1</sup> Departamento de Física, CAC, CNEA, Av. Gral. Paz 1499, (1650) San Martín, Buenos Aires, Argentina.

<sup>2</sup> CONICET, Buenos Aires, Argentina.

<sup>3</sup> DEINSO, UNIDDEF-CITEDEF, J.B. de la Salle 4397, (1603) Villa Martelli, Buenos Aires, Argentina.

<sup>4</sup> Escuela de Ciencia y Tecnología, UNSAM, M de Yrigoyen 3100, (1650) San Martín, Buenos Aires, Argentina.

<sup>5</sup> EaStChem, School of Chemistry, University of St. Andrews, North Haugh, St. Andrews, Fife, KY16 9ST, United Kingdom.

<sup>6</sup> Departamento de Ciencia de los Materiales e Ingeniería Metalúrgica y Química Inorgánica, Universidad de Cádiz, Campus Río San Pedro, Puerto Real, Cádiz, Spain.

rofuentes@conicet.gov.ar

Ceria-based mixed oxides are materials with a large technological impact, especially in the area of environmental protection. Nanostructured ceria materials can be used as supports for highly dispersed noble metal nanoparticles. The resulting catalyst systems exhibit much improved catalytic activity and redox properties. In particular, Pd-based catalysts are active for NO reduction and CO and hydrocarbon oxidation reactions. Enhanced metal-support interactions led to exceptionally high methane oxidation, with complete conversion below 400 °C. [1]

In this work, nanostructured Ce<sub>0.9</sub>Ln<sub>0.1</sub>O<sub>2- $\delta$</sub>  (LnDC; Ln: Gd, Pr, Tb) spheres previously obtained by microwave assisted hydrothermal homogeneous co-precipitation (HMW)[2,3] were impregnated with 1% wt Pd by incipient wetness impregnation (WI) of an aqueous Pd<sup>2+</sup> solution. Their properties were characterized by synchrotron radiation X-ray diffraction (SR-XRD), X-ray absorption near-edge spectroscopy (XANES) and scanning and high resolution electron microscopy (SEM and HRTEM) with X-ray spectroscopy (EDS). In situ XRD and XANES experiments were carried out under reducing and oxidizing conditions in order to investigate the redox behaviour of these materials. The addition of Pd to the LnDC increased the reducibility of the Ce in the mixed oxide. This was demonstrated by analysis of in situ XANES spectra obtained under reducing conditions. Clearly, the Pd improves the Ce<sup>3+</sup>/Ce<sup>4+</sup> redox couple in LnDC materials. High activity for CH<sub>4</sub> oxidation was observed in nanostructured Pd/LnDC spheres with a total conversion of CH<sub>4</sub> temperature lower than 400 °C. In fact, the reaction rates here reported at 350 °C show the highest efficiency per palladium atom in comparison with other palladium-based catalysts reported in literature.[1,4] These findings open up an interesting avenue for future working this area, and indicate a promising possible application for this particular system.

[1] M. Cargnello, J. Delgado Jaén, J. Hernández Garrido, K. Bakhmutsky, T. Montini, J. Calvino Gámez, R. Gorte, P. Fornasiero, *Science* 337, 713, (2012).

[2] F. Muñoz, L. Acuña, C. Albornoz, G. Leyva, R. Baker, R. Fuentes, *Nanoscale* 7, 271 (2015).

[3] L. Acuña, F. Muñoz, C. Albornoz, A. Leyva, R. Baker, R. Fuentes, *J. Mater. Chem. A* 3, 16120 (2015).

[4] F. Muñoz, R. Baker, A. Leyva, R. Fuentes, *Appl. Catal. B: Environmental* 136-137, 122 (2013).

*Acknowledgements:* This work has been supported by: the Brazilian Synchrotron Light Laboratory (LNLS, Brazil), under proposals D04B-XAFS1-13435 and D12A-XRD1-13437; Chinese Scholarship Council

---

(CSC, China); and Agencia Nacional de Promoción Científica y Tecnológica (Argentina, PICT 2012-1506). Electron Microscopy was performed at the Electron Microscopy Facility, University of St Andrews. The authors are grateful to Fernando Muñoz, Anna Paula da Silva Sotero Levinsky, Cristiane Rodella, Fábio Zambello and Simone Baú Betim for their invaluable experimental assistance at the LNLS.

# Cobalt-doped Zinc Oxide Nanoparticles Synthesis by a Fast Polymer Precursor Based Method

Leonardo Abreu Garcia<sup>1</sup>, Diógenes Ferreira de Almeida<sup>1</sup>, Claudia P. F. Perdomo<sup>2</sup> and Rodolfo Foster Klein-Gunnewiek<sup>1</sup>

<sup>1</sup>Universidade Federal de Alfenas, 37715-400, Campus Avançado de Poços de Caldas, Brazil;

<sup>1</sup>Universidade Federal de São Carlos, 13565-905, Departamento de Engenharia de Materiais, São Carlos, Brazil

leoabgarcia95@gmail.com

Zinc oxide is a versatile semiconductor material and have shown many applications as UV detector, piezoelectric devices, photocatalysis, photovoltaic devices and gas sensors. Furthermore, ZnO nanoparticles have shown an antibacterial activity, enhancing this property when doped with Cobalt [2]. Moreover, room temperature ferromagnetism is observed for a nanosized ZnO doped with many transitions metals, such as Mn, Ni and Co. In the present work, nanostructured Co doped-ZnO was synthesized by a modified fast polymeric precursor method based on soluble polymer. This method involved a water-based complexation of Zn and Co, with concentration from 0.1 to 5.0%-mol of cobalt, by water soluble polyacrylate [1]. The solution was dried and calcined by 120 minutes at 400, 450, 500 and 550 °C. The temperatures or thermal decomposition were determined using Differential Scanning Calorimetry (DSC). A Fourier-Transform Infra-Red Spectroscopy (FTIR) was proceeded to determine the structure of calcined product. X-Ray Diffraction was performed at LNLS (XRD1 beamline), showing very crystalline pattern, specially the powders thermally decomposed at 550 °C. Using Scherrer inference calculated from diffractogram peaks, nanoparticles under 50 nm are present. Scanning Electron Microscopy was also employed to study the morphology of the particles. This process yielded the synthesis of nanoparticles in very short time of about six hours, faster than conventional polymeric precursor methods as Pechini and sol-gel, and no ageing step was needed.

[1] R. F. K. Gunnewiek, C. F. Mendes, R. H. G. A. Kiminami, *Advanced Powder Technology*. 27, (2016) 1056-1061.

[2]M. G. Nair, M. Nirmala, K. Rekha, and A. Anukaliani, *Materials Letters*. 65,(2011) 1797–1800.

*Acknowledgements:* This work was supported by CNPEM LNLS (proposal number 20160371 (XRD1)), CAPES and FAPEMIG and the authors would like to thank the CNPEM LNLS beamline coordinator Alexandre M. G. Carvalho.

## **Advanced Modeling and Data Analysis of In-Situ SAXS investigations of silver nanoparticles nucleation**

P. R. A. F. Garcia<sup>1</sup>, V. Grasmik<sup>2</sup>, K. Pappert<sup>2</sup>, O. Prymak<sup>2</sup>, M. Epple<sup>2</sup> and C. L. P. Oliveira<sup>1</sup>

*1 Universidade de São Paulo, Instituto de Física da Universidade de São Paulo, Grupo de Fluidos Complexos, 05508090, São Paulo, Brazil; 2 University of Duisburg-Essen, Institute of Inorganic Chemistry, 45141, Essen, Germany  
pauloafg@if.usp.br*

Metallic nanoparticles are an important issue of the nanoscience nowadays. The understanding of the growth and nucleation processes is fundamental since these mechanisms determine the optical, electronic, magnetic and catalytic properties of the nanoparticles. In this work we investigated the growth and nucleation processes of silver nanoparticles during the synthesis process using “Small Angle X-Rays Scattering” in situ measurements. Using advanced modeling tools for the description of the scattering data, the temporal evolution of the volume and number fractions of the nanoparticles in the system as well as their average size could be determined. In addition, a hypothesis about the growth mechanism could be formulated based on the Lifshitz-Slyozov-Wagner (LSW) theory.

[1] Lindner, Peter, and Th Zemb. "Neutron, X-ray and light scattering: introduction to an investigative tool for colloidal and polymeric systems." (1991). [2] S. Banerjee, K. Loza, W. Meyer-Zaika, O. Prymak, and M. Epple, "Structural Evolution of Silver Nanoparticles during Wet-Chemical Synthesis," *Chemistry of Materials*, vol. 26, no. 2, pp. 951-957, Jan 28 2014. [3] I. M. Lifshitz and V. V. Slyozov, "The kinetics of precipitation from supersaturated solid solutions", *Journal of Physics and Chemistry of Solids*, vol. 19, no. 1-2, pp. 35-50, 1961.

Acknowledgements: This work was supported by CAPES, CNPq, FAPESP and INCT-FCx.

## Unravelling the nature of NIR plasmonic nanoprisms

L. Giovanetti<sup>1</sup>, M. A. Huergo<sup>1</sup>, M. S. Moreno<sup>2</sup>, C. M. Maier<sup>3,4</sup>, F. G. Requejo<sup>1</sup>, R. C. Salvarezza<sup>1</sup>, C. Vericat<sup>1</sup>

*1 Instituto de Investigaciones Fisicoquímicas Teóricas y Aplicadas (INIFTA), Universidad Nacional de La Plata – CONICET, Sucursal 4 Casilla de Correo 16, 1900 La Plata, Argentina. 2 Centro Atómico Bariloche - S.C. de Bariloche, Argentina. 3 Chair for Photonics and Optoelectronics, Department of Physics and Center for Nanoscience (CeNS), Ludwig-Maximilians-Universität München, Amalienstraße 54, 80799 Munich, Germany. 4 Nanosystems Initiative Munich (NIM), Schellingstraße 4, 80799 Munich, Germany*

*lisandro@fisica.unlp.edu.ar*

The selection of ideal materials for biomedical applications requires certain conditions not always easy to combine. Ideally, it is needed a nontoxic material, that could be reutilized to diminish doses to a minimum, with an adequate size for cell and tissues interaction and of course, that is efficient to remove malignant cells. Gold is an inert material that does not damage tissues itself due it does not chemically interact with them. This property makes it also very stable in an oxidative ambient, such as the biological medium. On the other hand, it is relatively easy to manipulate gold in the nanoscale, making it possible to grow nanostructures in the appropriate size to interact with cells and its components, that is neither too big, because it would not reach several locations, nor too small to become dangerous[1]. This malleability of gold allows scientists to synthesize nanoparticles (NP) with localized surface plasmon resonances (LSPR) in different positions of electromagnetic spectrum. In the last years, much effort has been done to improve the synthesis of gold nanoprisms because of the obvious advantages related to size and the energy of its LSPR in the NIR. One most popular strategy to synthesize gold nanoprisms is the use of sulfur compounds as reducing agents of the Au(III) ions. Sulfide and thiosulfate have been alternatively used to yield truncated gold nanoprisms with excellent NIR absorption but also to a collection of non-active NIR spherical nanoparticles [3]. In particular the thiosulfate synthetic route has attracted great interest due to the large yield of nanoprisms in relation to spherical particles. In this work we show preliminary results of the analysis of physical and chemical properties of Au NS resulting from the Au (III) reaction with thiosulfate ions. Our results shown that these NP are comparable in optical properties and bulk composition to those produced by the sulfide reaction, although with a better yield and easier control. Our data reveal that the thiosulfate synthesis proceeds by the same chemical route than that observed for the sulfide synthesis discarding the widely accepted route of thiosulfate oxidation to sulfate. XANES at the sulfur K edge reveals that the Thiosulfate decomposition to sulfide and the oxidation of these species to sulfur results in gold NP covered by a mixture of strongly adsorbed reduced sulfur species, similarly to those found when sulfide ions are used as reducing agents. The presence of Au<sup>0</sup> in the nanostructure bulk was confirmed by EXAFS signal at the Au L3 edge. The presence of these species on the nanostructure surface is crucial to understand and improve their biocompatibility, in particular when surface modification is made by the ligand exchange method [4].

---

[1] Chithrani, D. B. *Insciences J.* 1, 115–135 (2011). [2] Chithrani, B. D., Ghazani, A. A. & Chan, W. C. W. *Nano Lett.* 6, 662–668 (2006). [3] Saverot, S.-E., Reese, L. M., Cimini, D., Vikesland, P. J. & Bickford, L. R. *Nanoscale Research Letters* 10, 241 (2015). [4] Charchar, P., Christofferson, A. J., Todorova, N. & Yarovsky, I. *Small* 12, 2395–2418 (2016).

**Acknowledgements:** This work has been financially supported by ANPCyT (PICT 2012-0836, 2010-2554, 2012-1136 and 2015-2285) and CONICET (PIP 112-201201-00093 and 112-201101-01035). Partial support by Laboratório Nacional de Luz Síncrotron (LNLS) under proposals SXS 20150180 and XAFS2 20160225 is acknowledged.

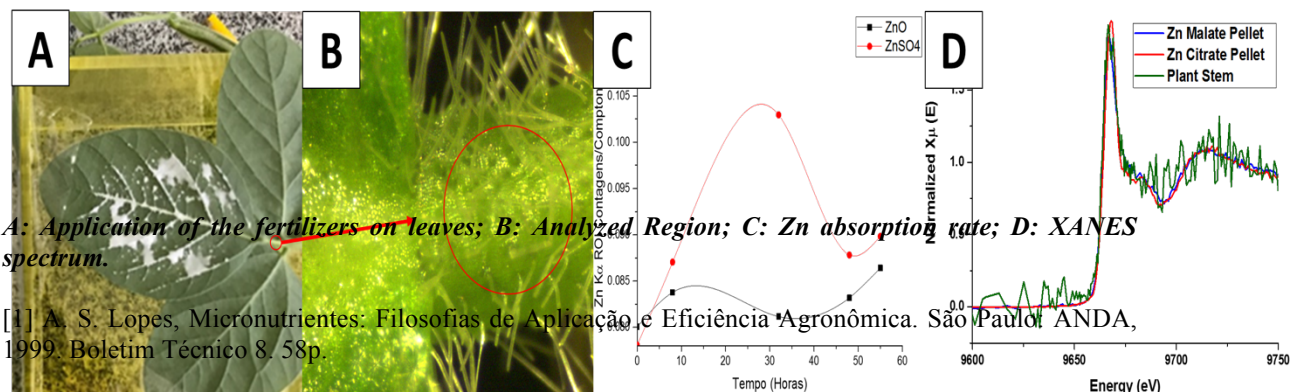
# In Vivo Evaluation of Zinc Foliar Absorption Applied by Sources with Different Solubility in Soybean

GOMES, M. H. F.<sup>1</sup>, RODRIGUES, E. S.<sup>1</sup>, DURAN, N. M.<sup>1</sup>, ALMEIDA, E.<sup>1</sup>, OTTO, R.<sup>2</sup>  
and CARVALHO, H. W. P.<sup>1</sup>

<sup>1</sup>Center for Nuclear Energy in Agriculture, 13416-000, Piracicaba-SP, Brazil; <sup>2</sup>Luiz de Queiroz College of Agriculture, 13418-900, Piracicaba-SP, Brazil

Email: marcos.gomes@usp.br

The application of fertilizers directly on plants leaves is a very common practice to supply nutrients. It aims at reducing problems of adsorption and leaching which occur when fertilizers are applied on the soil [1]. Nevertheless, the plant uptake efficiency for these nutrients is still low, e.g. between 2009 and 2012, the Brazilian agriculture applied 2.7 times the quantity of zinc exported by the main crops [2]. It is important to enhance the absorption efficiency of fertilizers, avoiding excessive accumulation in the environment and exhaustion of the global mineral sources. Aiming to analyze the zinc foliar absorption by soybean when applied by sources with different solubility, it was measured its concentration and determined the ligands in the stem of leaves before and application passed 5, 32, 48 and 55 hours. It was used a commercial ZnO (low solubility) and ZnSO<sub>4</sub> salt (high solubility) both with 23,000 mg Zn L<sup>-1</sup>. The fertilizers were spread on the abaxial face of the leaves using a brush (Figure A). The measures were performed on the stem 2 mm of the leaf edge (Figure B). The concentration analysis was performed using the Orbis PC EDAX  $\mu$ -XRF facility with a 1 mm excitation beam produced by a Rh anode operating at 40 keV and 900  $\mu$ A with a 25  $\mu$ m primary Ni filter. The XRF photons were detected by a 50 mm<sup>2</sup> SSD detector. The Zn chemical environment was characterized using XANES at the XRF beamline on the Brazilian Synchrotron National Laboratory. The beamline dispose of a double crystal monochromator working at the Zn energy band (from 9550 to 9800 eV). The readings were performed in fluorescence mode using a 264  $\mu$ m<sup>2</sup> excitation beam and the fluorescence produced were captured by a 30 mm<sup>2</sup> SSD detector. It was not observed absorption of zinc when applied as oxide. The sulphate uptake increased reaching maximum at 32 hours when start to decline, probably due to phytotoxicity caused by the high concentration of salt deposited on the leaf blade. The XANES analysis showed that zinc is naturally transported as Zn-malate, but when the absorption process increased, the transporter was gradually changed to citrate. At the maximum absorption rate zinc was totally bound to citrate and moved back to malate when the absorption normalized.



[1] A. S. Lopes, Micronutrientes: Filosofias de Aplicação e Eficiência Agronômica. São Paulo: ANDA, 1999. Boletim Técnico 8. 58p.

---

[2] J. F. Cunha, E. A. B. Francisco, V. Casarin and L. I. Prochnow, Balanço de Nutrientes na Agricultura Brasileira: 2009 a 2012. International Plant Nutrition Institute. Informações Agronômicas. nº 145. 13p. 2014.

# Mapping Out the Dynamics of Cation Exchange by Means of Synchrotron XRD

G. Grassi<sup>1,2</sup>, L. Michels<sup>3</sup>, M.A.S. Altoé<sup>4</sup>, C.L.S. da Fonsêca<sup>1</sup>, R. Droppa Jr.<sup>5</sup>, J.O. Fossum<sup>2</sup>, G.J. da Silva<sup>1</sup>

<sup>1</sup> Universidade de Brasília, Instituto de Física, 70910-900, Brasília, Brazil.

<sup>2</sup> Secretaria de Estado de Educação do Distrito Federal, 70040-020, Brasília, Brazil;

<sup>4</sup> Norwegian University of Science and Technology, Physics Institute, 7491, Trondheim, Norway.

<sup>4</sup> Universidade Federal do Espírito Santo, Departamento de Química e Física, 29500-000, Alegre, Brazil.

<sup>5</sup> Universidade Federal do ABC, Centro de Ciências Naturais e Humanas, 09210-580, Santo André, Brazil.

grassi@unb.br

In this work, we report X-Ray Diffraction (XRD) and Energy Dispersive X-Ray Spectroscopy (EDS) measurements to investigate the confined cation exchange process in saline aqueous suspensions of a synthetic clay mineral from Lithium-Fluorohectorite (Li-Fh) to Nickel-Fluorohectorite (Ni-Fh) as illustrated in Fig. 1 (a) and (b), as well as the reverse process from Ni-Fh to Li-Fh (Fig. 1 (c) and (d)) and also from Li-Fh to Sodium-Fluorohectorite (Na-Fh). The process consisted of mixing Li-Fh and salt  $\text{NiCl}_2(\text{H}_2\text{O})$  to replace  $\text{Li}^+$  with  $\text{Ni}^{2+}$  in the interlayer space and  $\text{NaCl}$  to exchange  $\text{Li}^+$  with  $\text{Na}^+$  in aqueous solution for two different pH values. The  $d_{001}$  of the samples at different times show that the interlayer space is of the same order of magnitude as traditional Ni-Fh, for which the exchange process was performed on the time-scale of months. The dynamics of the cation exchange to investigate if the Ni- or Li-Fh is observed at pH = 2 (Fig. 2 (a)) and pH = 7 (Fig. 2 (b)). The results show that the transitions from  $\text{Li}^+$  to a larger cation like  $\text{Na}^+$  and  $\text{Ni}^{2+}$  is faster than 5 minutes (Fig. 2 (c)). This was confirmed by EDS measurements. However, for the reverse path, from the traditional Ni-Fh ( $q_{001} = 4.326 \pm 0.002 \text{ nm}^{-1}$ ) to Li-Fh ( $q_{001} = 4.327 \pm 0.001 \text{ nm}^{-1}$ ), the change in the  $d_{001}$  was not observed during the same time scale, as illustrated in Fig. 1 (d), suggesting that the  $d_{001}$  will only decrease after most of the  $\text{Ni}^{2+}$  leave the interlayer space.

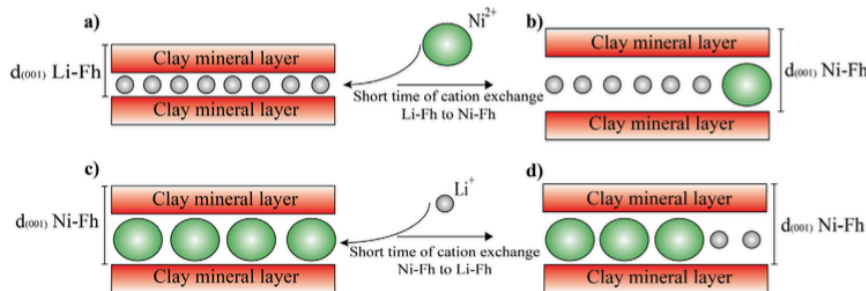
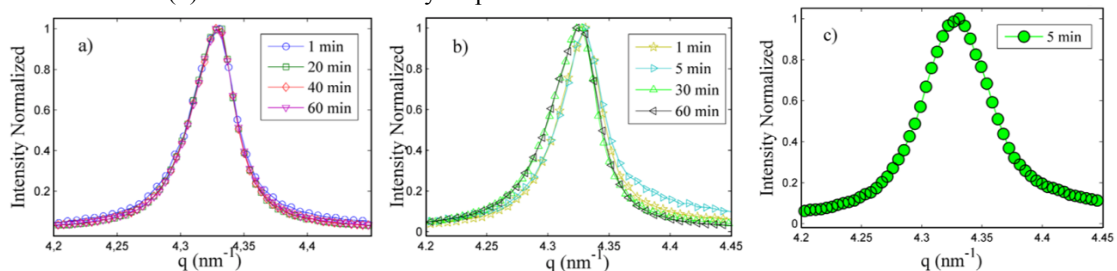


**Fig. 1.** Representation of (a) cation exchange from original Li-Fh to Ni-Fh. (b) Only few  $\text{Ni}^{2+}$  are necessary to change the interlayer space of the sample to one similar to Ni-Fh. (c) Cation exchange from the traditional Ni-Fh to Li-Fh. (d) The observed interlayer space after 5 minutes is similar to Ni-Fh.



---

**Fig. 2.** Powder samples extracted of a water solution of original Li-Fh and  $\text{NiCl}_2 \cdot 6(\text{H}_2\text{O})$  collected at different times after initial preparation for: a)  $\text{pH} = 2$  and b)  $\text{pH} = 7$ . c) Powder sample extracted of a water solution of traditional Ni-Fh and LiCl collected 5 minutes after initial preparation at  $\text{pH} = 2$ .

*Acknowledgements:* This work was supported by CAPES. The authors would like to thank the LNLS technical staff.

# Synthesis and structural characterization using synchrotron X-ray Powder Diffraction (S-XRD) of $\text{NdBa}_2\text{Cu}_3\text{O}_{6+\delta}$ with energy applications

Joaquín Grassi<sup>1</sup>, M. Macías<sup>2</sup> and L. Suescun<sup>1</sup>

<sup>1</sup> *Cryssmat-Lab/Cátedra de Física/DETEMA, Facultad de Química, Universidad de la República, Montevideo, Uruguay.* <sup>2</sup> *Departamento de Química, Universidad de los Andes, Carrera 1 N° 18A-12, Bogotá, Colombia*

joaquingrassi@fq.edu.uy

Solid Oxide Fuel Cells (SOFCs) are considered an excellent alternative among the different sources of clean energy, especially in the case of static and long-run applications due to its demonstrated efficiency, stability and fuel flexibility [1]. The principle of operation of a fuel cell involves the electrochemical reaction between a fuel and an oxidant in separate compartments to produce an electric current. The reactions take place on the surface of the electrodes, oxygen reduction reaction (ORR) at the cathode and fuel oxidation at the anode, while the circuit is closed by transporting anions through the ceramic electrolyte. Currently, the interest in those devices is focused especially in the so-called Intermediate Temperature Solid Oxide Fuel Cell (IT-SOFC) that operate between 600-800°C which creates the necessity for new materials with higher electrochemical activity in this temperature range. The higher catalytic activities have been reported for materials with  $\text{ABO}_{3-\delta}$  perovskite type structure with oxygen deficiencies ( $\delta > 0$ ) and a cubic or pseudocubic network. The most studied materials present a mixture of alkaline earth and lanthanide cations at A site and 3d transition metal mixtures at B site which ensures sufficient number of oxygen vacancies and mixed-valence B sites making these cathodes mixed ionic-electronic conductors (MIECs). We have already prepared and studied conventional cathodes with unconventional dopants as Cu [2]. Novel materials, however, need to be considered if fast progress wants to be achieved, since modification of traditional materials has proven to be a slow way forward. With this in mind we are in the search of other perovskite phases that show electrical conductivity and oxygen vacancies, able to act as MIECs and also provide good catalytic activity for the ORR. In collaboration with other groups we have already studied  $\text{La}_4\text{BaCu}_5\text{O}_{13-\delta}$  and doped variants, with mixed results [3]. Considering the large number and mobility of oxygen vacancies (even at room temperature) and high electric conductivity of traditional high TC superconductor  $\text{YBa}_2\text{Cu}_3\text{O}_7$  [4,5], our group focused on studying the possibility of using this type of material as an electrode (cathode) for SOFC. However YBCO shows an orthorhombic to tetragonal (O/T) phase transition associated with a strong change in oxygen content and mobility that may be a problem for IT-SOFC mechanical stability.

An extended study on  $\text{NdBa}_2\text{Cu}_3\text{O}_{6+\delta}$ , obtained through a combustion reaction path, the structural characterization and the evolution of the cell parameters as a function of temperature using synchrotron X-ray Powder Diffraction (S-XRD) is presented. We have found that the larger the RE (rare earth) cation reduces the O/T phase transition temperature, being eliminated in the RT-900°C range for Nd, making it a more promising IT-SOFC cathode material in process of being characterized.

- 
- [1] A.V. Da Rosa, *Fundamentals of Renewable Energy Processes*, third ed. Elsevier, Oxford, UK, 2013.
- [2] S. Vázquez, J. Basbus, A.L. Soldati, F. et al. *Journal of Power Sources* 274 (2015) 318-323.
- [3] M. A. Macías, M. V. Sandoval, N. G. Martínez et al. *Solid State Ionics* 288 (2016) 68–75.
- [4] E.B. Mitberg, M.V. Patrakeev, K.R. Poeppelmeier, et al. *Journal of Alloys and Compounds* 274 (1998) 103–109.
- [5] J.D. Jorgensen, M.A. Beno, D.G. Hinks, et al., *Phys. Rev. B* 36 (1987) 3608-3616.

*Acknowledgements:* This work was supported by ANII (PR\_FSE\_2015\_109493 and PD\_NAC\_2014\_1\_102409) and the Brazilian Synchrotron Light Laboratory (LNLS-CNPEN), Campinas, Brazil, through proposal XPD20160246.

## **Spectrochemical analysis of metals in gingival fluid of patients with dental implants and different prosthetic materials**

Miriam Grenón, Miriam<sup>1,2</sup>, David Fuks<sup>1</sup>, Manuel García<sup>3</sup>, Fabiana Oliva<sup>3</sup>, Juan C. Ibañez<sup>2</sup>, Maria C. Ibañez<sup>2</sup>, Maria A. Juaneda<sup>2</sup>, Carlos A. Pérez<sup>4</sup>, and Héctor J. Sánchez<sup>5,6</sup>

<sup>1</sup> Dept. of Periodontology, Faculty of Dentistry, Universidad Nacional de Córdoba (UNC), Córdoba, Argentina

<sup>2</sup> Dept. of Implantology, Faculty of Medicine, Universidad Católica de Córdoba (UNC), Córdoba, Argentina

<sup>3</sup> INFIQC, National Scientific and Technical Research Council (CONICET), CABA, Argentina

<sup>4</sup> Brazilian Synchrotron Light Source (LNLS), CNPEM, 13083-970 - Campinas, Brazil

<sup>5</sup> IFEG, National Scientific and Technical Research Council (CONICET), C1033AAJ - CABA, Argentina

<sup>6</sup> FaMAF, Universidad Nacional de Córdoba (UNC), Córdoba, Argentina

jsan@famaf.unc.edu.ar

Titanium dental implants are in an electrolytic hostile media composed by bacterial colonies, gingival fluid, and inflamed tissues. It triggers an electrochemical degradation process known as corrosion. During this process, different ions are released to the media and to the organism from the implant. This can result in the degradation of the implant surface, i.e., increase of the roughness and decrease of the TiO<sub>2</sub> protective layer. In addition, it leads to cytotoxic responses and inflammatory processes that can cause pathological conditions such as peri-implantitis.

Trace and ultra trace elements present in gingival fluid can be studied using very specialized spectrochemical techniques like total-reflection x-ray fluorescence analysis induced by synchrotron radiation (SR-TXRF).

In this paper, studies of metals in gingival fluid of patients with dental implants and different prosthetic materials were performed by SR-TXRF. Prosthetic materials based in zirconium, noble metals and nickel-chromium alloys were considered.

The results indicate that concentrations of Ni, Cu, and Zn in gingival fluid of patients with implants with prosthetic components of nickel-chromium alloys and inflamed gums are higher than those of patients with healthy gums. Similar (statistically) results were found for the same elements and vanadium when the prosthetic material was noble metals. In the case of prostheses made in base of zirconium, the only element with a significant statistical difference was titanium.

These results indicate the importance of metal release to the organism and the influence of it on the prosthetic restoration. Moreover, further research is needed regarding the release of metals by dental implant and prostheses in order to obtain clinical applications.

*Acknowledgements:* The authors would like to thank LNLS/CNPEM for partially supported this work  
Proposal:20150133

## Impact of the crystallization conditions on the polymorphism and crystalline size domain of Efavirenz

R. Guimarães<sup>1</sup>, A. Kuznetsov<sup>2</sup>, H.V.A. Rocha<sup>3</sup>, and S. L. Cuffini<sup>1</sup>

*1 Universidade Federal de São Paulo, ICT, São José dos Campos, Brazil; 2 Divisão de Metrologia de Materiais, Instituto Nacional de Metrologia, Qualidade e Tecnologia – Duque de Caxias, Brazil. 3 LaSiFA. Farmanguinhos-FIOCRUZ*

*rguimaraes42@gmail.com / scuffini@unifesp.br*

Efavirenz (EFV) is a compound used in High Activity Antiretroviral Therapy (HAART) [1]. A very critical problem in using drugs with low solubility is to assure their bioavailability. Previous studies [2] have shown that dissolution rate, as well as a bioequivalence of EFV depend on microstructure of its crystalline phase. However, the pharmaceutical industry does not include the control of this solid state property in quality control steps of EFV. In order to study the variability of the microstructure and other solid state properties, the samples of EFV were crystallized from solution at different crystal growth conditions: temperature, agitation and type of solvent. The produced samples were characterized by the X-ray powder diffraction method using synchrotron radiation (XPD beamline). X-ray diffraction patterns obtained using conventional X-ray sources allowed for identification of polymorphs present in the samples. However, a reliable determination of the average crystallite sizes for each sample required the use of synchrotron radiation. A combination of a highly crystalline powder sample of EFV and the standard reference material, Al<sub>2</sub>O<sub>3</sub> (NIST, SRM 1976), was used to determine the instrumental aberrations, mainly, at low  $2\theta$  diffraction angles, as there is no available standard reference material that covers low  $2\theta$  angle range typical for drugs diffraction. X-ray powder diffraction data were analyzed by Rietveld refinement method using TOPAS Academic software. It was established that crystal nucleation temperatures determine the EFV's polymorphism incidence while crystalline domain sizes, in turn, depend on polymorphism. Important correlations between type of solvent and agitation conditions, on the one hand, and crystalline size domain, on the other hand, are reported.

[1] de Aquino, R. J. A.; de Campos, L. M. M.; Alves, R. J.; Lages, G. P.; Pianetti, G. A. (J. Pharmaceut. Biomed. 2007), 43, 298–303. [2] Fandaruff, C., Silva, M.A.S., Bedor, D.C.G., Santana, D.P., Rocha, H.V.A., Rebuffi, L., Ricardo, C.L.A., Scardi, P., Cuffini, S.L., Correlation between microstructure and bioequivalence in Anti-HIV Drug Efavirenz, Eur. J. Pharm. Biopharm. 91 (2015) 52-58.

Acknowledgements: This work was supported by CAPES, UNIFESP, FIOCRUZ and INMETRO.

## Born Again vs. IsGisaxs:

### Application of these popular softwares in the characterization of nanopores embedded in ZnO films

E. Heredia<sup>1</sup>, C. Bojorge<sup>1</sup> and H. Cánepa<sup>1</sup>

<sup>1</sup> DEINSO – CITEDEF – UNIDEF. J. B. de la Salle 4397, (B1603ALO) Villa Martelli, Pcia. De Buenos Aires, Argentina

eheredia@citedef.gob.ar

Grazing-Incidence Small-Angle X-ray Scattering (GISAXS) is a surface scattering technique used to characterize the nanostructure of thin films. It is a versatile and powerful technique, which enables studies of nanoscale objects. These nanoparticles can be deposited on the surface or embedded in the film. GISAXS patterns provide information about the shape, size and distribution of nanoparticles.

Among the available techniques, the use of X ray scattering in the grazing incidence geometry is complementary to electronic microscopy techniques and presents several advantages:

- an averaged statistical information over all the sample;
- the technique can be applied in any kind of environments ranging from ultra-high vacuum to gas atmospheres;
- kinetic studies can be undertaken as function of temperature, gas pressure, etc.
- using the variable probed depth as function of the incidence angle, GISAXS offer the opportunity to characterize buried particles or interfaces.

In this work we present and compare GISAXS results obtained by using the free softwares Isgisaxs [1] and Born Again [2] for the analysis of nanopores embedded in ZnO thin films. IsGisaxs was widely used but its last update was made in the last decade. Although it delivers reliable results, this software operates under an unfriendly interface. Otherwise, Born Again is a new software which is periodically updated working in a very simple and visual way. Both programs allow modeling. By fitting selected parameters, it is possible to obtain the characteristics of the nanoparticles contained in the films.

Data collection using Gisaxs images was performed on the XRD2 line of the LNLS facilities.

[1] R. Lazzari, IsGISAXS: a program for grazing-incidence small-angle X-ray scattering analysis from supported islands, *J. Appl. Cryst.* 35 (2002) 406-421, <http://www.insp.jussieu.fr/oxydes/IsGISAXS/isgisaxs.htm>, Version 2.6.

[2] J. Burle, C. Durniak, J. M. Fisher, M. Ganeva, G. Pospelov, W. Van Herck, J. Wuttke (2017), BornAgain - Software for simulating and fitting X-ray and neutron small-angle scattering at grazing incidence, <http://www.bornagainproject.org>, Version 1.8.1.

*Acknowledgements:* This work was supported by MINDEF (PIDDEF 10/14).

# Structure of Sodium Caseinate-Stabilized Nanoemulsions Studied by Laser Scanning Confocal Microscopy and Small Angle X-Ray Scattering

M.L. Herrera<sup>1</sup>, J.M. Montes de Oca Ávalos<sup>1</sup>, M.V. Borroni<sup>1</sup> and R.J. Candal<sup>2</sup>

<sup>1</sup> *Institute of Polymer Technology and Nanotechnology (ITPN), University of Buenos Aires-CONICET, 1127, Buenos Aires, Argentina;* <sup>2</sup> *University of San Martín, Instituto de Investigación e Ingeniería Ambiental, 1650 San Martín, Provincia de Buenos Aires, Argentina.*

mlidiaherrera@gmail.com

Nanoemulsions are defined as a thermodynamically unstable colloidal dispersion consisting of two immiscible liquids, with one of the liquids being dispersed as small spherical droplets with radius sizes smaller than 100 nm (McClements, 2012). A conventional emulsion typically has particles with mean radii between 100 nm and 100  $\mu$ m. Nanoemulsions have been used for applications in the food industry such as beverage, healthier ice cream, frozen food or they have been designed for performing as carriers or delivery systems for lipophilic compounds. Recently, formulation of food grade O/W nanoemulsions has been an area of active research. Dairy proteins have been extensively used as emulsifiers in conventional emulsions since they adsorb to the oil droplet interface, forming a strong and cohesive protective film that helps prevent droplet aggregation. Sodium caseinate is widely used as an ingredient in the food industry due to its functional properties, which include emulsification, water and fat-binding, thickening and gelation. The aim of the present work was to investigate the physical properties of nanoemulsions stabilized with sodium caseinate. The effects of protein concentration and sucrose addition on physical properties were analyzed by dynamic light scattering (DLS), Turbiscan analysis, confocal laser scanning microscopy (CLSM) and small angle X-ray scattering (SAXS) with the aim of describing in a deeper way the stability behavior. Nanoemulsions were prepared using a combination of a high-energy homogenization and evaporative ripening methods previously reported for whey protein-stabilized systems with some minor changes (Lee and McClements, 2010). Oil phase was a blend of commercial SFO (15 wt.%) and ethyl acetate (85 wt.%). In all nanoemulsions the ratio NaCas/SFO was 0.6. Aqueous phase contained sucrose in concentrations of 0, 2, 4, 6, or 8 wt.% and NaCas in concentrations of 1.0, 2.0, 3.0, or 4.0 wt.%. Intensity vs.  $q$  curves were fitted with a model considering a hard core of sunflower oil and a shell of protein free to move. The results showed that stability behavior of NaCas-stabilized nanoemulsions was very dependent on droplets sizes. Systems with droplets smaller than 120 nm behaved in a different way of nanoemulsions prepared by a two-step method or than conventional emulsions. Because droplets sizes were smaller than the ones obtained by high-energy methods, gravitational forces on individual particles were negligible and destabilization by creaming was not noticeable. Selecting a protein concentration at which droplets aggregates were too small to interact to each other, flocculation may be avoided for a long time, even without addition of a co-adjuvant such as sucrose. The 4 wt.% NaCas-stabilized nanoemulsion was stable without sugar in the aqueous phase. CLSM images showed that nanoemulsions contained droplets sizes below microscope resolution. Homogeneous structures without flocs were obtained in all cases. Parameter  $N_{agg}$  (aggregation number) from SAXS model, which quantify the number of NaCas molecules on droplet surface, increased with sucrose concentration indicating that sodium caseinate had less tendency to aggregation and therefore were absorbed on droplets surface.

---

[1] D.J. McClements, *Soft Matter* 8, 1719 (2012).

[2] S.J. Lee and D.J. McClements, *Food Hydrocoll.* 24, 560 (2010).

*Acknowledgements:* This work was supported by the National Agency for the Promotion of Science and Technology (ANPCyT) through project PICT 2013-0897 and the Synchrotron Light National Laboratory (LNLS, Campinas, Brazil) through project SAXS1-20150056.

# **In situ synchrotron radiation evaluation of hydrogen embrittlement in stainless steels and of severe plastic deformation at cryogenic temperatures in metals**

J.J. Hoyos<sup>1,2</sup>, P. Craidy<sup>3</sup>, M.T.P. Paes<sup>3</sup>, A.J. Ramírez<sup>4,2</sup>, A. Tschiptchin<sup>5,2</sup>, O. Cintho<sup>1</sup>

<sup>1</sup> State University of Ponta Grossa, Department of Materials Engineering, 84030-900, Ponta Grossa, Brazil; <sup>2</sup> National Research Center for Energy and Materials (CNPEM), Metals Characterization and Processing Laboratory (CPM), Brazilian Nanotechnology National Laboratory (LNNano), Campinas, SP 13083970, Brazil; <sup>3</sup> Petrobras, Av. Horácio Macedo 950, Rio de Janeiro, RJ 21941915, Brazil; <sup>4</sup> Ohio State University, Department of Materials Science and Engineering, U.S.A.; <sup>5</sup> University of São Paulo, Department of Metallurgical and Materials Engineering, Polytechnic School, Brazil

jjhquintero@uepg.br

In situ synchrotron radiation measurements of axial strain were made in several materials, in order to evaluate the hydrogen embrittlement in stainless steels and dynamic recovery in cryogenic deformed metals. On one hand, this provides the first direct comparison between the kinetics of the main hardening mechanisms (martensitic transformation and dislocation density) as a function of strain for 316 austenitic stainless steel and 2507 duplex stainless steel under hydrogen effects. In both steels, the kinetics of the martensitic transformation did not have a clearly definite trend as a function of strain, suggesting that the strain-induced martensite is a result of plastic deformation and not the cause of the embrittlement phenomenon. While the necking and failure process took place around critical values of dislocation density. Therefore, the influence of the martensitic transformation on failure process seems to be lower than that of the dislocation density. On the other hand, a first in-situ evolution of microstrain as a function of strain is performed by X-ray diffraction during cryogenic deformation in several metals. As the microstrain can be related to dynamic recovery, dynamic recovery suppression seems to be easier in metals with lower stacking fault energy. Severe cryogenic deformation of metals leads to a considerable grain refinement and enhancement of the steel strength. This allows the production of nanocrystalline material without the disadvantage of the limited volume associated to the conventional methods of powder metallurgy, crystallization of amorphous alloys or deposition on a substrate.

*Acknowledgements:* This work was supported by CAPES (PNPD and Project Instituto Nacional de Ciência, Tecnologia e Inovação em Materiais Complexos Funcionais, Inomat) and CNPq (Projects 455275/2013-0 and 403530/2014-8). The authors are grateful to the LNNano/CNPEM for the technical support during the usage of the XTMS installation and LNLS/CNPEM for the infrastructure present in the XRD1 beamline.

## Isolation and characterization of nitrososulphide species ( $\text{SNO}^-$ / $\text{SNOH}$ ) stabilized by coordination to iridium (III)

Cristián Huck Iriart<sup>1</sup>, Ana Foi<sup>2</sup>, Leandro Andrini<sup>3</sup>, José Ramallo Lopez<sup>3</sup>, Yves Joly<sup>4</sup>,  
Florencia Di Salvo<sup>2</sup>, Fabio Doctorovich<sup>2</sup>

<sup>1</sup>. ECyT-UNSAM, San Martín, Argentina, <sup>2</sup>. DQIAQF/INQUIMAE, FCEN/CONICET, UBA, Buenos Aires, Argentina. <sup>3</sup>INIFTA-UNLP, La Plata, Argentina. <sup>4</sup>. Institut Néel, CNRS and Université Joseph Fourier, Grenoble, France  
chuck@unsam.edu.ar

Nitric oxide (NO) and hydrogen sulfide ( $\text{H}_2\text{S}$ ) are gaseotransmitters that regulate numerous physiological functions. Based on the similarity in their physiological effects, it is suggested a possible "link" between these two endogenous species [1]. Although the existence of S-nitrosothiols (RSNO) in biological systems is known since 1992 [2], the existence of the simplest RSNO, the thionitrous acid ( $\text{HSNO}$ ), was demonstrated in solution in 2012 [3]. The study of the reaction between  $\text{H}_2\text{S}$  and NO in the context of coordination chemistry was approached by Olabe et al., who studied the reaction of nitroprusside ( $[\text{Fe}(\text{CN})_5(\text{NO})]^{2-}$ ) with  $\text{HS}^-$  and detected formation of the species  $[\text{Fe}(\text{CN})_5\text{N}(\text{O})\text{SH}]^{3-}$  and then,  $[\text{Fe}(\text{CN})_5\text{N}(\text{O})\text{S}]^{4-}$ ; both characterized in solution [4]. The  $\text{NO}^+$  in the complex  $[\text{IrCl}_5(\text{NO})]^-$  (**1**) is the most nucleophilic known to date, specially due to the weak backbonding. On the other hand, thanks to the inertness of the  $[\text{IrCl}_5]^-$  moiety, several N-nitroso derivatives ( $\text{RXNO}$ ), highly instable species in their free form, were obtained by reaction of **1** with different nucleophiles and stabilized by coordination to the metal centre [5]. This background motivated us to study the reaction of **1** with  $\text{H}_2\text{S}/\text{HS}^-$  as nucleophiles. The reaction was studied at both 25 °C and -30 °C in different solvents and using  $\text{H}_2\text{S}(\text{g})$ , NaSH, and  $\text{Na}_2\text{S}$  in acid medium as  $\text{H}_2\text{S}/\text{HS}^-$  sources. In all the studied conditions, a red solid is immediately obtained as product. The product was characterized by standard spectroscopic techniques (UV-vis, IR), low-temperature high resolution ESI-MS studies and X-ray Absorption Fine Structure (XAFS) spectroscopy at the S K-edge and Ir  $L_3$ -edge. The geometry of the proposed Ir complex was optimized by DFT calculation using ORCA. S K edge XANES and Ir  $L_3$  EXAFS were simulated using FDMNES[6] and FEFF 9.6.4. The experimental and theoretical results show strong evidence of the stabilization of  $\text{SNO}^-/\text{SNOH}$  species through coordination to Ir(III). This work includes evidences for the formation and isolation in solid form of a  $\text{Ir}^{\text{III}}\text{-SNOX}$  coordination complex which is unprecedented. Thus, this study opens the way to use transition metals other than iron and ruthenium for S-nitrosylation of sulfides using NO and contributes to the understanding of species of physiological relevance.

[1] Yang, G. et al. *Science*, 322, 587–590 (2008)

[2] Stamler, J. S.; Singel, D. J.; Loscalzo, J. *Science*, 258, 1898–1902 (1992)

[3] Filipovic, M. R. et al. *J. Am. Chem. Soc.* 134, 12016–12027 (2012)

[4] Quiroga, S. L.; Almaraz, A. E.; Amorebieta, V.; Perissinotti, L. L.; Olabe, J. *Chem. Eur. J.*, 17, 4145–4156 (2011)

[5] Doctorovich, F.; Di Salvo, F. *Acc. Chem. Res.*, 40 985 (2007)

[6] Joly, Y. *Phys. Rev. B*, 63, 125120 (2001)

*Acknowledgements:* Authors wish to thank CONICET, ANPCyT-MinCyT and LNLS.

# Mn-Zn ferrite nanoparticles probed by synchrotron pair distribution function analysis and anomalous X-ray scattering

R. U. Ichikawa<sup>1</sup>, J. P. R. L. L. Parra<sup>2</sup>, O. Vallcorba<sup>3</sup>, I. Peral<sup>4,5</sup>, W. K. Yoshito<sup>1</sup>, M. J. Saeki<sup>2</sup>, X. Turrillas<sup>3,6</sup>, L. G. Martinez<sup>1</sup>

<sup>1</sup> Instituto de Pesquisas Energéticas e Nucleares, São Paulo - SP, Brasil (IPEN/CNEN).

<sup>2</sup> Universidade Estadual Paulista Júlio de Mesquita Filho, Botucatu - SP, Brasil (UNESP).

<sup>3</sup> ALBA Synchrotron, Cerdanyola del Vallès, Barcelona, Spain

<sup>4</sup> Université du Luxembourg, Faculté des Sciences, de la Technologie et de la Communication, Luxembourg.

<sup>5</sup> Luxembourg Institute of Science and Technology, Luxembourg.

<sup>6</sup> Institut de Ciència de Materials de Barcelona, Bellaterra, Spain (ICMAB/CSIC).

lgallego@ipen.br

Among the numerous applications of  $Mn_{1-x}Zn_xFe_2O_4$  nanoparticles we can highlight biomedical applications as magnetic tracer in Alternate Current Biosusceptometry (ACB), Magnetic Resonance Imaging (MRI), for diagnosis of cancer and others diseases as diabetes and Parkinson, whose severity can be monitored by analyzing the disturbances of the gastrointestinal motility [1,2]. Specifically, the former (ACB) method is promising because of its low cost, it is non-invasive method and because it can be conducted without ionizing radiation. Major advances have been achieved by developing a bio-nanocomposite based on ferrites for the theranostics [3] as well, of breast cancer, by carrying drugs or hyperthermia. Recently, we reported that  $Mn_{0.75}Zn_{0.25}Fe_{2.8}O_4$  nanoparticles with different surface charge can be produced precipitating them by NaOH with different concentrations [2]. This behavior is observed if an excess of Iron is introduced to the ferrite. Five samples precipitated with different NaOH concentrations were analyzed by X-ray synchrotron diffraction (XRD) which revealed a less crystalline phase contribution alongside the main peaks of the cubic spinel ferrite phase. Pair Distribution Function (PDF) analysis was used to probe the local structure and showed that Fe-Fe, Mn-Mn and Zn-Zn bond distances in the 3.0 up to 3.5 Å range are different from the ones usually reported in the literature. Lastly, for the sample with best magnetic behavior anomalous X-ray scattering (AXS) using three energies close to the absorption edges of Mn, Zn and Fe was applied to determine its cation distribution complementing the previous result from PDF analysis.

[1] Martins, M.L.; Calabresi, M.F.; Quini, C.; Matos, J. F.; Miranda, J.R.; Saeki, M.J.; Bordallo H.N. *Materials Science and Engineering*: C. v. 48, pp. 80–85, 2015.

[2] Parra, J. P. R.L.L.; Martins, M. L.; Moretto, G. M.; Ichikawa, R. U.; Martinez, L. G.; Corauto, F.; Miranda, J. R. A; Saeki, M. J. In: *Congress of Applied Physics to Medicine - CONFIAM*. Faculty of Medicine. UNESP. Botucatu, São Paulo. 2014.

[3] Martins, M. L.; Saeki, M. J.; Telling, M. T. F.; Parra, J. P. R. L. L.; Landsgesell, S.; Smith, R. I; Bordallo, H. N. *Journal of Alloys and Compounds*. v. 584, pp. 514–519, 2014.

*Acknowledgements:* The authors would like to acknowledge CAPES and CNPq (# 206983/2014-0) for the financial support. ALBA Synchrotron for the PDF measurements and LNLS (Proposal 20160591) for the anomalous X-ray scattering measurements. The author Inma Peral is supported by the National Research Fund of Luxembourg (Grant No FNR-Inter2015/LRSF).

# Crystal Structures of $\text{BaFe}_2\text{As}_2$ and $\text{Sr}(\text{Fe}_{0.08}\text{Co}_{0.20})_2\text{As}_2$ under Magnetic Field

Ulisses Ferreira Kaneko,<sup>1</sup> M. Piva,<sup>1</sup> M. E. Saleta<sup>1</sup> P. G. Pagliuso,<sup>1</sup> and E. Granado<sup>1</sup>

<sup>1</sup>“Gleb Wataghin” Institute of Physics, University of Campinas – UNICAMP, Campinas, São Paulo – 13083-859 Brazil.  
ulisses.kaneko@lnls.br

Iron-based superconductors (FeSCs) present high critical temperatures reaching 100 K, as it occurs in FeSe films. Large in-plane anisotropy below tetragonal-orthorhombic transition temperature  $T_{t-o}$  in electronic properties such as resistivity, magnetization and electron/hole occupation are important aspects to the physics of the FeSCs. Such anisotropies might be associated with an electronic nematic phase [1, 2], and the corresponding fluctuations may play an important role in the superconducting pairing mechanism [3]. Synchrotron x-ray diffraction experiments were performed on  $\text{BaFe}_2\text{As}_2$  and  $\text{Se}(\text{Fe}_{0.08}\text{Co}_{0.20})_2\text{As}_2$  single crystals as a function of temperature and applied magnetic field up to 6 T along two tetragonal  $[hhl]$  directions. For a  $\text{BaFe}_2\text{As}_2$  crystal with spin-density wave antiferromagnetic ordering temperature  $T_{AF} = 132.5$  K and  $T_{t-o} = 137$  K, the magnetic field favors the tetragonal phase in expense of orthorhombic domains at the vicinity of  $T_{AF}$ . For  $\text{Se}(\text{Fe}_{0.08}\text{Co}_{0.20})_2\text{As}_2$  with more separated magnetic and structural transitions ( $T_{AF} = 132$  K and  $T_{t-o} = 152$  K), the crystal structure also shows significant field-dependence only in a narrow temperature interval close to  $T_{AF}$ . These results are interpreted under a scenario where the structural/nematic transition is magnetically-driven in the 122 family of Fe pnictides [4,5].

- [1] J.-H. Chu *et al.*, Science **329**, 824 (2010).
- [2] A. Jesche *et al.*, Phys. Rev. B **86**, 134511 (2012).
- [3] H.-H. Kuo *et al.*, Science **352**, 958 (2016)
- [4] R.M. Fernandes *et al.*, Nature Phys. **10**, 97 (2014).
- [5] U.F. Kaneko *et al.*, Phys. Rev. B **96**, 014506 (2017).

# Chemical speciation of size-segregated aerosol samples collected at an urban location in Central Argentina

Bethania L. Lanzaco<sup>1</sup>, M.L. López<sup>2</sup>, L.E. Olcese<sup>1</sup> and B.M. Toselli<sup>1</sup>

<sup>1</sup> *Departamento de Físico Química / INFIQC / CLCM / CONICET. Facultad de Ciencias Químicas. Universidad Nacional de Córdoba. Ciudad Universitaria, 5000 Córdoba. ARGENTINA;* <sup>2</sup> *Facultad de Matemática, Astronomía y Física / IFEG / CONICET. Universidad Nacional de Córdoba. Ciudad Universitaria, 5000 Córdoba. ARGENTINA*

blanzaco@unc.edu.ar

Aerosol sampling was conducted for the winter-spring months of years 2014-2015 at an urban site of Córdoba City. Córdoba is the second largest city of Argentina and an important industrial and touristic centre. 175 samples were collected in 6-h intervals and five size fractions, using a SIOUTAS impactor (SKC). The impactor is a miniaturized cascade impactor consisting of four impaction stages and one after-filter. Particles in the aerodynamic diameter ranges  $< 0.25$ ,  $0.25-0.5$ ,  $0.5-1.0$ ,  $1.0-2.5$ , and  $2.5-10$  microns were collected on Teflon filters. The Sioutas impactor operates at a flow rate of  $9 \text{ L min}^{-1}$ . All the collected samples were later individually analyzed by SR-XRF at the Brazilian Synchrotron Light Source Laboratory (LNLS), in Campinas City. The measurements were carried out using the D09B-XRF beam line. Aerosol samples were excited with monochromatic beams of 10 keV and 13.5 keV to obtain size-segregated elemental aerosol mass concentrations for Mg, Al, Si, S, K, Ca, Ti, V, Cr, Mn, Fe, Co, Ni, Cu, Zn and Pb. The high sensitivity of SR-XRF allows for very low detection limits for most of the above elements [1].

It is recognized that the composition and size of particulate matter (PM) is largely determined by its source, making identification of them and its size-segregated components [2], critical to defining source-specific health risks. The results of the present study permitted to differentiate elements that are mainly emitted from mechanical processes from those that are emitted through the engine exhaust. The former have their origins in road resuspension (Al, Fe, Si, Ca, Ti) and are concentrated in the coarse size range (larger than 1 micron). The latter are mainly formed inside the engine and are concentrated in the finest fraction. However, there are some elements, such as Mn, Cr, Zn, Ni, and Cu, that by the size distribution, seems to have a double origin, i.e. in the interior of the engine and in mechanical wearing. The average elemental concentration measured in this work revealed that the most toxic metals (i.e. Cr, Zn, Ni, Cu, and Mn) tended to have an important contribution in the finest size fraction of the particulate matter.

In the present study, fine and ultrafine source identification was carried out by inspection of key species in source profiles, comparison with literature data and the knowledge of the city. As an outcome of this work, the results of detailed source apportionment of the finer fractions measured in the city are presented together with an analysis of the meteorological condition and number concentrations of the particulate matter for the same size fractions.

---

[1] N. Bukowiecki, P. Lienemann, C. N. Zwicky, M. Furger, A. Richard, G. Falkenberg, K. Rickers, D. Grolimund, C. Borca, M. Hill, R. Gehrig and U. Baltensperger. *Spectrochimica Acta Part B* 63, 929-938 (2008).

[2] M. Achad, M. L. López, S. Ceppi, G. G. Palancar, G. Tirao and B. M. Toselli. *Atmos. Environ.*, 92, 522-532, (2014).

*Acknowledgements:* We thank CONICET, SeCyT (UNC), FONCyT and the National Synchrotron Light Laboratory (Research Proposal D09B-XRF-20160044) for partial support of the work reported here. Bethania L. Lanzaco thanks CONICET for a graduate fellowship.

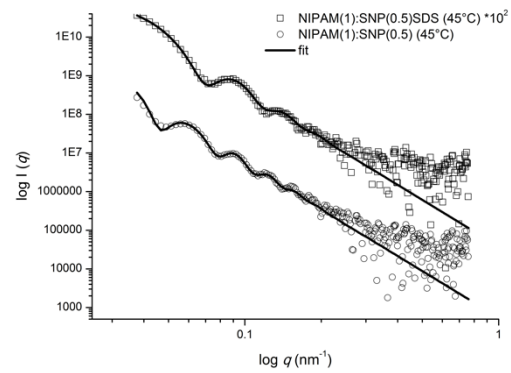
# Core-shell starch nanoparticles-*co*-p(NIPAM) hybrid microgels

D. C. Leite<sup>1</sup> and N. P. Silveira<sup>1</sup>

<sup>1</sup> Universidade Federal do Rio Grande do Sul, Instituto de Química, 91501-970, Porto Alegre, Brazil.

nadya@iq.ufrgs.br

Biomacromolecules, in particular starch polymers, are gaining increasing interest as components of stimuli responsive systems. Among those "smart" materials, microgels are versatile particles with an ability to rapidly swell and deswell in a reversible manner in response to various chemical and physical external stimuli [1]. One of the most stimuli-responsive polymers studied is poly(N-isopropylacrylamide) p(NIPAM), which has a lower critical solution temperature (LCST) of 32 °C [2]. In this work, we report the preparation of starch nanoparticles (SNPs) and the synthesis of cross-linked three-dimensional SNP-*co*-p(NIPAM) hybrid microgels by emulsion polymerization (EP) and surfactant-free emulsion polymerization (SFEP) in aqueous media with different NIPAM:SNP ratio. Herein, we present the results regarding the internal structure of these hybrid microgels, accessed through small angle X-ray scattering (SAXS). SAXS measurements of microgels in solution were performed on the D01B/SAXS1 beamline at the LNLS. The sample-to-detector distance was 3000 mm long, covering a scattering vector  $q$  ranging from 0.04 to 1.5 nm<sup>-1</sup>. Experiments were carried out below (20 °C) and above (45 °C) phase transition temperature (VPTT) of microgels, using a controlled thermobath. Water was measured as a background and subtracted from sample intensities, and it was also used for absolute normalization of the intensity. The data were fitted for a spherical shell form factor and a hard sphere structure factor with monodisperse approximation model using SASfit package (PSI, Switzerland). Size distribution was fitted using Schultz-Zimm model applying the same software. SAXS measurements have shown that starch nanoparticles are probably entangled onto the surface of microgels and, above VPTT, the hybrid materials exhibit a core-shell structure. SAXS curves were well fitted using a core-shell model, as can be seen in Figure 1. The core shell form factor can be understood on the basis of the slightly higher electron density of the polysaccharide compared to poly(NIPAM) assuming assembly of the SNPs on PNIPAM microgel cores. The formation of such kind of structure can be explained as starch nanoparticles being polymers, they are not able to enter inside p(NIPAM) network during its formation. SNPs disposal around p(NIPAM) structure also provide stability for the whole structure.



 SNP  
 p(NIPAM)

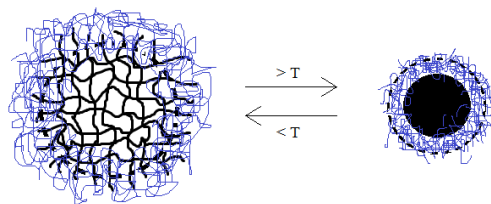


**Fig. 1** SAXS measurements of hybrid microgels above volume transition temperature (45 °C) (left) and proposed SNP-co-p(NIPAM) hybrid microgel structure.

- [1] M. Constantin et al. *Reactive & Functional Polymers* 84,1 (2014).  
 [2] R. H. Pelton and P. Chibante *Colloids and Surfaces* 20 (3), 247 (1986).

*Acknowledgements:* This work was supported by DAAD, Capes and CNPq.

# The Surface Atomic Structure of Black Phosphorus Studied by Photoelectron Diffraction

Luis Henrique de Lima<sup>1</sup>, Lucas Barreto<sup>2</sup>, Richard Landers<sup>1</sup> and Abner de Siervo<sup>1</sup>

<sup>1</sup>Universidade Estadual de Campinas, Instituto de Física "Gleb Wataghin", 13083-859, Campinas-SP, Brazil; <sup>2</sup>Universidade Federal do ABC, Centro de Ciências Naturais e Humanas, 09210-580, Santo André-SP, Brazil

lhlima@ifi.unicamp.br

Recently, orthorhombic black phosphorus (BP), the most stable phosphorus allotrope, has emerged as a "new" promising material for applications in nanoelectronics and nanophotonics [1]. The BP is formed by a stack of phosphorus layers arranged in a honeycomb structure known as phosphorene. Despite the difficulty and challenge in the preparation/characterization of the atomic structure of an isolated single layer, the surface of a single crystal can be a good approximation, since the surface is a natural break in the perpendicular periodicity. In this work, the surface atomic structure of single crystalline black phosphorus was studied by high resolution synchrotron-based photoelectron diffraction (XPD). The angle-scanned XPD experiments were carried out at the PGM beamline of the LNLS. The results show that the topmost phosphorene layer in the black phosphorus is slightly displaced compared to the bulk structure and presents a small contraction in the direction perpendicular to the surface. Furthermore, the XPD results show the presence of a small buckling among the surface atoms, in agreement with previously reported scanning tunneling microscopy results. The contraction of the surface layer added to the presence of the buckling indicates an uniformity in the size of the  $sp^3$  bonds between P atoms at the surface [2].

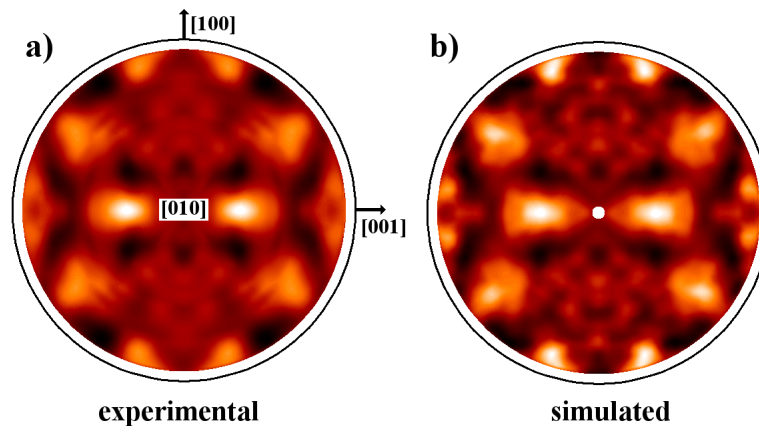


Figure 1: a) Experimental photoelectron diffraction pattern. The main

crystallographic directions are shown. b) Simulated photoelectron diffraction pattern. The patterns are orthographic projections.

[1] X. Ling, H. Wang, S. Huang, F. Xia and M. S. Dresselhaus, Proc. of Nat. Acad. of Sci. 112, 4523 (2015).

[2] L. H. de Lima, L. Barreto, R. Landers and A. de Siervo, Phys. Rev. B 93, 035448 (2016).

*Acknowledgements:* This work received financial support from FAPESP, CNPq, and CAPES from Brazil. XPD measurements were done at LNLS under Proposal No. PGM-19062. The authors thanks the LNLS staff, especially J. C. Cezar, for technical support during beam time.

# Crystallographic and Kinetic Analysis of NahK Mutants: A Decarboxylase from the Naphthalene Degradation Pathway

Marins, K. S., Guimarães, S. L. and Nagem, R. A. P.

Universidade Federal de Minas Gerais, Instituto de Ciências Biológicas, Departamento de Bioquímica e Imunologia, 31275-000, Belo Horizonte, Brazil

*karinsmarins@gmail.com & nagem@icb.ufmg.br*

Naphthalene is the simplest and most toxic polycyclic aromatic hydrocarbon (PAH) that constitutes crude oil<sup>1</sup>. Its metabolism by the bacterium *Pseudomonas putida* G7 occurs due to the presence of the plasmid NAH7 that carries the genes for such process<sup>2</sup>. In this organism, the enzyme NahK (4-oxalocrotonate decarboxylase, 28.4 kDa) belongs to the lower pathway of naphthalene degradation, catalyzing the reaction that converts 4-oxalocrotonate to 2-hydroxy-2,4-pentadienoate and CO<sub>2</sub><sup>3</sup>. This enzyme exists *in vivo* in a macromolecular complex with NahL, the next enzyme in the same pathway. In 2016, Guimarães *et al* proposed a reaction mechanism in which Glu109, Glu111, and Glu142 hold the Mg ion; Lys64, Lys72, and Ser164 share hydrogen bonds with the substrate stabilizing it, while Met76, Phe151, and Phe153 provide a hydrophobic environment which seems to be important for the catalysis<sup>3</sup>. Further mutation studies with these specific residues are important to confirm the decarboxylation mechanism. Hence, our aim was to structurally and kinetically characterize five NahK mutants, complexed or not with NahL and substrate analogues. To obtain the substrate of NahK to perform the kinetic assays, first we had to produce the previous enzyme, NahJ, which isomerizes 2-hydroxymuconate to 4-oxalocrotonate. We expressed and purified a recombinant NahJ, tested its activity and characterized its kinetic parameters. The enzymatic activity of the protein was evaluated analyzing the change of the absorbance curve over time in a spectral range sensitive to the absorption peak of the substrate (295 nm) and the product (236 nm). The kinetic parameters showed that recombinant NahJ, despite having low affinity to the substrate ( $K_M$  of  $373 \pm 36.3 \mu\text{M}$ ), has a high specificity constant ( $k_{\text{cat}} / K_M$  of  $5 \times 10^8 \text{ M}^{-1}\text{s}^{-1}$ ), evidencing that its catalysis is quite efficient. Besides, the enzyme was crystallized and preliminary diffraction data to 2.6 Å resolution was recently obtained at the MX2 Beamline at the Laboratório Nacional de Luz Síncrotron. From this, we focused to obtain the five NahK mutants. A mutagenesis protocol was used, changing the residues K64, K72, S164, F151, and F153 to alanine. Preliminary activity studies for NahK mutants showed that the mutation K64A and the double mutation Phe151A\_Phe153A promote the complete loss of the activity. On the other hand, the mutation S164A seemed to slightly reduce the reaction speed. These early results highlight the important role of these specific amino acids, corroborating the crystal structure analysis published in 2016<sup>3</sup> after NahK structure elucidation from X-ray data collected at MX2.

- 
- [1] Holliger, C. *et al.* (1997). Contaminated environments in the subsurface and bioremediation: organic contaminants. **FEMS Microbiol Rev**, 20, 517.
- [2] Sota, M. *et al.* (2006). Genomic and functional analysis of the IncP-9 naphthalenecatabolic plasmid NAH7 and its transposon Tn4655 suggests catabolic gene spread by a tyrosine recombinase. **J Bacteriol**, 188, 4057.
- [3] Guimaraes, S. L., *et al.* (2016). Crystal Structures of Apo and Liganded 4-Oxalocrotonate Decarboxylase Uncover a Structural Basis for the Metal-Assisted Decarboxylation of a Vinylogous beta-Keto Acid, **Biochemistry** 55, 2632-45.

*Acknowledgements:* This work was supported by CNPq. We would like to thank Dr. Masataka Tsuda and Dr. Masahiro Sota for kindly providing us the *P. putida* G7 strain, Dr. William H. Johnson Jr. for providing 2-hydroxymuconate for kinetic assays, and the Laboratório Nacional de Luz Síncrotron (LNLS, Campinas, Brazil) for provision of synchrotron-radiation facilities.

# *In situ* XRD studies of Copper-based methanol synthesis catalysts activation

M. I. S. de Mello<sup>1</sup>, P. Vinaches<sup>1</sup>, C. Rodella<sup>2</sup> and S. B. C. Pergher<sup>1</sup>

<sup>1</sup> Universidade Federal do Rio Grande do Norte, Laboratório de Peneiras Moleculares, 59078-970, Natal, RN, Brasil.

<sup>2</sup> Laboratório Nacional de Luz Síncrotron (LNLS), Centro Nacional de Pesquisa em Energia e Materiais (CNPEM), 13083-970, Campinas, São Paulo, Brasil.

mellomariele@gmail.com

Cu/Zn-based catalysts in combination with various metal oxides (i.e ZrO<sub>2</sub>) and support (mesoporous SBA-15) are extensively studied due to its high efficiency for methanol synthesis from CO<sub>2</sub> hydrogenation, [1, 2]. An important factor for these catalysts development and optimization is the influence of the preparation and activation parameters in the structural properties [3-5]. Thus, this research focus on the *in situ* XRD analysis of the reduction process of the Cu/ZnO and Cu/Zn/ZrO<sub>2</sub> catalysts to evaluate the ZrO<sub>2</sub> effect in the structure of the catalyst. *In situ* X-ray diffraction (Figure 1) revealed that the ZnO allowed the CuO reduction at lower temperatures (190 and 230 °C) compared with pure CuO. It was also observed that the addition of ZrO<sub>2</sub> in the catalyst helps to decrease even more the reduction temperature (around 100 °C). ZnO and/or ZrO<sub>2</sub> were not reduced neither varied their structure up to 500 °C as expected, and the Cu was in its reduced form even at room temperature after the activation.

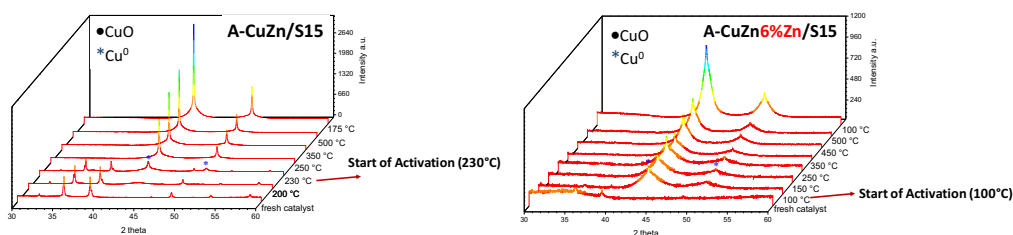


Figure 1: X-ray diffractions of the *in situ* reduction of fresh catalysts.

The ability of catalytic reduction, after their use in methanol synthesis reaction (H<sub>2</sub>/CO<sub>2</sub> = 3, P = 5.0 MPa, T = 240 °C), was similarly evaluated. Initially, the catalysts were half reduced half oxidized. When they were subjects of further reduction, the same reduced completely without structure modifications (Figure 2). There was an exception, the A-CuZn/S15 catalyst (20%Cu/10%Zn), which remained completely reduced after its use and handling. This shows that the catalysts can be recycled to be used again in the catalytic reaction.

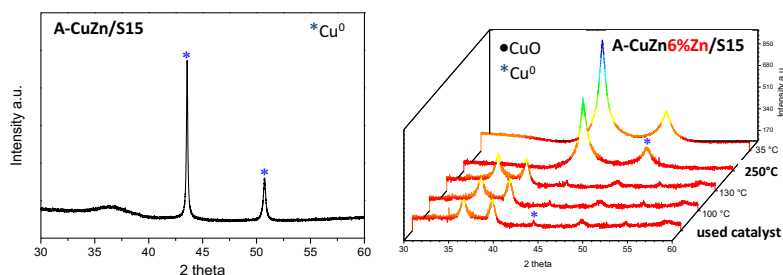


Figure 2: X-ray diffractions of the *in situ* reduction of used catalysts.

- 
- [1] Guo X, Mao D, Lu G, Wang S, Wu G., Catal Commun 12, 12 (2011).  
[2] Raudaskoski R, Niemela MV, Keiski RL., Top Catal. 45, 1-4 (2007).  
[3] Behrens M, Schlögl R., Zeitschrift für Anorganische und Allgemeine Chemie., 639, 15 (2013).  
[4] Zander S, Kunkes EL, Schuster ME, Schumann J, Weinberg G, Teschner D, et al., Angew Chem. 52, 25 (2013).  
[5] Schumann J, Tarasov A, Thomas N, Schlögl R, Behrens M., Appl Catal A Gen. 516 (2016).

*Acknowledgements:* The authors would like to thank UFRN for the infrastructure, and LNLS/CNPEM for the XPD measurements performed within the proposal number 20160653 entitled “In situ studies of activation Copper-based methanol synthesis catalysts”.

## Synthesis and characterization of ligand-free Ni nanoclusters

Martín Mizrahi<sup>1</sup>, Ana Sol Peinetti<sup>2</sup>, David Buceta<sup>3</sup>, José Martín Ramallo-López<sup>1</sup>, Graciela González<sup>2</sup>, Félix Requejo<sup>1</sup>, Arturo López-Quintela<sup>3</sup> and Fernando Battaglini<sup>2</sup>

<sup>1</sup> Instituto de Investigaciones Fisicoquímicas Teóricas y Aplicadas – INIFTA (CONICET y Dto. Química, Fac. Cs. Ex., UNLP), 1900 La Plata, Argentina.

<sup>2</sup> INQUIMAE (CONICET) – Depto. de Química Inorgánica, Analítica y Química Física, Fac. Cs. Ex. y Nat., Universidad de Buenos Aires, Ciudad Universitaria, Pabellón 2, C1428EHA Buenos Aires, Argentina.

<sup>3</sup> Departamento de Fisicoquímica, Universidad de Santiago de Compostela, 15782 Santiago de Compostela (España).

mizrahi@fisica.unlp.edu.ar

Metal nanoclusters (NC) are a new class of materials which attract a great interest due to their new properties, related with their unique geometric and electronic structures.<sup>1, 2</sup> The intrinsic features of these structures do not change monotonically, rather drastically, with the number of atoms, therefore, the control over the synthesis of these assemblies is highly relevant. In this work, the electroreduction of Ni<sup>2+</sup> ions inside an ordered mesoporous alumina was studied as function of the current density applied (J). These samples were characterized by AFM, SEM, UV-Vis fluorescence and XAS techniques. Applying a J= 3 mA/cm<sup>2</sup> we are able to generate a ligand-free NC of metallic Ni of about 0.7 nm of diameter (see Fig. 1). When the current density is increased, it leads to the generation of nanoparticles (NP) and nanorods (NR). In these cases, we have observed that the metallic state start to disappears to become Ni oxide NP or NR (see Fig. 2). As an example, we use these ligand-free Ni clusters to catalyze the reduction of methylene blue showing an excellent performance.

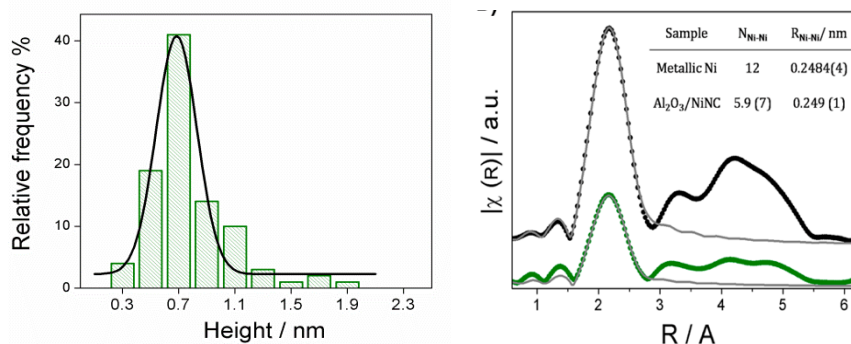


Figure 1: Left: AFM topography images of Ni NC deposited on a mica substrate. Center: Histogram distribution heights. Right: Fourier transform of Ni foil (blank dots) and Ni NC (green dots) with their respective fits (blank lines).

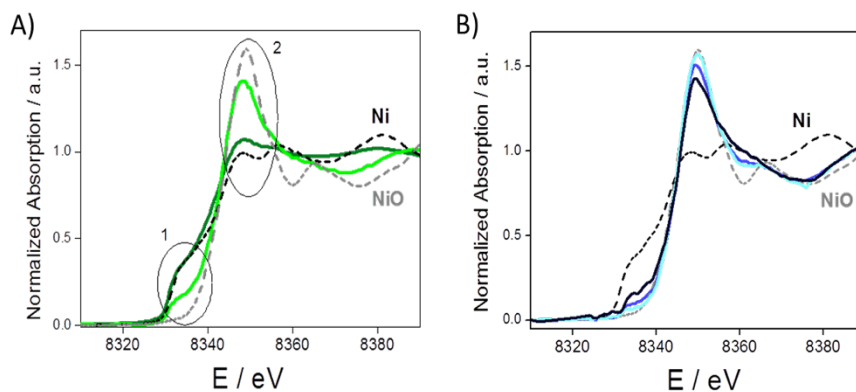


Figure 2: Normalized XANES spectra at the Ni K-edge of: A) Ni NC @  $J=3 \text{ mA/cm}^2$  (dark green) and  $J=10 \text{ mA/cm}^2$  (light green). B) Ni NC @  $J=25 \text{ mA/cm}^2$  applying 5 pulses (black), 50 pulses (blue) and 100 pulses (light blue). Metallic Ni (dashed black line) and NiO (dashed gray line) references are also plotted in both graphics.

[1] Yamazoe, S.; Koyasu, K.; Tsukuda, T. *Acc. Chem. Res.* **2014**, *47* (3), 816.

[2] Oliver-Messeguer, J.; Liu, L.; García-García, S.; Canós-Giménez, et al.. *J. Am. Chem. Soc.* **2015**, *137* (11), 3894.

*Acknowledgements:* This work was supported by: LNLS (XAFS2 beamline proposal 20160632) and grants: UBACYT 20020130100262BA, PIP1035 CONICET and PICT 2015 - 2285 ANPCYT.

## Structure-property relations of polyurea elastomers prepared by sol-gel process

Eduardo Ferreira Molina<sup>1</sup> and Vinicius Henrique Bonattini<sup>1</sup>  
*1Universidade de Franca, 14400-600 Franca – São Paulo, Brazil Email:  
eduardo.molina@unifran.edu.br*

Polyureas (PU), are a class of elastomeric polymers that are broadly similar to segmented polyurethane copolymers.[1,2] In this study, we synthesized polyureas containing alternating soft segments (polyethers) and hard segments (triisocyanate) by sol-gel route using an appropriate solvent. Thermodynamic incompatibility between hard and soft segments gives rise to a nanoscale segregated morphology that plays a critical role the physical and mechanical properties of these materials. Changing the concentrations of the polymer and the crosslinker lead to the formation of an elastomeric material. The dry PU are sensitivity to the humidity, it can be seen that the xerogels are opaque or transparent. Moreover, the PUs are rubbery, flexible and insoluble in aqueous medium. The opaque characteristic of the PU is due to the presence of a crystallinity PEO segment. The macroscopic swelling experiments demonstrated the hydration of the matrix, leading to the expansion of the network by the water molecules diffusion into the PEO. The contact angle result demonstrated a fast absorption of the drop water by PU hydrogel, evidencing a very hydrophilic surface. This behavior is due to the functional groups (urea and polyether backbone) present in the structure of the PU xerogel. IR spectroscopic analyses of all the polyether urea elastomers show new peaks at 1569 cm<sup>-1</sup> (CO-N-H amide II) and at 3334 cm<sup>-1</sup> (N-H, hydrogen bonded) which indicates the urea formation. We performed preliminary measures of a polyurea sample on SAXS1 beamline. We observe a broad peak at low q values centered on 0.17 nm<sup>-1</sup>, which corresponds to the phase separation of the hydrogen bonding hard domains from the soft polyether domains. The incorporation of antimicrobial/anticancerous curcumin in the preparation of PU xerogels was successfully obtained which show promising applications as biomaterials.

[1] Lucie Chagnon, Gilles Arnold, Sylvain Giljean, Maurice Brogly, Progress in Organic Coatings 2013, 76, 1337. [2] Marlene Jacquemond, Nicolas Jeckelmann, Lahoussine Ouali, Olivier P. Haefliger, Journal of Applied Polymer Science 2009, 114, 3074.

Acknowledgements: This work was supported by FAPESP (n° 2016/16804-0). The authors would like to thank Brazilian Synchrotron Light Laboratory (LNLS) for providing beamtime at the D01A-SAXS1 beamline and for assistance with the X-ray scattering experiments.

# Changes in the Structural Characteristics of Titania Photocatalysts Probed by Multivariate Analysis Applied to SAXS Profiles and FT-IR Spectra

Yolice P. Moreno<sup>1</sup>, Marco Ferrão<sup>2</sup>, and João H. Z. Dos Santos<sup>2</sup>

*1 Universidade Federal Rio Grande do Sul, Departamento de Engenharia Química, Porto Alegre, RS, Brazil; 2 Universidade Federal Rio Grande do Sul, Instituto de Química, Av. Bento Gonçalves, Porto Alegre, RS, Brazil  
yppureno@gmail.com*

The nature of the support is one of the most important concerns of research in heterogeneous catalysis because the characteristics of the material may affect the performance of the catalyst. In photocatalysis, the metal nanoparticles may have limitations on their reuse due to their size and may suffer aggregation problems [1]. To overcome these limitations, the nanoparticles of the catalysts can be immobilized on a solid support, for example on a micrometer silica particle surface, this strategy allows expand its application to photocatalysis, and enhance the thermal stability of catalysts. The structural analysis of supports and catalysts can be investigated by the Fourier transform infrared (FT-IR) and small-angle X-ray scattering (SAXS) methods. In this study, we applied multivariate analysis, such as, principal component analysis (PCA) and hierarchical cluster analysis (HCA) to analyze the variance and to detect similarities between spectroscopic and scattering data [2]. Nanoparticles and structured mixed silicas, including functionalized and hybrids ones were prepared employing six routes, using several reagents, such as tetraethoxysilane, SiCl<sub>4</sub>, octadecylamine, Pluronic®L-31, and Tween®80. These materials were used as catalysts supports for rhodamine B (RhB) photodegradation and H<sub>2</sub> photogeneration. We monitored structural changes in samples through simultaneous multivariate data analyses (PCA and HCA) applied to techniques with different principles, such as SAXS curves and FT-IR spectra. It was determined that only two principal components accounted for over 96.5 and 89.7% of variance (FT-IR and SAXS, respectively) within the sample set. The functionalized particles with chlorine atoms depicted high degrees of similarity (85.6% from FT-IR spectra and 88.5% from SAXS curves). The catalytic activity of the structured mixed catalysts was influenced by factors such as: (i) textural characteristics (the zeta potential and the specific surface area,  $r_{Sp} > 0.779$ ); (ii) the clusters fractal structure,  $r_{Sp} > 0.745$ , it was observed a transition from mass fractal to fractal surface, according to the power law values; (iii) the presence of functional groups, in agreement with the FTIR/SAXS/multivariate analysis results. The resulting photocatalyst systems reheaded 68% in RhB photodegradation and they used in H<sub>2</sub> generation showed much higher performance than commercial TiO<sub>2</sub> catalyst (11.200  $\mu\text{mol H}_2 \cdot \mu\text{mol Ti}^{-1} \cdot \text{hr}^{-1}$  and 0.776  $\mu\text{mol H}_2 \cdot \mu\text{mol Ti}^{-1} \cdot \text{h}^{-1}$ , respectively), under UV radiation.

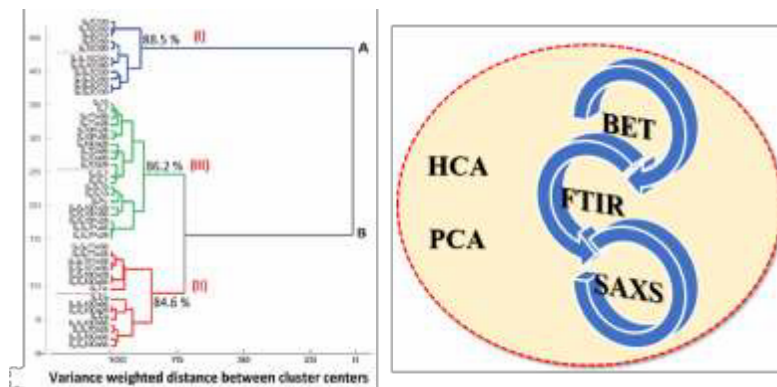


Figure 1. Dendrogram obtained from HCA applied to the SAXS profiles.

[1] B. Wang B Wang, F. de Godoi, Z. Sun, Q. Zeng, R. L. Frost, et al. *J. Colloid interface Sci.*, 438, p. 204-211 (2015). [2] Y. P. Ruiz, M. F. Ferrão, M. B. Cardoso, J. H. dos Santos, et al. *RSC Advances*, 6, 72306-72316, (2016).

Acknowledgements: This Project was partially financed by CNPq. Yolice P. Moreno is grateful for the grant provided by CAPES. The Brazilian Synchrotron Light Laboratory (Campinas, Brazil) are thanked for the analysis of the SAXS (Projects SAXS1 - 20160537).

# Calculation of Two-Dimensional Scattering Patterns for Oriented Systems

Cristiano L. P. Oliveira<sup>1</sup>, C. Alves<sup>2</sup> and J. S. Pedersen<sup>3</sup>

<sup>1</sup> *Institute of Physics, University of São Paulo, Rua do Matão 1371, São Paulo, São Paulo, 05508-090, Brazil*

<sup>2</sup> *Department of Engineering and Sciences, Federal University of Parana, Rua Pioneiro 2153, Palotina, Parana, 85950-000, Brazil*

<sup>3</sup> *Department of Chemistry and Interdisciplinary Nanoscience Center (iNANO), Aarhus University, Gustav Wieds Vej 14, Aarhus, DK-8000 C, Denmark*

crisipo@if.usp.br

A versatile procedure to calculate two-dimensional scattering patterns of oriented systems is presented. The systems are represented by a set of dummy atoms with different scattering length densities which allows the construction of very complex shapes either for single particles or for sets of particles. By the use of oriented pair distances distribution functions it is possible to perform a fast calculation of the scattering intensity from the oriented system in a given direction in the scattering vector ( $q$ ) space and generate the 2D scattering pattern on a given  $q$  plane. Several examples of the calculations are presented, demonstrating the method and its applicability. The presented results open new possibilities for the analysis of scattering patterns obtained from oriented systems [1].

[1] Alves, C., J.S. Pedersen, and C.L.P. Oliveira, Calculation of two-dimensional scattering patterns for oriented systems. *Journal of Applied Crystallography*, 2017. 50(3): p. 840-850.

*Acknowledgements:* This work was supported FAPESP, CAPES, CNPq and INCT-FCx.

# Grazing incidence X-ray off specular scattering on biomembrane Langmuir monolayers

R. Oliveira<sup>1</sup>, J. Pusterla<sup>1</sup>, A. Gasperini<sup>2</sup>, X. Puentes-Martinez<sup>2</sup>, L. Cavalcanti<sup>2</sup>

<sup>1</sup>*Centro de Investigaciones en Química Biológica de Córdoba (CIQUIBIC-CONICET) - Departamento de Química Biológica, Facultad de Ciencias Químicas, Universidad Nacional de Córdoba, Ciudad Universitaria, X5000HUA, Córdoba, Argentina;* <sup>2</sup>*Brazilian Synchrotron Light Laboratory - LNLS, CNPEM, Rua Giuseppe Maximo Scolfaro, 10000, Campinas, SP 13083-070, Brazil.*

rafaelg\_oliveira@yahoo.com.ar

Grazing incidence X-ray off specular scattering (GIXOS) is a technique that produces analogous information to specular X-ray reflectivity on systems with conformal roughness in just a single measurement. This technique is mainly applied to Langmuir monolayers at the air/water interface which serves as biomembrane model systems. We performed GIXOS at XRD-2 (LNLS) on Langmuir monolayers of myelin lipids. These measurements play a central role for comparison with myelin lipid bilayers (measured by SAXS) on one side, and myelin lipid monolayers measured in a new setup based on light reflectivity using a Brewster Angle Microscope (BAM). Our BAM setup, with variable refractive index on the subphase, allows the matching of the refractive indexes from the monolayer and the subphase, and thus the determination of the monolayer refractive index. The last plus the reflectivity renders the thickness of the monolayer. Nevertheless, due to the fact that the monolayer is not optically homogeneous in the z direction, it was not clear what includes the measured thickness. In this sense, comparisons between SAXS, GIXOS and BAM on the same material in monolayers and bilayers allowed us to conclude that the BAM setup measures all the thickness of the monolayer. Additionally, we found that the phosphor to phosphor thickness of the bilayer (4.60 nm) is bigger than twice the monolayer (2.13 nm each) even in the thicker state. We postulate that this is due to roughness at the air/water interface that under monolayer apposition, in order to build up a bilayer generates a steric repulsion. This force separates each monolayer from the contact plane by half roughness, which is 0.15 nm. This separation reconstitutes the correct P-P thickness as well as the proper electron density profiles of the methylene minimum as seen by SAXS in bilayers [1].

[1] JM. Pusterla, AA. Malfatti-Gasperini, XE. Puentes-Martinez, LP. Cavalcanti, RG. Oliveira, BBA Biomem. 1859, 924 (2017).

*Acknowledgements:* This work was supported by grants from CONICET (PIP 2012-14 #11220110100624), SECyT (2014-2015 203/14) (UNC), FonCyT (PICT 2012-2583) and CeBEM (09-2012) (Argentina). We acknowledge to the Brazilian Synchrotron Light Laboratory for beamtimes at SAXS-2 beamline under research proposals SAXS1-10716 and SAXS1-13462 and XRD-2, proposal 20150072. R.G.O. thanks to FAPESP for the program of visiting researcher (grant number 14/18526-1).

## Study of the profile of layer formed in plasma nitride austenitic stainless steel

D.Olzon-Dionysio<sup>(1,a)</sup>, S. D. de Souza<sup>(1)</sup>, L. G. Martinez<sup>(2)</sup>, M. Campos<sup>(3)</sup>, E. H. da Silva<sup>(4)</sup>, and M. Olzon-Dionysio<sup>(1)</sup>

<sup>(1)</sup>UFVJM- Diamantina, MG, Brazil, <sup>(2)</sup> IPEN- São Paulo, SP, Brazil, <sup>(3)</sup>UNESP- Tupã, SP, <sup>(4)</sup>Belgian Nuclear Research Centre (SCK-CEN)/Vrije Universiteit Brussel (VUB), LABO and BEFY, Brussels, Belgium,

(a) Corresponding author: [dolzon@gmail.com](mailto:dolzon@gmail.com)

The ASTM F138 and AISI 316L stainless steels are used as biomaterials and for industrial applications. Studies related to the application of plasma nitriding to such materials have been given much attention and it has been the subject of a systematic study in our research [1-5]. If temperatures up to 400<sup>o</sup> C is used in the process, a nitrided layer of some micrometers is produced, which improves important properties in this context as high hardness, wear resistance and also corrosion resistance. The nitrided layer is formed by the **composite layer** which consists of iron and chromium nitrides, and concentrates on the surface, as well as the nitrogen **diffusion layer** which is located in the inner region, known as expanded austenite  $\gamma_N$ . Compared to matrix  $\gamma$ -phase reflections,  $\gamma_N$ -phase diffraction peaks are broader and shifted to lower angles. The  $\gamma_N(200)$  peak positions are more deviated relatively to  $\gamma(200)$  than other planes, demonstrating a distortion from the cubic fcc unit cell. Up to now, the crystalline structure of this phase is still a matter of debate and it has not been completely clarified. We have developed some measurements using synchrotron radiation, which allows for both a higher intensity and a better resolution, in order to elucidate this important phase formed in the nitriding process [4,5]. With the aim of investigate the depth distribution of composite layer of some ASTM F138 samples, which were nitrided at 400<sup>o</sup> C at different conditions of AC voltage frequency, synchrotron radiation diffraction was carried out using 7.0 keV energy. The XRD patterns were measured using different grazing angles. Measurements revealed that the iron and chromium nitrides, from the composite layer, decrease rapidly with depth. The results will be presented and discussed, contributing to better elucidate this important phase formed in the nitriding process.

[1] S. D. de Souza, M. Olzon-Dionysio, E. J. Miola and C. O. Paiva-Santos. *Plasma Nitriding of sintered AISI 316L at Several Temperatures*- Surf. Coat. Technol. 184/2-3 (2004) 176.

[2] M. Olzon-Dionysio, S.D. de Souza, R.L.O. Basso, S. de Souza. *Application of Mössbauer spectroscopy to the study of corrosion resistance in NaCl solution of plasma nitrided AISI 316L stainless steel*-Surf. Coat. Technol. 202 (2008) 3607.

[3] S.D.de Souza, M.Olzon-Dionysio, R.L.O.Basso, S.de Souza *Mössbauer spectroscopy study on the corrosion resistance of plasma nitrided ASTM F138 stainless steel in chloride solution*-Mater.Character. (2010) 992 DOI 10.1016/j.matchar.2010.06.015

[4] M. Campos, S. D.de Souza, L. G. Martinez; M.Olzon- Dionysio *Study of expanded austenite formed in plasma nitrided AISI 316L samples using synchrotron radiation diffraction*-Mater.Res.(2014) 17(5): 1302-1308 DOI:10.1590/1516-1439.285914

[5] M. Campos, *Investigação das fases formadas na superfície do aço inoxidável AISI 316L nitretado a plasma*- São Carlos. PhD thesis-DF- UFSCar, Advisor : M.Olzon- Dionysio, finished in abril/2013.)

*Acknowledgements:* This work was supported by FAPESP, CAPES and FAPEMIG.

# Studying the 4f electrons in the Kondo lattice antiferromagnet $\text{Ce}_2\text{RhIn}_8$

K. R. Pakuszewski<sup>1</sup>, W. S. Silva<sup>2</sup>, C. Giles<sup>1</sup>, F. Rodolakis<sup>3</sup>, Julio C. Cezar<sup>2</sup>, J. C. Campuzano<sup>4</sup>, P. G. Pagliuso<sup>1</sup>, and C. Adriano<sup>1</sup>

<sup>1</sup> Instituto de Física "Gleb Wataghin", UNICAMP, Campinas-SP, 13083-859, Brazil; <sup>2</sup> Laboratório Nacional da Luz Síncrotron, C. P. 6192, 13083-970, Campinas-SP, Brazil; <sup>3</sup> Northwestern University Argonne National Laboratory Institute of Science and Engineering (NAISE), Northwestern University, Evanston, Illinois 60208, USA; <sup>4</sup> Department of Physics, University of Illinois at Chicago, Chicago, Illinois 60607, USA.  
raduenz@ifi.unicamp.br

Materials which exhibit the heavy fermion behavior, such as Ce-based materials, are of great interest, as the Kondo scattering continuously grows with decreasing temperature, until it can no longer be treated as a perturbation. The electron-electron interactions can easily be tuned, leading to a variety of sometimes exotic ground states, including complex magnetic ordering and unconventional superconductivity. In some cases, it is possible to tune these ground states from antiferromagnetic to superconducting state and this tenability involves, to some extent, the control of the f-conduction electron hybridization and of the Kondo interaction [1]. Here we directly probe the temperature evolution of the 4f states of  $\text{Ce}_2\text{RhIn}_8$  heavy fermion compound by means of Ce 4d-4f resonant angle-resolved photoemission spectroscopy (ARPES) technique. The experiments were performed at the LNLS-PGM beamline in an ARPES chamber using photon energy of 121 eV with a resolution of about 100 meV and a PHOIBOS-SPECS spectrometer. The samples were cleaved *in situ* perpendicular to the [001] direction, and measurements along cuts parallel to the [100] direction in a pressure better than  $1 \times 10^{-11}$  Torr. The results show that a flat f-derived band is observed with distinct temperature dependence and a k-dependent spectral weight. At some distinct points we could also observe structures resulting from the interaction between heavy and light bands related to the Kondo-lattice formation.

[1] G. R. Stewart, Rev. Mod. Phys. 56, 755 (1984); H. V. Lohneysen et al., Rev. Mod. Phys. 79, 1015 (2007); A. C. Hewson, *The Kondo Problem to Heavy Fermions*, (Cambridge University Press, Cambridge, 1993).

*Acknowledgements:* This work was supported by FAPESP (grant #2015/18544-2 and #2012/04870-7) and CNPq (grant # 462368/2014-9).

## CoAl-terephthalate hydrotalcite materials with high aluminum contents

L. Palacio<sup>1</sup>, T. Coelho<sup>2</sup>, S. Arias<sup>2</sup>, Y. Licea<sup>2</sup> and A. Faro<sup>2</sup>

<sup>1</sup>Instituto de Química, Universidade do Estado do Rio de Janeiro, Rua São Francisco Xavier, 524, 20550-013 Rio de Janeiro, Brazil; <sup>2</sup>Instituto de Química, Universidade Federal do Rio de Janeiro, Ilha do Fundão, CT bloco A, 21941-909 Rio de Janeiro, Brazil

lpalacio@uerj.br

Terephthalate LDHs (layered double hydroxides) are useful as catalyst precursors, as the terephthalate anion (TA) provides a larger expansion of the inter-layer galleries, being effective for the incorporation of oxometalates by ion-exchange [1]. The corresponding mixed oxides may be obtained by calcining the exchanged LDHs, and they can be used as precursors for several catalysts, such as the ones used in the hydrotreating of petroleum fractions [2]. In this work, LDH with high aluminum content (aluminum atom fractions 0.3 and 0.5, samples called Co70Al30 and Co50Al50) and terephthalate were successfully synthesized in the system Co-Al, using a co-precipitation method with controlled pH. Different characterization techniques (XRD, FTIR, ICP, AAS, TGA and CHN) showed that the terephthalate ions are vertically placed within the interlayer galleries and the cations were effectively included in the layers. The unusually large limiting value for the intralayer aluminum proportion is possibly associated with the larger length and polarizability of the terephthalate anion as compared to the usual small inorganic anions (carbonate, nitrate or hydroxyl).

As there are several assumptions involved in determining the aluminum atom fractions values from chemical analysis data (CHN, ICP and TGA), it is important to confirm them using an independent technique, and we chose EXAFS for this purpose, as it provides information on the near-neighborhood of an X-ray absorbing element, Co in the present case. The X-ray absorption spectra at the Co K-edge were obtained at the XAFS1 line at the LNLS, Campinas, Brazil. The Athena program [3] was used to extract the EXAFS oscillations in  $k$  space, in terms of  $\chi(k)k^3$ . Simulations of the EXAFS spectra were performed in  $R$ -space using the Artemis program [3].

The larger second shell intensity (see Fig. 1) relative to the first one in the Co70Al30 spectrum is due to the smaller amount of Al atoms present, since the Co-Co and Co-Al scattering waves interfere destructively. This is the main difference between the Co K-edge spectra for both materials. Simulated EXAFS spectra were obtained by multiplying the Co-Co path by  $(1-x)$  and the Co-Al path by  $x$  in the second and higher order mixed Al and Co shells. The  $x$  values (corresponding to aluminum atom fractions) are in good agreement with those derived from chemical analysis.

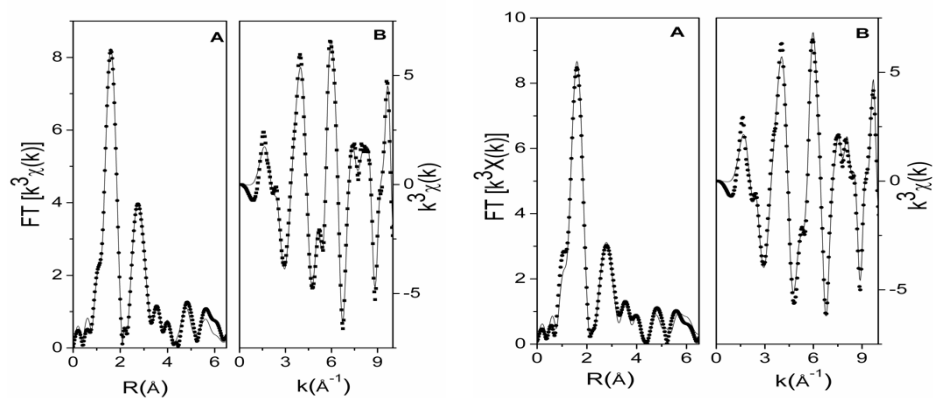


Figure 1. Co K-edge spectrum and fitting function (continuous line) for the samples (Left) Co70Al30 and (Right) Co50Al50. (A) R space and (B) Fourier transformed  $k^3\chi(k)$ .

Our results show that it is possible to prepare CoAl-terephthalate LDH with Al fractions within the layers up to 0.5, considerably higher than the generally accepted upper limit of 0.3.

[1] M. Drezdson, Inorg. Chem. 244, 4628 (1988)

[2] S. Arias, Y.E. Licea, L.A. Palacio, A.C. Faro Jr. Catal. Today 213, 198 (2013)

[3] B. Ravel, M. Newville, J. Synchrotron Radiat. 12, 537 (2005)

*Acknowledgements:* The authors would like to thank to Laboratório Nacional de Luz Síncrotron -LNLS (Campinas, Brazil) for project D04B-XAFS1 10916 approval and financial support during XAFS measurements.

## Cooling induces phase separation in isolated Central Nervous System myelin membranes

Julio Pusterla<sup>1</sup>, Emanuel Schneck<sup>2</sup>, Sérgio Funari<sup>3</sup>, Bruno Demé<sup>4</sup>, Motomu Tanaka<sup>5</sup> and Rafael Oliveira<sup>1</sup>

<sup>1</sup> *Centro de Investigaciones en Química Biológica de Córdoba (CIQUIBIC)-Departamento de Química Biológica, Facultad de Ciencias Químicas, Universidad Nacional de Córdoba, Haya de la Torre y Medina Allende, Ciudad Universitaria, X5000HUA, Córdoba, Argentina.*

<sup>2</sup> *Biomaterials Department, Max Planck Institute of Colloids and Interfaces, D-14476 Potsdam, Germany.*

<sup>3</sup> *HASYLAB at DESY, Notkestrasse 85, D22603 Hamburg, Germany.*

<sup>4</sup> *Institut Laue-Langevin 6 Rue Jule Horowitz, F38042 Grenoble Cedex 9, France*

<sup>5</sup> *Biophysical Chemistry II, Institute of Physical Chemistry and BIOQUANT, University of Heidelberg, D69120, Heidelberg, Germany.*

*jpusterla@fcq.unc.edu.ar*

Purified myelin membranes (PMMs) are the starting material for biochemical analyses such as the isolation of detergent-insoluble glycosphingolipid-rich domains (DIGs), which are believed to be representatives of functional lipid rafts. The normal DIGs isolation protocol involves the extraction of lipids under moderate cooling. Here, we thus address the influence of cooling on the structure of PMMs and its sub-fractions. Thermodynamic and structural aspects of periodic, multilamellar PMMs are examined between 4 °C and 45 °C and in various biologically relevant aqueous solutions. The phase behavior is investigated by small-angle X-ray scattering (SAXS) and differential scanning calorimetry (DSC). Complementary neutron diffraction (ND) experiments with solid-supported myelin multilayers confirm that the phase behavior is unaffected by planar confinement. SAXS and ND consistently show that multilamellar PMMs in pure water become heterogeneous when cooled by more than 10 – 15 °C below physiological temperature, as during the DIGs isolation procedure. The heterogeneous state of PMMs is stabilized in physiological solution, where phase coexistence persists up to near the physiological temperature. This result supports the general view that membranes under physiological conditions are close to critical points for phase separation. In presence of elevated Ca<sup>2+</sup> concentrations (> 10 mM), phase coexistence is found even far above physiological temperatures. The relative fractions of the two phases, and thus presumably also their compositions, are found to vary with temperature. Depending on the conditions, an “expanded” phase with larger lamellar period or a “compacted” phase with smaller lamellar period coexists with the native phase. Both expanded and compacted periods are also observed in DIGs under the respective conditions. The observed subtle temperature-dependence of the phase behavior of PMMs suggests that the composition of DIGs is sensitive to the details of the isolation protocol.

# The structure of Co species in novel active and selective Co/MCM41 catalyst in the COProx reaction prepared by supercritical CO<sub>2</sub> reactive deposition

José M. Ramallo-López<sup>1</sup>, Martín Mizrahi<sup>1</sup>, Soledad Aspromonte<sup>2</sup>, Esther Alonso<sup>3</sup> and Alicia Boix<sup>2</sup>

<sup>1</sup> Instituto de Investigaciones Fisicoquímicas Teóricas y Aplicadas – INIFTA (CCT La Plata – CONICET, UNLP) – Diagonal 113 y calle 64, 1900, La Plata, Argentina.

<sup>2</sup> Instituto de Investigaciones en Catálisis y Petroquímica – INCAPE (FIQ, UNL-CONICET) - Santiago del Estero 2829, 3000, Santa Fe, Argentina.

<sup>3</sup> High Pressure Processes Group – Chemical Engineering and Environmental Technology Department, University of Valladolid, C/ Dr. Mergelina s/n, 47011, Valladolid, Spain

ramallolopez@gmail.com

Co/MCM41 catalyst with 4.3 wt. % Co (Co/sc) has been prepared by supercritical CO<sub>2</sub> reactive deposition (SCFRD) and characterized by different physicochemical techniques. This synthesized method was compared with others conventional methodologies such as template-ion exchanged (Co/TIE) and incipient wet impregnation (Co/IWI) with similar cobalt content. All the samples were studied as catalysts on the CO total oxidation (COTox) and preferential oxidation of CO on H<sub>2</sub>-rich streams (COProx). The Co/sc catalyst was the most active and selective for the COProx reaction. This enhanced performance of the Co/sc catalyst has been explained in terms of the characteristics of the Co active sites. Temperature-Programmed Reduction (TPR), X-ray Photoelectronic (XPS) and X-ray Absorption spectroscopic (XANES/EXAFS) studies suggested that TIE and IWI methods can provide tetrahedrally coordinated Co(II) ions mainly dispersed on the internal surface of MCM41. The SCFRD method generated the Co<sub>3</sub>O<sub>4</sub> spinel nanoparticles and Co(II) species into the framework of MCM41. Even though IWI and TIE methods are simpler for cobalt incorporation, they caused a significant loss of surface area, thus blocking the pores. In particular, a core-shell structure was formed with TIE method, with outer cobalt layers. Thus, the combination of Co<sub>3</sub>O<sub>4</sub> nanoparticles and Co(II) sites interacting with the siliceous structure, highly dispersed on the surface and inside the mesoporous support obtained by the SCFRD method resulted in a more active and selective catalyst for the COProx reaction.

*Acknowledgements:* This work was supported by LNLS, Brazil (Project XAFS-18859), UNL (CAI+D 2011), ANPCyT (PICT 2013-0354, PICT 2015-2285), UNLP and CONICET (PIP 112-200801-03079/112-201301-00062).

## Mesoporous silica: in situ SAXS investigation of synthesis processes

Helena Ø. Rasmussen<sup>1,2</sup>, Francisco M. Neto<sup>1</sup>, Marcia C. A. Fantini<sup>1</sup> & Cristiano L. P. Oliveira<sup>1</sup>

*<sup>1</sup>Instituto de Física, Universidade de São Paulo, Caixa Postal 66318, 05314-970, São Paulo, SP, Brazil*  
*<sup>2</sup>Department of Chemistry and iNANO Interdisciplinary Nanoscience Center, University of Aarhus, DK-8000 Aarhus, Denmark*  
*crislp@if.usp.br*

In this study synthesis routes for SBA-15 will be investigated, primarily using in situ small-angle X-ray scattering (SAXS). Furthermore, the effects of the swelling agents TMB (1,3,5-Trimethylbenzene) and TIPB (1,3,5-Triisopropylbenzene) are investigated when the swelling agent is added in several stages during the synthesis, together with the Pluronic P123 and tetraethyl orthosilicate (TEOS), which is the silica source for the formation of the ordered structure. The results from in situ measurements are further complemented by studies of nitrogen absorption, powder diffraction, transmission electron microscopy (TEM) and scanning electron microscopy (SEM). As will be shown, a detailed structural investigation is obtained for the several synthesis conditions, indicating the correlation between the synthesis parameters and structural parameters obtained from the characterization techniques and advanced modeling of the SAXS data [1]. The information obtained from this study is very important since it enable a fine-tuning of the pore sizes and structural ordering for the hexagonal phase of this mesoporous material, with many potential applications [2,3].

[1] Sundblom, A., et al., Modeling in Situ Small-Angle X-ray Scattering Measurements Following the Formation of Mesostructured Silica. *Journal of Physical Chemistry C*, 2009. 113(18): p. 7706-7713. [2] Mariano-Neto, F., et al., Physical properties of ordered mesoporous SBA-15 silica as immunological adjuvant. *Journal of Physics D-Applied Physics*, 2014. 47(42). [3] Scaramuzzi, K., et al., Nanostructured SBA-15 silica: An effective protective vehicle to oral hepatitis B vaccine immunization. *Nanomedicine-Nanotechnology Biology and Medicine*, 2016. 12(8): p. 2241-2250.

Acknowledgements: This work was supported by CAPES, FAPESP and CNPq.

# Specific procedures for experiments of multiple diffraction at XRD2 beamline (LNLS) applied to micro organic crystals

Cláudio M. R. Remédios<sup>1</sup> and Sérgio L. Morelhão<sup>2</sup>

<sup>1</sup> Federal University of Pará , Institute of Exact Sciences, Belém, PA, Brazil; <sup>2</sup>University of São Paulo, Institute of Physics, São Paulo, SP, Brazil.

rocha@fisica.ufc.br

The versatility of XRD2 beamline has been explored in XRDMD measurements with very small crystals sample. High-resolution X-ray Renninger Scan were obtained to bis (L-histidinato) nikel (II) monohydrated micro organic crystals. X-ray multiple diffraction (XRMD) occurs when two or more set of crystallographic planes satisfy Bragg's law at the same time for a certain incident X-ray beam [1]. A straightforward approach to obtain this phenomenon is to adjust a primary reflection to the exact Bragg condition and Spin the crystal around diffraction vector ( $\phi$ -rotation). For certain angles, different secondary reflections also diffract the incident X-ray beam. As result, one obtains the X-ray Renninger Scan that consists of a plot of the intensity versus phi angles [1]. Several peaks originated from interference between the waves diffracted are observed. This obtained pattern is known to contain structural information such as lattice parameters, symmetry and crystal quality [2-3]. Usually, samples with a size of the order of centimeters are used on XRMD. However, some organic crystals hardly grow in these sizes, especially, very important organic crystals of amino acids, drugs and proteins. So, it was necessary to develop specific procedures for experiments of multiple diffraction with microcrystals. In this work, we have used XRDMD to provide structure information about microcrystals of bis (L-histidinato) nikel (II) monohydrated. It was clear demonstration, XRDMD measurements can be realized with microcrystals also in XRD2 beamline.

[1] Chang, S. L. (1984). Multiple Diffraction of X-rays in Crystals. Berlin, Heidelberg, New York: Springer Verlag.

[2] Z.A. Amirkhanyan, C.M.R. Remédios, Y.P. Mascarenhas, S.L. Morelhão. Analyzing structure factor phases in pure and doped single crystals by synchrotron x-ray renninger scanning. J. Appl. Cryst. 47, 160 (2014).

[3] S.L. Morelha, Z.G. Amirkhanyana and C.M.R. Remédios. Absolute refinement of crystal structures by X-ray phase measurements. Acta Cryst. A 71. (2015).

*Acknowledgements:* The authors would like to thank Brazilian funding agencies CAPES, CNPQ and LNLS (proposals 20160261 and 20150290, XRD2).

## Stability and reactivity of copper clusters with five atoms

Félix G. Requejo<sup>1</sup>, Lisandro J. Giovanetti<sup>1</sup>, José M. Ramallo-López<sup>1</sup>, Cristián H. Iriart<sup>1</sup>, Carlos Escudero-Rodríguez<sup>2</sup>, David Buceta<sup>3</sup> and M. Arturo López-Quintela<sup>3</sup>

*1 Instituto de Investigaciones Físico Químicas Teóricas y Aplicadas (INIFTA), CONICET – FCE-UNLP, CP 1900 La Plata, Argentina; 2 BL24- CIRCE, Experiments Division, ALBA SYNCHROTRON LIGHT SOURCE, Barcelona, Spain; 3 Physical Chemistry Department, Faculty of Chemistry, and NANOMAG Laboratory, Research Technological Institute, University of Santiago de Compostela, E-15782 Santiago de Compostela, Spain  
requejo@fisica.unlp.edu.ar*

We report the XAFS (X-ray absorption fine structure) and NAP-XPS (Near Ambient Pressure XPS) characterization and catalytic properties of subnanometric Cu atomic clusters (atomic quantum clusters: AQC) in water without any surfactant or protective agent. The original synthesis is based on the kinetic control of the reaction, which is achieved with an electrochemical method and using a solution with almost no conductivity (i.e., without added electrolytes commonly used in electrochemical methods). AQC with five copper atoms (Cu<sub>5</sub>) were initially characterized by ultraviolet–visible (UV–vis) and fluorescence spectroscopies, atomic force microscopy and electrospray ionization time-of-flight mass spectrometry. For further studies focused on structure and stability of Cu AQC, we performed Cu K-edge XANES and EXAFS and NAP-XPS experiments under controlled oxygen pressure and temperature. Contrary to what should be expected, such clusters are very stable and remain unaltered in water solution and supported on different substrates like graphite or gold in presence of oxygen at higher temperatures than 200 °C. The reason for such stability resides on their huge band gap (4.07 eV). Moreover, such Cu<sub>5</sub> clusters are extremely stable to UV irradiation, temperature, and wide variations of pH values. In present contribution we show the particular features of Cu-K XANES spectra, away from the usual concept referred to the position of the edge according to the oxidation state of the absorbing element. Additionally, through NAP-XPS, an “anomalous” behavior can be observed for the oxidation and reversible reduction of the Cu state in oxygen atmosphere. These particular characteristics can be only explained because the unique electronic structure of Cu<sub>5</sub> AQC. The same electronics of Cu<sub>5</sub> may have significant catalytic implications, such as high oxidative capacity, as it is also shown by a control experiment of cysteine oxidation by S-K XANES experiments.

[1] Shahana Huseyinova, José Blanco, Félix G. Requejo, José M. Ramallo-López, M. Carmen Blanco, David Buceta, and M. Arturo López-Quintela. Synthesis of Highly Stable Surfactant-free Cu<sub>5</sub> Clusters in Water. *J. Phys. Chem. C*, 120 (29), 15902 (2016)

Acknowledgements: this work was partially supported by ANPCyT (PICT 2015-2285)

# Effects of B4C Addition on Microstructure and Mechanical Properties of a Beta Titanium Alloy

V. V. Rielli<sup>1#</sup>, R. J. Contieri<sup>1</sup>

<sup>1</sup>*School of Applied Sciences/FCA, University of Campinas, UNICAMP, Campus Limeira, 1300, Pedro Zaccaria St., 13484-350 Limeira, SP, Brazil*

<sup>#</sup>*Corresponding author: vitorrielli@gmail.com*

The increasing demand for materials with a high ratio between mechanical resistance and weight has led to greater use of metastable beta titanium alloys [1]. Low mechanical resistance and low modulus of elasticity are some characteristics of the  $\beta$  phase of titanium alloys [2]. However, this mechanical behavior may be drastically modified when new processing routes are used and also through the addition of ceramic particles. In this work, the effects on the phase transformation and consequently on the mechanical properties of the  $\beta$  metastable titanium alloy: TIMETAL 21S (Ti-15Mo-3Nb-3Al-0.2Si) with different concentrations of B4C additions is investigated. The following steps were carried out in the present study: (a) preparation of the alloy by arc melting; microstructural homogenization in high temperatures followed by the analysis of resulting metastable structures owing to different cooling methods; (b) evaluation of the effects of different amounts of B4C; (c) investigation of the effects of heat treatments on microstructure and mechanical properties.

[1] HUANG, J.; WANG Z.; ZHOU, J., Cyclic Deformation Response of  $\beta$ -Annealed Ti-5Al-5Mo-5V-3Cr Alloy under Compressive Loading Conditions, Metallurgical and Materials Transactions A 42 (2011) 2868.

[2] DUERIG T.W.; WILLIAMS J.C., "Overview: Microstructure and Properties of Beta Titanium Alloys", Beta Titanium alloys in the 80's: Proceedings of the Symposium, Atlanta, GA, EUA, 1984. p.19-67.

# Compact XRF spectrometer for CARNAUBA beamline at SIRIUS

J. I. Robledo<sup>1,2</sup>, C. A. Pérez<sup>3</sup>, R. Ribeiro<sup>3</sup>, M. Honnicke<sup>4</sup> and H. J. Sánchez<sup>1,2</sup>

<sup>1</sup> Universidad Nacional de Córdoba, Facultad de Matemática, Astronomía y Física, Córdoba, Argentina; <sup>2</sup> Consejo Nacional de Ciencia y Técnica, Instituto de Física Enrique Gaviola, Córdoba, Argentina; <sup>3</sup> Centro Nacional de Pesquisas em Materiais, Laboratorio Nacional de Luz Síncrotron, Campinas, Brazil; <sup>4</sup> Universidad Federal de Integración Latinoamericana (UNILA), Foz de Iguazú, Brazil.

jorobledo@unc.edu.ar

We have been working on the design of a compact, high resolution, x-ray spectrometer for CARNAUBA beamline at SIRIUS. The spectrometer is thoroughly designed as Wavelength Dispersive System (WDS) consisting of an integrated conical crystal analyzer and a position sensitive detector. The proposed focusing scheme [1] allows reducing detector area and optical aberrations thus making a very compact design (~16 cm sample–detector distance), similar to that shown by Morishita *et al.* [2]. A program written in MATLAB was developed to calculate the main parameters of the x-ray spectrometer such as crystal dimensions, energy resolution, energy bandwidth and peak location at the position sensitive detector. Simulations were also performed using the McXtrace code [3] to confirm previous results from calculations. From the above, we are proposing a x-ray spectrometer consisting of a bent Si(220) wafer of 4.1 cm × 9.6 cm covering an energy range of from 5.3 to 7.1 keV having a resolution of approximately 10 eV in this energy range. For the detection system, three sequential MEDIPIX detectors [4] has been proposed covering an effective area of 14 × 42 mm<sup>2</sup>. We have also been working on the construction of this first prototype to test it at the XRF-D09B beamline at the LNLS, Campinas, Brazil.

[1] T. A. Hall, *J. Phys. E* **17**, 110 (1984).

[2] K. Morishita, K. Hayashi, and K. Nakajima *Rev. Sci. Inst.* **83**, 1, 013112 (2012).

[3] E. B. Knudsen, A. Prodi, J. Baltser, M. Thomsen, P. K. Willendrup, M. Sanchez del Rio, C. Ferrero, E. Farhi, K. Haldrup, A. Vickery, et al. *J. Appl. Cryst.*, **46**, 3, 679-696, (2013).

[4] E.N. Gimenez *et al*, *IEEE Trans. Nucl. Sci.* **99**, 3 (2010).

*Acknowledgements:* This work is partially supported by CONICET and the LNLS.

# Molecular Orientation and Ultrafast Charge Transfer Dynamics Studies on the P3HT:PCBM Blend

M. L. M. Rocco<sup>1</sup>, B. G. A. L. Borges<sup>1</sup>, A. G. Veiga<sup>1</sup>, L. Tzounis<sup>2</sup>, A. Laskarakis<sup>2</sup> and S. Logothetidis<sup>2</sup>

<sup>1</sup>*Institute of Chemistry, Federal University of Rio de Janeiro, 21941-909, Rio de Janeiro, RJ, Brazil;* <sup>2</sup>*Lab for Thin Films, Nanobiomaterials, Nanosystems & Nanometrology (LTFN), Physics Department, Aristotle University of Thessaloniki, 54124, Thessaloniki, Greece*

luiza@iq.ufrj.br

Ultrathin films of poly(3-hexylthiophene) (P3HT) blended with 6,6.-phenyl-C61-butyric acid methyl ester (PCBM) were investigated by X-ray Absorption Spectroscopy (XAS) and resonant Auger spectroscopy (RAS) in the context of the core-hole approach at the sulfur K absorption edge [1]. P3HT:PCBM blend is a well-known system widely used as a bulk heterojunction (BHJ) photoactive layer in organic photovoltaics (OPV). Its morphology, phase separation and ordering of the constituent phases have been proven to significantly affect the performance of the resulting OPV devices. Herein, thermally annealed P3HT:PCBM films at optimum conditions, in terms of power conversion efficiency (PCE) of the resulting fully-printed OPV modules (2.22% for 8 cm<sup>2</sup> active area modules), have been proven to be well-ordered films as revealed by the XAS spectra measured at different angles of the incoming photons. Moreover, electron delocalization times were calculated as a function of the excitation energy, resulting in a very low delocalization time in the femtosecond regime.

[1] C.F.N. Marchiori et al, *Spectrochimica Acta. Part A*, 171, 376 (2016).

*Acknowledgements:* Research partially supported by LNLS – National Synchrotron Light Laboratory, Brazil and the NMP.2012.1.4-1 Project SMARTONICS (under Grant Agreement number 310229) part of the European Union Seventh Framework Program. M.L.M.R. would like to thank CNPq for financial support.

## Lectins from *Parkia biglobosa* and *Parkia platycephala*: A comparative study of structure and biological effects

Bruno A M Rocha<sup>1</sup>, Alpha U Bari<sup>1</sup>, Mayara Q Santiago<sup>1</sup>, Vinícius J S Osterne<sup>1</sup>, Vanir R Pinto-Júnior, Livia P Pereira<sup>2</sup>, José Caetano Silva-Filho<sup>3</sup>, Henri Debray<sup>4</sup>, Plinio Delatorre<sup>3</sup>, Claudener S Teixeira<sup>3</sup>, Corneville C Neto<sup>1</sup>, Ana Maria S Assreuy<sup>3</sup>, Kyria S Nascimento<sup>1</sup> and Benildo S Cavada<sup>1</sup>

<sup>1</sup> Departamento de Bioquímica e Biologia Molecular, Universidade Federal do Ceará, 60440-970, Fortaleza, Ceará, Brazil; <sup>2</sup> Universidade Estadual do Ceará, 60714-242, Fortaleza, Ceará, Brazil; <sup>3</sup> Departamento de Biologia Molecular, Universidade Federal da Paraíba, Paraíba, Brazil; <sup>4</sup> University of Science and Technology of Lille, Lille, France; <sup>5</sup> Universidade Federal do Maranhão, Maranhão, Brazil

bruno.rocha@ufc.br

Lectins are defined as a structurally heterogeneous group of proteins or glycoproteins that possess at least one non-catalytic domain that binds reversibly to a specific mono- or oligosaccharide [1]. Legume Lectins are the most studied group of plant lectins [1]. Among the studies of lectins from *Leguminosae*, many are focused on members of the tribe *Phaseoleae*, subfamily *Papilionoideae*, while investigations of lectins of the other two subfamilies, *Caesalpinioideae* and *Mimosoideae*, are scarce [2]. In the *Mimosoideae* subfamily, the glucose/mannose-specific lectin isolated from *Parkia platycephala* seeds (PPL-1) is the best characterized with regard to its structural features. PPL-1 contains a single, nonglycosylated polypeptide chain composed of three tandemly arranged jacalin-related domains [3]. The resolution PPL-1 crystal structure showed a novel circular arrangement of  $\beta$ -prism domains [3]. Our group recently reported the purification, characterization and primary structure of a lectin from *Parkia biglobosa* seeds, named PBL [2]. PBL is a mannose-binding jacalin-related lectin and exhibits important anti-inflammatory activity, associated to leukocyte mobilization, and antinociceptive activity, associated to inflammatory pain. The relation structure-activity of the *Mimosoideae* lectins of *Parkia platycephala* (PPL) and *Parkia biglobosa* (PBL) was analyzed in this study. PBL was solved by X-ray crystallography at a resolution of 2.1 Å, and the crystal structure belonged to the C2221 space group. Structural organization and binding sites were also characterized. Specifically, PBL monomer consists of three  $\beta$ -prism domains tandemly arranged with each one presenting a different carbohydrate recognition domain (CRD). PPL showed antinociceptive activity in the mouse model of acetic acid-induced writhes with maximal inhibitory effect by 74% at 1 mg/mL. PPL also demonstrated anti-inflammatory effect causing inhibition of leukocyte migration induced by both direct and indirect chemoattractants. These PPL activities were compared to that of PBL described previously. Molecular docking of both PBL and PPL demonstrated some differences in carbohydrate-lectin interaction energy. Comparing structure and biological effects of the two lectins provided new data about their structure and the relation with its biological activities.

[1] E.J.M. Van Damme, W.J. Peumans, A. Barre, P. Rougé, Crit. Rev. Plant Sci. 17 (1998) 575–692.

[2] H.C. Silva, A.U. Bari, B.A.M. Rocha, K.S. Nascimento, E.L. Ponte, A.F. Pires, P. Delatore, A.H. Teixeira, H. Debray, A.M.S. Assreuy, C.S. Nagano, B.S. Cavada, J. Mol. Recognit. 26 (2013) 470–478.

[3] F.G. Del Sol, C.S. Nagano, B.S. Cavada, J.J. Calvete, J. Mol. Biol. 353 (2005) 574–583.

*Acknowledgements:* This work was supported by CNPq and CAPES.

## Mapping of elemental distribution of Cu, Fe and Zn in human prostatic carcinoma cell spheroid culture using synchrotron radiation based on Microbeam X-ray Fluorescence

K.M.J. Rocha<sup>1</sup>, R.G. Leitão<sup>2</sup>, E.G.Oliveira-Barros<sup>3</sup>, M.A. Oliveira<sup>3</sup>, C.G.L. Canellas<sup>2</sup>, M.J. Anjos<sup>1,2</sup>, L.E. Nasciutti<sup>3</sup>, R.T. Lopes<sup>1</sup>

<sup>1</sup> Nuclear Instrumentation Laboratory, Federal University of Rio de Janeiro, RJ, Brazil.

<sup>2</sup> Physics Institute, Stated University of Rio de Janeiro, RJ, Brazil.

<sup>3</sup> Institute of Biomedical Sciences, Federal University of Rio de Janeiro, RJ, Brazil.

*kjose@nuclear.ufrj.br*

Prostate cancer continues to be one of the most common fatal cancers in men. The main function of the prostate is the high production and secretion of citrate which is possible due to the unique accumulation of zinc by prostatic epithelial cells. Iron plays a vital function in oxygen metabolism, oxygen uptake, and electron transport in mitochondria, energy metabolism, muscle function, and hematopoiesis. Copper plays an important role in the aetiology and growth of tumours however, whether intratumoral copper is actually elevated in prostate cancer patients has not been established. Zinc is an essential trace element, critical for diverse biological functions in the human body. The X-ray microfluorescence technique ( $\mu$ XRF) is a rapid and non-destructive method of elemental analysis that provides useful elemental information about samples without causing damage or requiring extra sample preparations. This study investigated the behavior of cells in spheroids of human prostate cells, tumour cell line (DU145) and normal cell line (RWPE- 1), after supplementation with zinc chloride by 24 hours using synchrotron X-ray microfluorescence ( $\mu$ SRXRF). Besides that, it too was analysed cell viability through colorimetric cytotoxicity assay (MTT) and evaluated the organization of cytoskeleton cell, in order to better characterize morphologically the established cellular spheroids, by fluorescence microscopy. The measurements were performed with a standard geometry of 45° of incidence, excited by a white beam using a pixel of 25  $\mu$ m and a time of 300 ms/pixel at the XRF beamline at the Synchrotron Light National Laboratory (XRF - 18905 proposal). It was observed that the iron intensity in the normal cells spheroids did not present a standard with respect to the treatment of zinc chloride, whereas in the tumor cell increased from the treatment of 100  $\mu$ M, whereas in the treatment of 50  $\mu$ M the intensity remained constant. There was a decline in the intensity of copper in the tumor cells in the treatment of 50, in the treatments of 100, 150, 200 and 250  $\mu$ M there was an increase when compared to the control. It was observed that the highest intensities were observed in the treatments of 150 and 200  $\mu$ M. In the normal cells, the intensity of copper did not present a standard with respect to the treatment of zinc chloride, however the intensity remained lower in all the treatment when compared to the control. In the case of zinc, it has been observed that despite the treatment the tumor cell suffers a decrease in the ability to accumulate zinc when compared to normal cells. MTT assay's results showed no significant difference, which indicates that the cell viability was not changed, regardless of treatment in both cell types tested, so the cells are viable. Finally, immunofluorescence assay allowed to evaluate the organization of the cytoskeleton and cellular phenotype, through the identification of cytokeratin and vimentin filaments.

---

Acknowledgements: This work was supported by the National Council for Scientific and Technological Development (CNPq), the Rio de Janeiro State Research Foundation (FAPERJ), Coordenação de Aperfeiçoamento de Pessoal de Nível Superior (CAPES) and the National Synchrotron Light Laboratory (LNLS) (Project XRF – 18905).

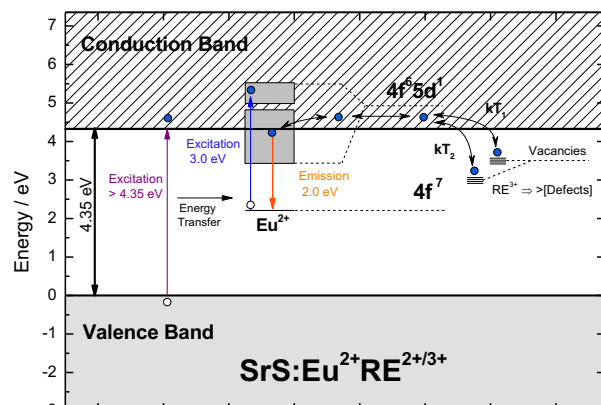
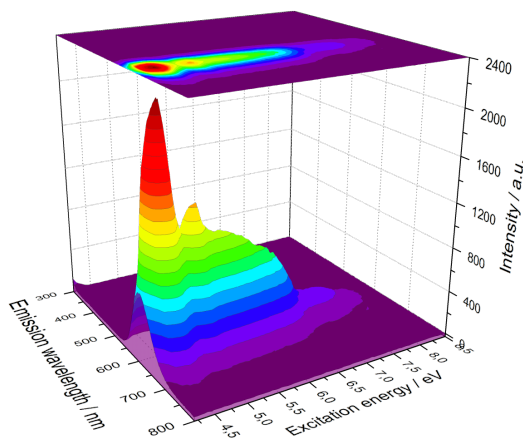
# Advances in the Red/NIR-persistent luminescence materials design with VUV luminescence spectroscopy

Lucas C.V. Rodrigues<sup>1</sup>, Danilo O.A. Santos<sup>1</sup>, Miguel A.S.G. Barbará<sup>1</sup>, Douglas L. Fritzen<sup>1</sup>, Otávio P. Bezzan<sup>1</sup>, and Verônica C. Teixeira<sup>2</sup>

<sup>1</sup> University of São Paulo, Institute of Chemistry, 05508-000, São Paulo-SP, Brazil; <sup>2</sup> Brazilian Center for Research in Energy and Materials (CNPEM), Brazilian Synchrotron Light Laboratory, 13083-100, Campinas-SP, Brazil.

lucasavr@iq.usp.br

Most of Persistent Luminescent (PeL) materials have their emission at blue-green region (400 – 550 nm) [1-3]. Red and Near Infrared (NIR) emitters are rare and often very expensive or inefficient [2]. These Red/NIR emitting materials have great potential for applications on energy storage and bioimaging. For an efficient application of these emitters, their luminescence should persist for hours after ceasing the charging with visible light irradiation [3-5]. The design of PeL materials is normally done in a trial-error basis leading to high financial, time and environment costs. In this work we present a detailed analysis of the VUV luminescence spectroscopy of four different Red/NIR PeL materials:  $\text{CaTiO}_3:\text{Pr}^{3+}$ ,  $\text{Cd}_2\text{SiO}_4:\text{Pr}^{3+}$ ,  $\text{SrS}:\text{Eu}^{2+}, \text{RE}^{2+,3+}$  and  $\text{LaAlO}_3:\text{Cr}^{3+}, \text{Sm}^{3+}$ . This analysis allowed the determination of important parameters as the band gap energy (Figure left) and energy levels position, leading to the development of the mechanisms (Figure right). The persistent luminescence decays showed that three main mechanisms dominate the PeL materials: i) some materials must be irradiated below the band gap indicating that the trapping only happens under ion excitation ( $\text{Eu}^{2+}$  and  $\text{CaTiO}_3:\text{Pr}^{3+}$  case); ii) Only close to band gap irradiation generates PeL ( $\text{Cd}_2\text{SiO}_4:\text{Pr}^{3+}$ ), i.e., ion excitation does not store energy and iii) Only high energy irradiation processes are effective ( $\text{LaAlO}_3:\text{Cr}^{3+}, \text{Sm}^{3+}$ ). These new data on different mechanisms allow the design of excitation-tuned PeL materials that are efficient for bioimaging, solar cell conversion and even LED illumination.



---

Figure: SrS:Eu<sup>2+</sup> 3D VUV-excitation spectrum (left) and its persistent luminescence mechanism.

- [1] H.F. Brito, J. Hölsä, T. Laamanen, M. Lastusaari, M. Malkamäki, L.C.V. Rodrigues, *Opt. Mater. Express* 2, 371 (2012).
- [2] J. Hölsä, *Electrochem. Soc. Interface* 18, 42 (2009).
- [3] C.M. Abreu, R.S. Silva, M.E.G. Valerio, Z.S. Macedo, *J. Solid State Chem.* 200, 54 (2013).
- [4] Z. Pan, Y. Lu, F. Liu, *Nature Mater.* 11, 58 (2012).
- [5] Y. Katayama, H. Kobayashi, S. Tanabe, *Appl. Phys. Express* 8, 012102 (2015).

*Acknowledgements:* This work was supported by CNPq, CAPES and FAPESP.

# Impact of oxidized lipid in the structural parameters of biological model membranes as seen by Small Angle X-Ray Scattering (SAXS)

Raffaela de Rosa<sup>1</sup>

<sup>1</sup> *University of São Paulo, Institute of Chemistry, 05508-000, São Paulo-SP, Brazil*

In this work, we investigated the alterations caused in membrane mimetic systems due to the presence of oxidized lipids in their composition. The study was performed using two different oxidized lipids: 1) hydroperoxide lipid of POPC (POPC-OOH) whose structure shows a hydroperoxide group in the 9-10 carbon region of one of the acyl chains, giving a more hydrophilic character in this region, 2) The lipid PAzPC (1-palmitoyl-2-azelaoyl-sn-glycero-3-phosphocholine) containing a carboxyl group at the end of one of the C9-truncated chains. Large unilamellar vesicles composed of POPC-OOH, POPC: PAzPC and POPC: POPC-OOH: PAzPC with different molar ratios were investigated by SAXS at the National Laboratory of Synchrotron Light (LNLS). The scattering curves for vesicles composed of oxidized lipids showed significant changes in the electron density profile. Vesicle analysis was performed via the 3-region model of different electron densities for the membrane (polar, CH<sub>2</sub> and CH<sub>3</sub> regions) relative to the density of the aqueous solvent using the GENFIT software [1]. The results showed that there is a decrease in the thickness of the lipid bilayer as we increase the proportion of oxidized lipid in the membrane. For the POPC:POPC-OOH system, it was verified that the thickness of the lipid bilayer decreased from 46.8 Angs. For pure POPC membranes, to 42.4 Angs. When the membrane is composed of 33% POPC-OOH and 37.6 Angs. To 100% POPC-OOH. However, the systems composed of two oxidized lipids (POPC: POPC-OOH: PAzPC) showed a small displacement of the SAXS curve at higher scattering angles with the increase of the percentage of PAzPC in the membrane. The results indicate that the presence of POPC-OOH predominantly determines the observed changes. It is worth noting that the parameters obtained for the POPC / PAzPC membranes containing 25 mol% POPC-OOH are similar to those of POPC: POPC-OOH 67:33. Using a model considering the position of each chemical group in the membrane [1] we could observe that both hydroperoxide and carboxil groups are located at the interface hydrophob/hydrofilic region.

# Study of hydration of sulphoaluminate cement by *in situ* synchrotron diffraction

C.M. Rossetto<sup>1</sup>, L.G. Martinez<sup>2</sup>, R.U. Ichikawa<sup>2</sup>, G.L. Carezzato<sup>2</sup>, A.M.G. Carvalho<sup>3</sup>  
and X. Turrillas<sup>4</sup>

<sup>1</sup>Faculdade de Tecnologia de São Paulo, FATEC-SP, São Paulo, Brazil

<sup>2</sup>Instituto de Pesquisas Energéticas e Nucleares, IPEN-CNEN/SP, 05508-000, São Paulo, Brazil

<sup>3</sup>Laboratório Nacional de Luz Síncrotron, LNLS, Campinas, Brazil

<sup>4</sup>Institut de Ciència de Materials de Barcelona, ICMAB/ CSIC, Barcelona, Spain

lgallego@ipen.br

The hydration of calcium sulphoaluminate cement mixtures was studied *in situ* by synchrotron X-ray diffraction at the XRD1 beamline at the Laboratório Nacional de Luz Síncrotron (LNLS – Campinas). The specimens were analyzed in borosilicate glass capillary tubes of 0.7 mm and imbued with deionized water. As the hydration reaction is very fast, the data collection was started after two minutes of mixing with water. The X-ray wavelength chosen to get an adequate flux for these short time acquisitions was 1.033258 Å (12 keV), determined with a corundum standard. Diffraction patterns were collected every 35 seconds at temperatures ranging from 40 °C to 55 °C with accuracy better than 0.1 °C attained with a hot air blower. The diffracted signal was collected with an array of 24 Mythen detectors [1]. The diffraction patterns accumulated had appropriate statistics to determine the kinetics of the reaction either by quantitative Rietveld analysis or by fitting isolated diffraction peaks to Gaussian curves as a function of time. The most important phases involved in the hydration are Klein's salt, also known as Ye'elimite,  $\text{Ca}_4(\text{AlO}_2)_6\text{SO}_4$ , and gypsum,  $\text{CaSO}_4 \cdot 2\text{H}_2\text{O}$  to yield Ettringite,  $\text{Ca}_6\text{Al}_2(\text{SO}_4)_3(\text{OH})_{12} \cdot 26\text{H}_2\text{O}$ , phase responsible for the mechanical properties. These studies show the potential of XRD1 beamline to investigate at controlled temperatures *in situ* fast reactions involving crystalline phases with time resolutions inferior to one minute, which is ideal for the hydration of cementitious mixtures.

The series of diffraction patterns collected for one and half hour are shown in Figure 1(a) and (b). In Figure 1(c) the evolution of the relative proportions of crystalline phases can be seen. Non-crystalline phases such as CSH gel or  $\text{Al}(\text{OH})_3$  (gibbsite) are not taken in consideration [2].

The figures clearly show that the ettringite formation happens in two stages, the second one starting after approximately forty minutes. It is also interesting to notice that this stages seem to coincide with the depletion of  $\text{Ca}_2\text{SiO}_4$  (C2S) for the first stage and the depletion of  $\text{Ca}_3\text{SiO}_5$  (C3S) for the second one.

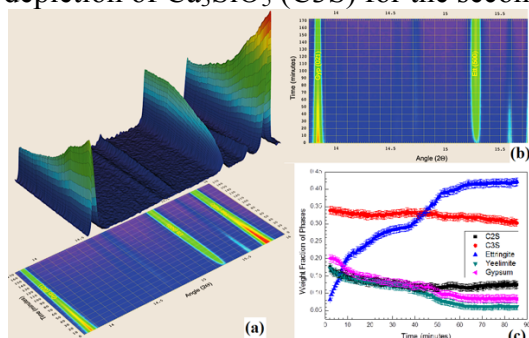


Figure 1: Sequence of diffraction patterns in a pseudo- 3D fashion as a function of time on a narrow angular domain to illustrate the evolution of the main crystalline phases involved in hydration: (a) 3D assembly of patterns; (b) projection as 2D contour map; (c) weight fractions of the crystalline phases plotted as determined by quantitative Rietveld analysis with GSAS. Some other non-crystalline products such as gibbsite and CSH gel are not taken in consideration.

[1] A. M. G. Carvalho et al.; J. Synchrotron Rad. 23 (2016) 1501.

[2] C. M. Rossetto, R. U. Ichikawa, L. G. Martinez, Carezzato, G. L., A. M. G. Carvalho and X. Turrillas. *In situ* hydration of sulfoaluminate cement mixtures monitored by synchrotron x-ray diffraction. Submitted to Mat. Sci. Forum (2017).

## Local structure on BaFe<sub>2</sub>As<sub>2</sub>: formation of nanotwins studied by atomic pair distribution function

M.E. Saleta<sup>1,2</sup>, D. Tobia<sup>1,3</sup>, M.M. Piva<sup>3</sup>, C.B.R. Jesús<sup>3</sup>, P.F. Rosa<sup>3,4</sup>, R.R. Urbano<sup>3</sup>, E. Granado<sup>3</sup> and P.G. Pagliuso<sup>3</sup>

<sup>1</sup> Laboratorio de Resonancias Magnéticas - Centro Atómico Bariloche (CNEA), S.C. de Bariloche-RN, Argentina;

<sup>2</sup> Laboratório Nacional de Luz Síncrotron (LNLS), Campinas-SP, Brazil; <sup>3</sup> Instituto de Física "Gleb Wataghin", Universidade de Campinas (UNICAMP), Campinas-SP, Brazil; <sup>4</sup> University of California, Irvine-CA, United States.

*martin.saleta@cab.cnea.gov.ar*

The recent discovery of high-T<sub>c</sub> superconductivity in iron-arsenide-based materials has accelerated further investigations to understand the nature of the superconducting state and the interplay between superconductivity and magnetism. In particular, non-doped compounds of the oxygen-free AFe<sub>2</sub>As<sub>2</sub> family (A=Ba, Ca, Eu, Sr) commonly exhibit a structural phase transition with an adjacent antiferromagnetic order, and a “so called” nematic order is claimed to play a crucial role on these transitions. Hence, the relation between the magnetic order and structural distortion is one of the vital issues in the investigations of such compounds, with possible close connection with the emergent unconventional superconductivity in the doped members.

Here we focus on the BaFe<sub>2</sub>As<sub>2</sub> (Ba122) compound. Ba122 crystallizes in a tetragonal cell, but for low temperature, the system undergoes a structural phase transition to an orthorhombic structure. The Tetra-to-Orthorhombic distortion has been associated with the stabilization of a *spin density wave* (SDW) phase on the Fe sub-lattice. These transitions, at  $T_S$  and  $T_{SDW}$ , were originally found to coincide in the non-doped Ba122, but further studies demonstrated  $T_S \neq T_{SDW}$  for this system. We have exhaustively studied high quality Ba122 single crystals [1]. Heat capacity measurements clearly exhibit two jumps related to the onset of the structural transition at  $T_S$  and to the Fe SDW ordering at  $T_{SDW}$ , and the magnetic susceptibility drops monotonically for temperatures below  $T_{SDW}$ .

In order to further investigate the local structure of the Ba122 we employed the **atomic pair distribution function** (PDF) technique. PDF is an attractive technique to analyze X-ray total scattering data and is a powerful characterization tool in material science. It is an alternative to conventional XRD and XAS [2]. Contrary to XRD, that only reflects information about the average structure, PDF analysis allows the detection of small local distortions [2], bringing information of the local and medium-range order.

In this work we present a PDF structural study of Ba122. We studied milled crystals, grown by In-metal flux, at XDS beamline (LNLS) [3], at different temperatures below and above the  $T_S / T_{SDW}$ . Strain broadening of the Bragg peaks caused by the milling procedure in our samples prevented us to unambiguously determine the structural phase transition by a conventional analysis of the XRD patterns. Nonetheless, this transition could be clearly detected with our PDF investigation using the very same experimental data, illustrating the usefulness of the PDF analysis for this kind of material. We found that all PDF curves (below and above the  $T_S / T_{SDW}$ ) could not be modeled with the same structure in all the r-range. This variation in the local structure in the Ba122 system is a good evidence of the presence of nanotwins in the sample. A previous PDF work reported the presence of nanotwins at 30 K [4], but no systematic study of the evolution in temperature was conducted. Our work focuses on the thermal evolution of the nanotwins and our results show that the variation of the local structure seems to be more important at low temperature.

- ^
- [1] T.M. Garitezi, et al., Bras.J.Phys. 43, 223 (2013); T.M. Garitezi, et al., J.Appl.Phys, 115, 17D711 (2014).
  - [2] T. Egami& S. Billinge, "Underneath the Bragg peaks: structural analysis of complex materials (Pergamon, 2003).
  - [3] F.A. Lima, M.E. Saleta et al., J. Synchr. Rad. 23, 1538 (2016).
  - [4] J.L. Niedziela, et al, Phys Rev. B. 86, 174113 (2012).

*Acknowledgements:* Experiment performed at LNLS under project nº XDS - 19016. The authors thank XDS beamline staff and LQU staff, for their technical support during the experiment.

# Pressure-induced Phase Transition and Phonon Anomalies in Sr<sub>2</sub>IrO<sub>4</sub>

Kousik Samanta<sup>1</sup>, D. S. Rigitano<sup>1</sup>, F. M. Ardito<sup>2</sup>, N. M. Souza-Neto<sup>2</sup>, and E. Granado<sup>1</sup>

*<sup>1</sup>Institute of Physics "Gleb Wataghin", UNICAMP, 13083-859 Campinas, SP, Brazil <sup>2</sup>Laboratório Nacional de Luz Síncrotron, Caixa Postal 6192, 13083-970, Campinas, SP, Brazil Email: ksamanta@gmail.com*

The combination of strong spin-orbit interaction and moderate electronic correlation makes the 5d transition metal oxide Sr<sub>2</sub>IrO<sub>4</sub> a potentially interesting system for its novel and exotic spin-orbit entangled  $J_{\text{eff}} = 1/2$  Mott-insulating state. The application of external pressure can tune the inter atomic distance and atomic arrangements, leading to a tuning of spin-orbit interaction, as well as the electronic and magnetic ground states. The lattice parameters and vibrations of Sr<sub>2</sub>IrO<sub>4</sub> were investigated by simultaneous Raman scattering and x-ray powder diffraction experiments as a function of pressure up to 45 GPa. The XRD and Raman experiments were carried out using XDS beamline of LNLS ( $E = 20$  KeV) and 514.5 nm laser line, respectively. The Sr<sub>2</sub>IrO<sub>4</sub> belongs to a distorted tetragonal structure with space group I41/acd. The a lattice parameter compressed much faster (30%) than c-axis with pressure, indicating an increased non-cubic crystal field with increasing pressure. We have observed the anomalies of lattice parameters and line-width at two pressure regions at  $\sim 16$  and 35 GPa, indicative of phase transition, without clear accompanying change in lattice symmetry. Raman scattering studies of Sr<sub>2</sub>IrO<sub>4</sub> shows the disappearance of two A<sub>1g</sub> modes at 179 and 255 cm<sup>-1</sup> at  $\sim 17$  GPa. A Fano-type asymmetric line shape of B<sub>2g</sub> mode at 386 cm<sup>-1</sup> was observed in the pressure between 16 to 35 GPa; this asymmetry disappear out of this pressure range. The Fano-interference is revealing that the low-energy orbital dynamics of Ir<sup>4+</sup> (5d<sup>5</sup>) electrons is impacted by the transitions. These results reveal a competition between distinct spinorbit configurations tuned by external pressure.

Acknowledgement: This work was supported by FAPESP; Grant Number: 2016/00756-6.

# Copper Chemical Environment in *Daphnia magna* exposed to copper nanoparticles

SANTOS, J.R.P.<sup>1</sup>, COSTA JR, G. T.<sup>1</sup>, GOMES, M.H.F.<sup>1</sup>, MONTEIRO, R.T.R.<sup>1</sup>, CARVALHO, H.W.<sup>1</sup>

<sup>1</sup> Centro de Energia Nuclear na Agricultura, University of São Paulo, Laboratory of Nuclear Instrumentation, 13416-000, Piracicaba

joyceribeiro123@gmail.br

Nanomaterials have been used in several segments because of their unique properties, which are consequence of their shape, size and chemical composition [1]. However, little is known so far about their behavior in soils, since they can remain in the organic matter or be leached into the aquatic environment [2]. If leached, they can affect filtering organisms as *Daphnia magna*, a model organism used to indicate environmental quality [1]. Literature shows that most papers are related to silver, titanium and zinc nanoparticles that are commonly determined by Transmission Electronic Microscopy (TEM) and Inductively Coupled Plasma Optical Emission Spectrometry (ICP-OES). These techniques afford determining their location and concentration, but they are not able to assess the speciation of these elements in daphnids, therefore, not allowing investigating any possible biotransformation. Thus, we probed the copper chemical environment in *D. magna* exposed to CuO nanoparticles (nCuO). For this, neonates and adults of *Daphnia* were exposed to nCuO dispersions (0.01 to 16 mg L<sup>-1</sup>), fixed in paraformaldehyde (4%), washed with phosphate buffer (pH 7.3) and analyzed by  $\mu$ -XANES technique, available at the XRF beamline, on the Brazilian Synchrotron Light Laboratory, Campinas/SP. The exposure time of neonates was 48 hours, while for adults was 21 days at lethal and effective concentrations that kills 100% of organisms, respectively. These concentrations were determined by acute and chronic assays made previously. In addition, nine reference compounds synthesized in our laboratory were also analyzed by  $\mu$ -XANES, at the XRF beamline. As daphnids are aquatic organisms, it was necessary to cover them with ultralene film on the support wrapped by kapton film to avoid drying the sample during  $\mu$ -XANES analysis (Fig. 1). The results show that there are chemical speciation of the nCuO to copper carbonate and copper oxide in *Daphnia* (neonates and adults) exposed to nCuO 80 nm at lethal and effective concentration. In adults exposed to nCuO 40 nm at effective concentration there is chemical speciation to copper oxide (Fig1). In a study about synchrotron irradiation in *Xiphinema vuittenezi* (nematode) exposed to CuSO<sub>4</sub>, is possible to compare similarity among glycine, glutamate acid and histidine spectra by XANES [3]. Theses results demonstrate that there may be biotransformation of copper compounds within invertebrates. The spectra indicate that copper bound to other compounds (biotransformation) may be associated with toxicity and death of *Daphnia* exposed to nCuO.

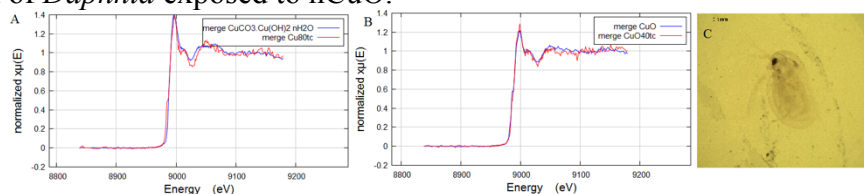


Figure 1. Merge spectra of CuCO<sub>3</sub>, Cu(OH)<sub>2</sub>.nH<sub>2</sub>O (A), CuO (B) and adults of *D. magna* exposed nCuO 80 and 40 nm. *D. magna* covered by ultralene film.

[1] Adam, N.; Vakurov, A.; Knapen, D.; Blust, R. J. Hazard. Mater. 283 (2015).

[2] Bashirnezhad, K.; Rashidi, M. M.; Yang, Z.; Bazri, S.; Yan, M. J. Thermal. Anal. Calorim. 122 (2015).

[3] Savoly, Z.; Pepponi, G.; Nagy, P.I.; Strelci, C.; Buzanich, G.; Chinea-Cano, E.; Zaray, G. X-ray Spectrom. 42 (2013).

**Acknowledgements:** This work was supported by CAPES. The authors would like to thank CENA/USP and CNPEM/LNLS.

# μ-XANES analysis for understanding of the interaction of ZnO nanoparticles in seeds of common bean

Savassa, S.M.<sup>1</sup>, Duran, N. M.<sup>1</sup>, Rodrigues, E.S.<sup>1</sup>, Pereira de Carvalho, H.W.<sup>1</sup>

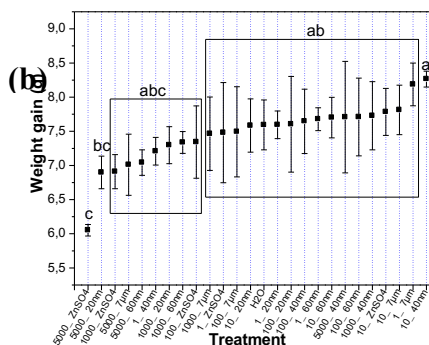
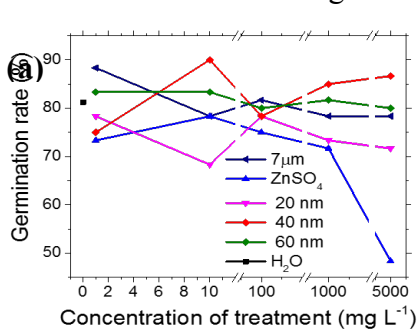
<sup>1</sup> Centro de Energia Nuclear na Agricultura-CENA, Universidade de São Paulo- USP, 10000-000, Piracicaba, Brazil;

susisavassa@gmail.com

Nanomaterials are present in our daily reality. It is necessary to understand how they interact in the environment. The number of scientific researches articles about this relevant subject increase each year, principally around the study of nanomaterials and plants. In this work, was study how nano ZnO nanoparticles interact and are transformed in common bean (*Phaseolus vulgaris*). The effect of nano ZnO on the germination of seeds and root absorption were investigated. Five different concentrations (5000; 1000; 100; 10 and 1 mgL<sup>-1</sup>) and different sizes of water dispersed non-coated nano ZnO (20; 40 and 60 nm) were evaluated. The higher concentration presented the worst results in the germination assay for all sizes tested when compared with the negative control (water). On the other hand, for the ZnO 40 nm at 10 and 100 mg L<sup>-1</sup> was possible to observe gain in germination rate and quantity of matter

observe gain in germination rate and quantity of matter

Figure 1: germination rate of the sizes 20; 40 and 60 nm at five concentrations 1000 and 5000 mg L<sup>-1</sup>. Figure 2 (a) and (b) shows the best result for ZnO 40nm 10 mg L<sup>-1</sup> treatment. The highest concentration of all treatments was toxic.



possible to observe gain in germination rate and quantity of matter

Results of assay testing and 60nm in different concentrations (1; 10; 100; 5000 mg L<sup>-1</sup>). The rate (a) and weight gain (b) shows the best result for ZnO 40nm 10 mg L<sup>-1</sup> treatment. The highest concentration of all treatments was toxic.

Analyzing seeds under these treatments in a bench top Micro X-ray Fluorescence Spectrometry (Micro-XRF) it is possible to see a Zn gradient of the external to internal part. Using the microbeam of XRF beamlines were performed in XRF beam line in LNLS, with the micro beam to discover the chemical environment of zinc in different points of the seed. Figure 2 present the experimental setup and Table 1 shows that for different concentrations of ZnO 40nm treatments present different quantities of each Zn ligand. These results indicate that zinc provided by nanoparticles of ZnO is incorporated by seed in germination and is modified in this process.

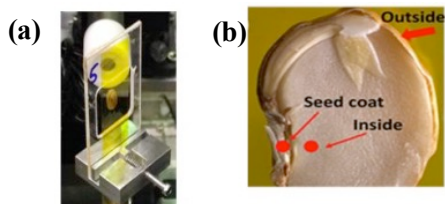


Figure 2 : Experimental setup of analyse in XRF beamline (a). In red, points of analyses in seeds (b).

Using the microbeam of XRF beamlines were performed in XRF beam line in LNLS, with the micro beam to discover the chemical environment of zinc in different points of the seed. Figure 2 present the experimental setup and Table 1 shows that for different concentrations of ZnO 40nm treatments present different quantities of each Zn ligand. These results indicate that zinc provided by nanoparticles of ZnO is incorporated by seed in germination and is modified in this process.

Sampled region	Percentual Fraction						Fit disagreement
	ZnO	Zn-Malate	Zn-Citrate	Zn-Hystidine	ZnSO <sub>4</sub>	Zn-Phytate	
<b>Seeds treateds</b>							
Seed coat with 40nm ZnO 5000 mg L <sup>-1</sup>	93.4	-	-	6.6	-	-	0.0007139
Cotyledon with 40nm ZnO 5000 mg L <sup>-1</sup>	-	-	-	100	-	-	0.002295
Seed outside region with 40nm ZnO 100 mg L <sup>-1</sup>	18.3	74.7	7.0				0.000962
Seed coat-inside region with 40nm ZnO 100 mg L <sup>-1</sup>	27.2	48.5	24.3				0.002862

Table 1: Percentual fractions values of different Zn ligands for the ZnO 40nm 5000 and 100 mg L<sup>-1</sup> treatments in bean seeds.

Acknowledgements: This work was supported by CNPQ, FAPESP and CAPES. The authors would like to thank the support time of XRF and XAFS2 beam line.

## Structure of CoO thin films under mechanical stress

JÚLIA SBORZ<sup>1,2</sup>, A. BORDIN<sup>1</sup> AND M. M. SOARES<sup>1</sup>

<sup>1</sup> Laboratório Nacional de Luz Síncrotron, 13083-100, Campinas, Brazil; <sup>2</sup> Universidade Federal de Santa Catarina, 88.906-072, Araranguá, Brazil.

julia.sborz@lnls.br

Cobalt oxide (CoO) is a unique antiferromagnetic (AFM) oxide due to its high magnetocrystalline anisotropy, Néel Temperature close to the room temperature and significant magnetostriction. Spintronic devices based on antiferromagnetic tunneling anisotropic magnetoresistance, for instance, may benefit from its properties [1]. Despite the fact that AFM materials have low susceptibility, it has been shown that it is possible to control orbital moment and spin orientation of CoO through strain. For CoO epitaxially grown on a substrate with smaller lattice parameter (compressive stress) the Co spin are oriented parallel to the film plane [2,3], while for a substrate with larger lattice parameter (tensile stress) spins are out-of-plane [2]. Aiming to control the spin orientation on CoO through deformations of its crystalline structure, we have grown CoO films on a flexible and stretchable substrate (Kapton) via sputtering and analyzed them under different levels of strain. We have optimized the ranges of oxygen and argon flux at 27 °C and at 300 °C to form stoichiometric CoO. An increase in the oxygen flux leads to the formation of Co<sub>3</sub>O<sub>4</sub> while a decrease forms Co. Performing XRD with in situ application of tensile stress, we have measured the strain in the film as a function of the applied stress by following the position of the diffraction peaks both in the direction of the applied stress (peaks shift to smaller angles) and perpendicular to it and to the film plane (peaks shift to higher angles). CoO showed a good adherence to Kapton and we were able to determine its elastic deformation region.

[1] K. Wang et al., Scientific Report 5, 15498 (2015).

[2] S. I. Csiszar et al., Physical Review Letters 95, 187205 (2005).

[3] A. Lamirand et al., Physical Review B 88, 140401(R) (2013).

## Study of the zeolitic precursor (P)MCM-22: nucleation and growth.

A. J. Schwanke<sup>1</sup>, P. Vinaches<sup>1</sup>, F. Meneau<sup>2</sup>, E. Morgado Jr<sup>3</sup> and S. B. C. Pergher<sup>1</sup>

<sup>1</sup>Universidade Federal do Rio Grande do Norte, Laboratório de Peneiras Moleculares, 59078-970, Natal, RN, Brasil.

<sup>2</sup>Laboratório Nacional de Luz Sincrotron (LNLS), Centro Nacional de Pesquisa em Energia e Materiais (CNPEM),

13083-970, Campinas, São Paulo, Brasil. <sup>3</sup>Petrobras/CENPES, 21941-915, Rio de Janeiro, RJ, Brasil

sibelepergher@gmail.com

The zeolitic precursor (P)MCM-22 is an aluminosilicate that can be adapted to a variety of catalytic applications by performing different treatments, such as expansion, delamination, pillaring or disorganization [1-4]. This versatility makes this material promising for industry and reveals the need of further studies aiming to optimize the synthesis procedure. So, in the present research work the nucleation and crystallization of the layered zeolitic precursor (P)MCM-22, with Si/Al gel ratio of 25, was followed by different characterization techniques. The first signals of nucleation were found within the second day of synthesis by X-ray diffraction (XRD, Figure 1-left). Scanning electron microscopy (SEM) analyses corroborated the XRD results since several small planar particles were noticed from the second day of crystallization. On the seventh day the formation of discoid-like crystallites was observed. The band at 3745 cm<sup>-1</sup> appearing in the Fourier-transformed infrared spectra (FTIR) indicated the decrease of the external silanol quantity when the crystallization time increases [5] due to the silica condensation and polymerization. It was also observed that the bands attributed to the organic structural agent (hexamethyleneimine, HMI) increases up to the seventh day. Finally, it was possible to identify the beginning of the nucleation after 1 day by small angle X-ray scattering (SAXS, Figure 1-right). These results also indicated the existence of a particle population in every sample, allowing the identification of the lamellar morphology in the smaller average size population [6].

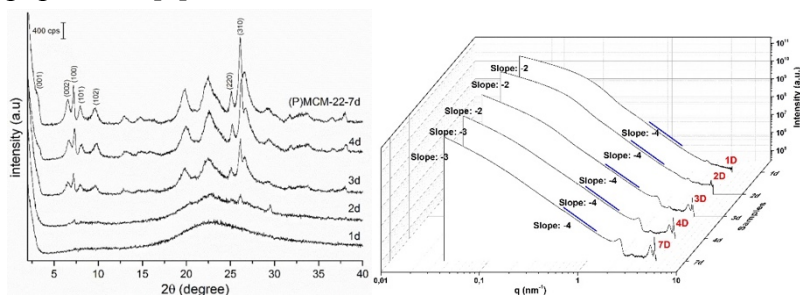


Figure 1. XRD (left) and SAXS (right) results of the samples.

[1] S.B.C. Pergher, A. Corma, V. Fornés. *Química Nova*, 26, 795 (2003). [2] M.V. Opanasenko, W.J. Roth, J. Cejka. *Catal. Sci. Technol.*, 6, 2467 (2016). [3] S.B.C. Pergher, A. Corma, V. Fornés. *Química Nova*, 26, 828 (2003). [4] A. Corma, V. Fornés, S.B.C. Pergher, T.L.M. Maesen, J.G. Buglass. *Nature*, 396, 353 (1998). [5] A. Corma, C. Corell, V. Fornés, W. Kolodziejski, J. Pérez-Pariente. *Zeolites*, 15, 576 (1995). [6] H. Schnablegger and Y. Singh, *The SAXS Guide* (Anton Paar GmbH, 2013).

Acknowledgements: This work was supported by PETROBRAS and CAPES. The authors would like to thank PPGCEM, UFRN and ITQ for the infrastructure, and LNLS/CNPEM for the SAXS measurements performed within the proposal number 20160104 entitled “In situ studies of MCM-22 synthesis”.

## Magnetite nanoparticles for hyperthermia cancer treatment

Willian Takemitsu Shigeyosi<sup>1</sup>, Fernanda Cristina Costa<sup>2</sup>, Jörg Kobarg<sup>3</sup> and Mateus Borba Cardoso<sup>4</sup>

<sup>1</sup> Universidade Federal de São Carlos, Departamento de Física, São Carlos, Brazil;

<sup>2</sup> Universidade Estadual de São Paulo, Instituto de Ciências Físicas e Biomoleculares, São Carlos, Brazil;

<sup>3</sup> Universidade Estadual de Campinas, Instituto de Biologia, São Carlos, Brazil;

<sup>4</sup> Centro Nacional de Pesquisa em Energias e Materiais, Laboratório Nacional de Nanotecnologia, Campinas, Brazil.

willian.takemitsu@gmail.com

One of the largest challenges on medicine has been developing treatments for several types of cancer. Moreover, conventional treatments for cancer such as chemotherapy and radiotherapy have been presenting undesirable secondary effects [1,2]. As an alternative, nanomaterials have the premise of improving and creating a new route of treatment and diagnosis. Currently, iron oxide nanoparticles are strongly studied especially because of their ability to produce heat when they are subjected to an alternating magnetic field. The mechanism of induced heating via external magnetic field is called magnetic hyperthermia [3] and, through this mechanism, it becomes possible to make the biothermic applications and use drug delivery system. The advantage of using a magnetic nanomaterial comes from the unusual feature known as superparamagnetism. The superparamagnetic systems does not present spontaneous magnetization nor coercive field therefore their magnetization curves do not present hysteresis losses. This way, the nanomaterial will not exhibit remanent magnetization.

This work aims to deal with fundamental aspects of cell biocompatibility and properties about physical and chemical characterization of Fe<sub>3</sub>O<sub>4</sub> nanoparticles. In this context, it will be approaching some questions about the use of iron oxide nanoparticles with distinct types of coatings. Discussing the advantages and disadvantages of each coating according to its physico-chemical characteristics as well as its cytotoxicity. In addition, this work approaches the hyperthermic magneto potential of these superparamagnetic coated nanoparticles by comparing their respective performances in the treatment of human's embryonic kidney cells HEK293T.

Through the development of this work it was observed that for a good bioapplicability's samples must present a low cytotoxicity, in this case the coatings formed by surfactants like centrimonium bromide and sodium dodecyl sulfate presented a high rate of cellular mortality not being indicated for the treatment. Finally, the potential of magnetic hyperthermia for a biocompatible nanomaterial should be evaluated, in this case the best results associated to hyperthermia treatment were obtained for nanoparticles coated with chitosan, polyethylene glycol and PEGylated phospholipid.

[1] Baskar R, Lee KA, Yeo R, Yeoh K. Cancer and Radiation Therapy : Current Advances and Future Directions. Int J Med Sci. 2012;9. doi:10.7150/ijms.3635.

[2] Jr ES, Urban C de A, Lima RS de, Iris Rabinovich, Spautz CC. Radioterapia e quimioterapia no tratamento do câncer durante a gestação - revisão de literatura. Rev Bras Cancerol. 2007;53(1):41-46.

[3] Wust P, Hildebrandt B, Sreenivasa G, et al. Review Hyperthermia in combined treatment of cancer. Lancet Oncol. 2002;3:487-497.

*Acknowledgements:* This work was supported by CNPEM, CAPES, FAPESP and CNPq

# Qualitative structure and strain determination of CeO<sub>2</sub> nanoparticles using atomic pair distribution function analysis

F.P. Silva<sup>1</sup>, M.S. Silva<sup>2</sup> and N. S. Ferreira<sup>1</sup>

<sup>1</sup> *Universidade Federal do Amapá, Departamento de Ciências Exatas e Tecnológicas, Macapá, Brazil;*

<sup>2</sup> *Instituto Federal do Sertão Pernambucano, Departamento de Mecânica, Ouricuri, Brazil.*

*Francimario.passos@gmail.com*

In this experiment, we aim to measure medium-range correlation lengths and size in undoped and Cr-doped CeO<sub>2</sub> nanoparticles using pair distribution function (PDF) analysis. Based on the obtained findings, we expect to make significant contributions to both amount of non-stoichiometric defects near grain boundary and variation of lattice strain influence on the ferromagnetic ordering in this system. Although all previous characterizations suggested that in our case the observed ferromagnetism in the Cr-doped CeO<sub>2</sub> samples is due to their intrinsic nature, it is not straightforward to judge from these measurements whether this ferromagnetism comes from Cr ions substituting the Ce site or structural defects etc. Therefore, our research is at a critical juncture that hinges on pinpointing the intrinsic structure of the amorphous/crystalline phase of DMS systems. Our accumulated experience so far dictates the need of using experimental techniques that can zero in on the disorder in the nanoparticle atomic lattice. It is well known that the PDF technique allows both the Bragg and diffuse scattering to be analyzed together without bias, revealing the short and intermediate range order of the material regardless of the degree of disorder even in the case of polydisperse nanoparticles. Thus, a PDF analysis through the combination of SQUID, HRTEM, XRD and XPS techniques will get a better insight into the room temperature ferromagnetism of Cr-doped CeO<sub>2</sub> samples. Therefore, the purposed PDF studies made it possible to observe the presence of defects in the nanoparticle structure could cause a lattice distortion and the crystalline core and amorphous grain boundaries in the CeO<sub>2</sub> nanoparticles. Then, the results from this proposed experiment will help us to elucidate where is this magnetism located in the CeO<sub>2</sub> nanoparticles and also whether the observed ferromagnetism in the Cr-doped CeO<sub>2</sub> samples is indeed due to Cr ions substituting the Ce site, non-stoichiometric defects near grain boundary or lattice strain.

<sup>1</sup> N. S. Ferreira and M. A. Macêdo, *Advanced Materials Research* **975**, 7 (2014).

<sup>2</sup> N. S. Ferreira, L. G. Abraçado, and M. A. Macedo, *Physica B* **407** (16), 3218 (2012).

<sup>3</sup> N. S. Ferreira, L. G. Abraçado, and M. A. Macêdo, *J Supercond Nov Magn* **26** (7), 2549 (2013).

# A study of M-type $MFe_{12}O_{19}$ (M=Ba and Sr) nanoparticles by X-ray diffraction and atomic pair distribution function

F.P. Silva<sup>1</sup>, M.S. Silva<sup>2</sup> and N.S. Ferreira<sup>1</sup>

<sup>1</sup> Departamento de Física, Universidade Federal do Amapá, 68902-280, Macapá, AP, Brazil

<sup>2</sup> Instituto Federal de Educação, Ciência e Tecnologia do Sertão Pernambucano, 56000-000, Salgueiro, PE, Brazil

nilsondsf@gmail.com

The hexagonal ferrites nanoparticles have been extensively studied because of its possibility of different technological, such as magneto-optic devices, microwave devices, microelectromechanical systems, and transformer cores [1]. Recently, M-type hexagonal ferrites, i.e.,  $MFe_{12}O_{19}$  (M=Ba, Sr and Pb), have been widely investigated for its relatively large magnetization, high performance permanent magnetic and material high Curie temperature [2,3]. In this work, all samples were synthesized by a citric acid based sol-gel method. Both  $BaFe_{12}O_{19}$  and  $SrFe_{12}O_{19}$  nanoparticles were obtained by thermal treatment at 900 and 1000 °C for 1 h. The local structure of M-type  $BaFe_{12}O_{19}$  nanoparticles have been studied using synchrotron X-ray diffraction (SCXRD), Rietveld refinement, and the atomic pair distribution function (PDF) technique. SCXRD patterns data and PDF confirmed the hexagonal structure of space group  $P6_3/mmc$  for  $BaFe_{12}O_{19}$  and  $\alpha-Fe_2O_3$  as main impurity phase. Rietveld refinement from SCXRD and PDF results showed that lattice parameters values are in the range  $5.879 \leq a = b \leq 5.882 \text{ \AA}$  and  $23.018 \leq c \leq 23.037 \text{ \AA}$ . The first nearest neighbor distances for samples were about at  $r = 2.335 \text{ \AA}$  from a  $Fe^{3+} - Fe^{3+}$  pair. This is a of the most intense peaks because is metal-metal bonding, which is more perceptible in the total X-ray scattering. The second strong and intense peaks was also of metal-metal bonding with distances of  $3.834 \text{ \AA}$ , which represent  $Ba^{2+} - Ba^{2+}$  for samples  $BaFe_{12}O_{19}$ . The third peak more intense is from a covalently bonded  $Fe^{3+} - O^{2-}$  pair. Moreover, high values of atomic displacement parameters determined by PDF analysis suggest a certain local disorder of atoms in the hexagonal crystal lattice. This disorder is due to nearest Fe(2)-O(1) bond lengths thermal treatment dependent, which results in the oxygen bipyramid distortion around the Fe(2) crystallographic position of  $Fe^{3+}$  cation. The structural coherence length is approximately 50-70 nm, in good agreement with Scherrer method observations. The combination of synchrotron X-ray diffraction and atomic PDF proved to be a powerful technique able to reliably determine the atomic scale crystal structure of hexagonal ferrites nanoparticles.

[1] V. Šepelák, M. Myndyk, R. Witte, J. Röder, D. Menzel, R. H. Schuster, H. Hahn, Paul Heitjans, and K-D. Becker. *Farad. Discuss.* 170, 121(2014).

[2] F.N. Tenorio-González, A.M. Bolarín-Miró, F. Sánchez-De Jesús, P. Vera-Serna, N. Menéndez-González, and J. Sánchez-Marcos. *J. Alloys Compd.* 695, 2083 (2017).

[3] W.M.S. Silva, N.S. Ferreira, J.M. Soares, R.B. da Silva, and M.A. Macêdo. *J. Magn. Magn. Mater.* 395, 263 (2015).

*Acknowledgements:* This work was supported by the the Santander Bank through the Iberoamerican grants for Young Professors and Researchers (Edital No. 07/2015/PROCRI/UNIFAP). The authors acknowledge support from the CNPq (Grant No. 152026/2016-9) and LNLS/CNPEM (Brazilian Synchrotron Light Laboratory e Brazilian Center for Research in Energy and Materials) (proposal XDS#20160288).

# Micelles and hybrid silicas formation with tripropylammonium surfactants and different hydrophobic tails

Laura L. da Silva, Iago W. Zapelini, Pedro P. Modesto, Ana F. P. Campos, Lucas B. de Oliveira, Juliana F. da Silva, Dilson Cardoso

Federal University of São Carlos, Chemical Engineering Department, Catalysis Laboratory, 13565-905, São Carlos, Brasil, [www.labcat.org](http://www.labcat.org),

*dilson@ufscar.br*

Mesoporous materials have several applications and arouse the interest of many researchers. In this type of materials, the M41S silicas stands out because of its properties: high surface area and porosity and adjustable pore diameter. These properties depend on several factors during the synthesis steps, like: molar composition of the reaction mixture, silica source and the type of cationic surfactant used for mesopores formation. The type and the molar concentration of surfactant, the temperature and pH of aqueous dispersion change the micellar diameter, the aggregation number ( $N_{ag}$ ) and the critical micelle concentration (CMC). In this sense, this work aims to evaluate the influence of alkyltripropylammonium surfactants with different hydrophobic tails length ( $C_n$ TPABr,  $n = 14, 16, 18, 20$  e  $22$ ) on the micelles formation in aqueous dispersions and on the formation of mesoporous silicas. The CMC of the surfactants were determined by electric conductivity. The results showed the increasing of hydrophobic tail reduces the CMC, indicating the facility to aggregation and then, more micelles are formed. These results accord to small angle X-ray scattering (SAXS) curves, in which was observed the increasing of micellar organization by the increasing of the surfactant hydrophobic tail. The SAXS curves also showed the decreasing of intermicellar distance when hydrophobic chain increase, what is attributed to high micelles diameter provided by long tails. X-ray patterns of the hybrid silicas prepared with  $C_n$ TPABr ( $n = 14, 16$  and  $18$ ) showed that the structure of these materials have low organization, presenting only one diffraction peak, corresponding to (100) plane. Increasing the number of carbons ( $n = 20$  and  $22$ ), there were observed the formation of MCM-41 structure, with (110), (200) and (210) peaks. This result can be explained by the facility of micelle formation of  $C_{20}$ TPABr e  $C_{22}$ TPABr surfactants, confirmed by SAXS, what probably favors the cooperative mechanism during the synthesis.

[1] V. K. Aswal, P. S. Goyal, H. Amenitsch, S. Bernstorff, *Pramana - J Phys.*, 63: 333 (2004).

[2] A. F. P. Campos, A. R. O. Ferreira, and D. Cardoso, D., *Química Nova*, 39(3), 279 (2016).

*Acknowledgements:* The authors would like to thank to FAPESP (2016/21033-2) and CAPES for the financial support.

# Long-term drug release using SiO<sub>2</sub>-Poly(oxypropylene)hybrid matrix: correlation between the release mechanism and the physical-chemical characteristics.

Silva, R.<sup>1,\*</sup>; Dahmouche, K.<sup>1</sup>; Santilli, C.V.<sup>2</sup>

<sup>1</sup>UFRJ, Rio de Janeiro, Brazil.    <sup>2</sup>I.Q. UNESP, Araraquara, SP, Brazil.

\* raniellesilva@ima.ufrj.br

Organic-inorganic hybrids have received increasing attention in the last decade as emerging materials for applications in diverse areas such as energy, environment, health or optics [1]. The flexible, transparent and chemically stable materials, obtained through a Sol-Gel process, consist of siloxane nanoparticles interconnected to polyoxypropylene (PPO) chains by means of urea bridges (Si-PPO) that bring particularly promising characteristics. As a consequence of these peculiarities, these materials are currently being investigated for biological applications such as controlled drug release. In particular, we synthesized these hybrids with the intent to utilize them as drug delivery systems for Propranolol Hydrochloride, a hypertension-related drug. The influence of the polymeric phase on the drug release has been investigated comparing two hybrid materials distinguished by two different polymer chain lengths: the first hybrid, named Si-PPO-4000, synthesized with a PPO molar mass of 4000 g/mol, and hence having a more marked hydrophobic nature. On the contrary, the second hybrid, with a polymer chain molar mass of 230 g/mol and named Si-PPO-230, is characterized by a less hydrophobic nature and different mechanical and optical properties due to a higher hydrophilic/hydrophobic moiety ratio. As a consequence, the drug release kinetics occurs through two different regimes along an uncommonly prolonged period: 1500 hours for the Si-PPO-4000 samples and about 5000 hours for the Si-PPO-230.

Different techniques (DRX, TGA, DSC, FTIR and SAXS) have been used to characterize each stage in the release process. As regard the PPO-4000 sample, XRD, TGA and DSC showed that water intake into the matrix and drug release did not occur homogeneously but they start from the outer regions of the sample and proceed gradually toward the core. By way of a simultaneous XRD and DSC measurement, this water uptake has been confirmed through the observation of different phase transitions: two endothermic peaks (DSC), linked to water melting and evaporation, and a peculiar thermal transition between -28°C and -38°C. This has been associated to the presence of meta-stable water or to a combination between a cubic and hexagonal water crystal phases thanks to the appearance of characteristic peaks in the XRD plot [2]. SAXS measurements have also revealed a complex structure formed by a network of loosely packed polymer chains interconnected by silica and regions with silica aggregates within densely packed polymer chains. The size of these aggregates has been observed to evolve during the release process while these changes have been correlated with each of the release mechanisms.

SAXS analysis of the Si-PPO230 sample showed the presence, and subsequent size variations, of silica aggregates. Moreover, this sample displayed, after circa 700 hr of release, the appearance of an electron scattering attributed to the presence of secondary aggregates. These are formed by the intralamellar interaction of urethane moieties that connect the organic and inorganic phases in the hybrid network.

These results suggest that the structural modifications of the system - such as the formation of confined water regions in the hybrid network, the size variation of the nanometric aggregates and the formation of urethane aggregates - are related with the different stages, and the consequent mechanisms, of drug release.

1. C. Sanchez *et al.* *Chemical Society Reviews*. **2011**, 40, 696.
2. T. Yamaguchi *et al.* *Journal of Molecular Liquids*. **2006**, 129, 57.

# Radiation damage caused by soft X-rays in sulfur tripeptides in solution: Why should we care?

SIMÕES, G.<sup>1</sup>, GONZALEZ, J.C.<sup>1</sup>, BERNINI, R.B.<sup>2</sup>, COUTINHO, L. H.<sup>3</sup> and DE SOUZA, G.G.B.<sup>1</sup>

<sup>1</sup> Universidade Federal do Rio de Janeiro, Instituto de Química, 21941-909, Rio de Janeiro, Brazil;

<sup>2</sup> Instituto Federal do Rio de Janeiro, 25050-100, Rio de Janeiro, Brazil;

<sup>3</sup> Universidade Federal do Rio de Janeiro, Instituto de Física, 21941-909, Rio de Janeiro, Brazil.

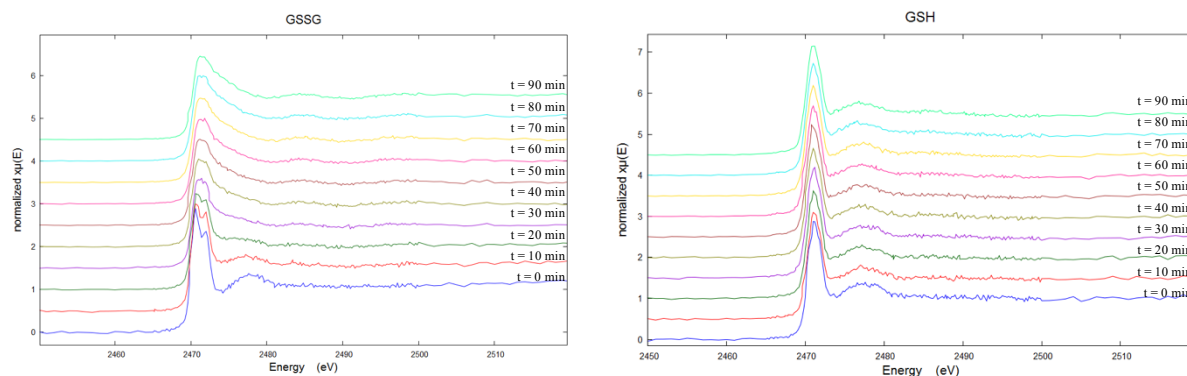
grazielisimoes@iq.ufrj.br

Glutathione (GSH) is a tripeptide ( $\gamma$  glutamylcysteinylglycine) present in a broad range of organisms, plants and humans. Plants cannot survive without glutathione or related homologues. The biological functions of GSH relate principally to reversible redox reactions of the cysteine sulfur group, resulting in the coexistence of a reduced state (GSH) and an oxidized state (GSSG) [1,2].

The oxidized state presents a disulfide bridge which is usually formed by two cysteine molecules, pertaining to proteins polypeptide chains. The (tertiary and quaternary) form of proteins composed of more than one chain can be altered by the action of various agents, such as: organic solvents, temperature, pH and radiation damage among others.

In previous work, our group already discussed the effects of radiation damage in solid insulin [3]. The aim of the present work is to bring additional insight and to examine structural modifications towards the analysis of the radiation damage of sulfur-containing biomolecules in liquid phase by the exposure of soft X-rays during the photoabsorption analysis (NEXAFS).

The experiments were performed at SXS beamline of LNLS. NEXAFS spectra were obtained in the fluorescence mode, around the S 1s edge. The tripeptide solutions were prepared in a buffer (tris(hydroxymethyl)aminomethane/HCl) at pH 7,5 and were exposed for 1.5 hours to soft X-rays. NEXAFS spectra of GSSG and GSH are shown in the Figures below.



[1] Noctor G., *et al.* Glutathione in plants: an integrated overview (Plant, Cell and Environment, 2012) p 454.

[2] D.Voet, J.G.Voet, C.W.Pratt, Fundamentos de Bioquímica (Artmed Editora, 1999).

[3] G.Simões, F.N.Rodrigues, R.B.Bernini, C.S.C. Castro and G.G.B. de Souza, A NEXAFS and mass spectrometry study of cysteine, cystine and insulin irradiated with intermediate energy (0.8 keV) electrons (J.El.Spectr.Rel.Phen, 2014) p 21.

*Acknowledgements:* The authors would like to thank CNPq, CAPES, PGQu-IQ/UFRJ and LNLS for financial support.

# Thermo-mechanical stability of austenite in post weld heat treated supermartensitic stainless steel weld metal

H. G. Svoboda<sup>1,2</sup>, L. Tufaro<sup>1,3</sup> and S. Zappa<sup>2,4</sup>

<sup>1</sup> Universidad de Buenos Aires, Facultad de Ingeniería, INTECIN, GTSyCM3, 1127, Buenos Aires, Argentina; <sup>2</sup> CONICET, Buenos Aires, Argentina; <sup>3</sup> Instituto Nacional de Tecnología Industrial, Centro de Mecánica, San Martín, Argentina; <sup>4</sup> Universidad Nacional de Lomas de Zamora, Facultad de Ingeniería, Lomas de Zamora, Argentina.

hsvobod@fi.uba.ar

Supermartensitic stainless steels (SMSS) were developed based on the classical martensitic stainless steels (11-14% Cr), reducing the C content and increasing the Ni and Mo contents. SMSS have been developed as a technological alternative of a lower cost with good mechanical properties and corrosion resistance to be applied in the petrochemical industry and pipelines to transport oil and gas, both onshore platforms and "off-shore". Semiautomatic welding process is recognized as a very interesting technological alternative for the welding of these materials and their industrial implementation has grown in recent times. In these steels, post-weld heat treatments (PWHT) are usually necessary to adjust the final properties of weld deposits, based on microstructural evolution (control of martensite, martensite tempered, austenite, delta ferrite, carbides contents, etc.). The PWHTs used are single and double tempering to ensure a full martensite tempered and maximize the retained austenite. This is the most important phase in these steels because it can modify the hardness, tensile properties, toughness and corrosion resistance, reaching high values for certain heat treatments. Austenite contains a high density of dislocations and enrichment of Ni and C with respect to the matrix [1,2]. One of the main characteristics of this phase is to be stable at room temperature and does not transform to martensite with subsequent cooling. The mechanical stability of the austenite is defined as the susceptibility of austenite to transform into martensite, as induced by plasticity. An austenite of higher mechanical stability needs more strain to transform into martensite than that of lower mechanical stability. Regarding the mechanical stability of the austenite in SMSS has not been widely studied in the literature. At low temperatures, retained austenite is less stable and transforms to martensite easily [3]. Under mechanical load, cooling below ambient temperature or combinations thereof retained austenite can be transformed into martensite. This fact can modify the structural integrity of welded component. In this sense, the study of the mechanical stability of the austenite in SMSS weld metals is an aspect that presents scientific and technological relevance and there is scarce information published about it. The aim of this work is to analyze in -situ the stability of the austenite in SMSS weld metals under mechanical loads, for different welding conditions and PWHT's using a XTMS station. Evaluation of the effect of temperature and strain rate in the mentioned stability is also considered. In this sense, samples with different welding conditions and PWHT were mechanically tested in a Gleeble machine, at different temperatures (60 to -20 °C) and strain rates (0,1 mm/min to 10 mm/min), with in-situ monitoring of austenite evolution. It could be determined the austenite transformation during mechanical testing, obtaining a critical strain, for each temperature and strain rate. The mechanisms involved in the austenite transformation in this material was discussed.

[1] Bilmes, P. D., Solari, M. y Llorente, C. L.; *Materials Characterization*; 46; 2001.

[2] Gooch, T. G., Wolling, P. y Haynes, A. G.; *Supermartensitic Stainless Steel*, Brussels, Belgium; 1999.

[3] Berrahmoune M.R., et al.; *Materials Science and Engineering A*; 378 2004.

*Acknowledgements:* This work was supported by ANPCYT and APUEMFI. The authors would like to thank ESAB, Air Liquide, INTI-Mecánica, INTECIN and Ing. Leonardo Wu (LNNano).

# New method in the growth of thin films of Ag<sub>2</sub>Se and structural study through Synchrotron radiation X-ray grazing incidence diffraction with *in situ* heating

J A Perez Taborda<sup>1,2</sup>, F Briones<sup>1</sup> and M S Martin Gonzalez<sup>1</sup>

<sup>1</sup>*Instituto de Microelectrónica de Madrid, CSIC, 28760 Tres Cantos, Madrid, Spain*

<sup>2</sup>*Sociedad Colombiana de Ingeniería Física, SCIF, Colombia*

In this work, we propose a new route to obtain Ag<sub>2+x</sub>Se, which consists of a reactive sputtering method that gives rise to highly crystalline films of controlled stoichiometry in a matter of minutes. We have previously reported the development and fabrication of this new system, namely *Pulsed Hybrid Reactive Magnetron Sputtering* (PHRMS) <sup>[1]</sup>, which is based on a DC reactive sputtering. This method includes a fine control on the amount of selenium present in the alloy, fast growth rate, accurate control over the stoichiometry, and it is easily scalable for industrial production.

It is known that Ag<sub>2</sub>Se has two temperature-dependent phases, termed as low-temperature orthorhombic ( $\beta$ )-phase and high-temperature cubic ( $\alpha$ )-phase, with the structural phase transition temperature around 133 °C. In the high-temperature phase, the selenium atoms form a body-centred cubic (bcc) packing, while the silver atoms are statistically distributed over several interstitial sites. Ag<sub>2</sub>Se was investigated by means synchrotron radiation grazing incidence X-ray diffraction (SR-GIXRD) in National Synchrotron Light Source at the Brazilian Synchrotron (LNLS)—XRD2 beamline—in Campinas, Brazil. The SR-GIXRD diffraction patterns obtained from room temperature to 300 °C and its subsequent controlled cooling to room temperature again in a controlled argon atmosphere are shown.

[1] J. A. Perez-Taborda, L. Vera, O. Caballero-Calero, E. Lopez, J. J. Romero, D. G. Stroppa, F. Briones, and M. Martin-Gonzalez, *Advanced Materials Technologies* (2017).

## Magnetic Structures and Transitions of RNiSi<sub>3</sub> (R = Gd-Ho)

Rodolfo Tartaglia<sup>1</sup>, D. V. A. Giraldo<sup>2</sup>, M. A. Avila<sup>2</sup> and E. Granado<sup>1</sup>

*<sup>1</sup> Universidade Estadual de Campinas, Departamento de Eletrônica Quântica, 13083-859, Campinas, Brazil; <sup>2</sup> Universidade Federal do ABC, Centro de Ciências Naturais e Humanas, 09210-580, Santo André, Brazil  
rodolfotartaglia.s@gmail.com*

Rare earth-based materials have received considerable attention over the years due to many interesting physical phenomena, such as highly anisotropic magnetic properties associated with the unquenched orbital moments are commonly observed. Recently, a new series of rare earth intermetallic compounds RNiSi<sub>3</sub> (R = Y, Gd-Tm) were synthesized, based on the isostructural compound YbNiSi<sub>3</sub>. Magnetic susceptibility measurements indicate antiferromagnetic phases at low temperatures (T<sub>N</sub> = 2-32 K) with fairly marked anisotropy. However, the magnetic structures, among the different possibilities for an antiferromagnetic ordering, still need to be determined. Knowing that photons are also sensitive to the electronic magnetic moments, leading to the appearance of magnetic Bragg peaks in the ordered phase of the material, we intend to contribute to the characterization and understanding of the magnetism of such systems by means of resonant magnetic x-ray diffraction experiments. These peaks may be strongly intensified when the energy of the X-rays coincides with some absorption edge of the magnetic element, causing a resonant scattering condition. This gives to the technique the advantage of being element-selective and allow us to solve the magnetic structures and investigate the phase transitions induced by temperature and, if possible, magnetic field. The diffraction measurements described above will be carried out at the XDS (X-ray Diffraction and Spectroscopy) beamline of LNLS, starting the second semester of 2017.

Acknowledgements: This work was supported by CAPES and FAPESP.

# In-situ electrochemical cell for lithium ion batteries and X-ray absorption studies.

J.E. Thomas<sup>1</sup>, L.J. Giovanetti<sup>1</sup>, M.A. Sanservino<sup>1</sup>, G. Azevedo<sup>2</sup>, F.G. Requejo<sup>1</sup> and A. Visintin<sup>1</sup>

<sup>1</sup>Instituto de Investigaciones Físicoquímicas Teóricas y Aplicadas (INIFTA), Facultad de Ciencias Exactas, (UNLP), CCT La Plata-CONICET, CC 16, Suc. 4, 1900 La Plata, Argentina

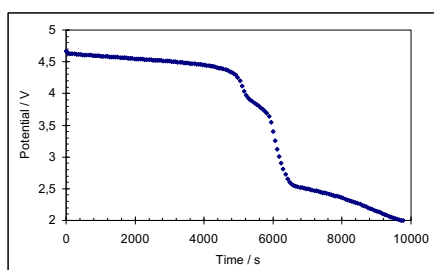
<sup>2</sup>Brazilian Synchrotron Light Laboratory (LNLS), Campinas, SP, Brazil

enryjt@inifta.unlp.edu.ar

To improve the performance and efficiency of Li based batteries is indispensable to have a clear comprehension of the processes that occurs during the use of these systems. But some times, these physicochemical processes can not be detected by electrochemical measurements, and in the case of lithium ion batteries, the possibility to make electrochemical experiments in a classical three electrodes open cell joined to other chemical or physical techniques is very hard. Typical impediments to this type of experiment are, for example, the nature of the electrodes, electrolytes and working conditions of these types of batteries. For this reason we develop an in-situ lithium ion battery cell system capable to work in typical current/potentials experiments for these kinds of batteries and at the same time allow performing X-Ray absorption experiments over the active materials.

With this setup it is now possible to characterize different anodic and cathodic active materials by X-ray spectroscopy techniques like XANES and EXAF at different working conditions i.e. different states of charge (SOC) or during a potentiodynamic running and also under normal operation conditions like charge-discharge cycles. The aim of this work is focused the use of the same electrochemical cell not only to XAFS but also to other types of techniques (XRD, XRF, etc) working at faster potentiodynamic experiments or higher current conditions. In this work we present our recent results obtained in the DXAS beam line at the LNLS with a home made 5 Volts spinel ( $\text{LiNi}_{0.5}\text{Mn}_{1.5}\text{O}_4$ ) cathode under working conditions. Figure 1(a) shows a picture of the in-situ cell ensemble (inside of the adapter) ready to work in the beam line and (b) discharge potential profile of the cell working at  $-300\mu\text{A}$  between 5V and 2V. Figure 1(c) shows XANES spectra of Mn and Ni K-edges during a discharge.

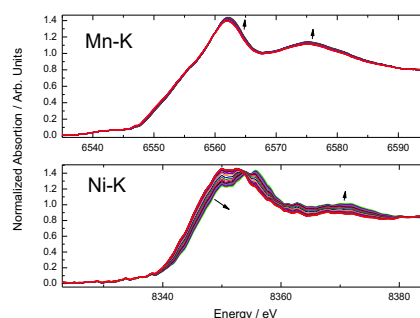
a)



b)



c)



**Acknowledgements:** This work was supported by CONICET, Agencia Nacional de Promoción Científica y Tecnológica, Universidad Nacional de La Plata and Laboratorio Nacional de Luz Síncrotron (DXAS proposal 20160731). The authors would like to thank Prof. Dr. Luciano Montoro for his invaluable support.

## X-Ray Absorption Study on Native Defects of Cu<sub>2</sub>O

Milton A. Tumelero<sup>1</sup>, Iuri S. Brandt<sup>2,3</sup> and Andre A. Pasa<sup>2</sup>

*1 Instituto de Física, Universidade Federal do Rio Grande do Sul,  
UFRGS, C.P. 15051, Porto Alegre, RS 91501-970, Brazil*

*2 Laboratório de Filmes Finos e Superfícies, Departamento de Física, Universidade Federal de  
Santa Catarina, Florianópolis, Brazil*

*3 Programa de Pós-Graduação em Ciência e Engenharia de Materiais,  
Departamento de Engenharia Mecânica, Universidade Federal de  
Santa Catarina, Florianópolis 88040-900, Brazil*

Cuprous oxide (Cu<sub>2</sub>O) is semiconductor material with wide bandgap of 2.1 eV and natural p-type doping, that have been extensively studied for the development of electronics, spintronics, optoelectronics and photovoltaics efficient devices. Most recently, this compound has attracted attention for the construction of photoelectrochemical cell (PEC), for hydrogen generation. One of main attributes of Cu<sub>2</sub>O, in comparison to other oxides and semiconductors used for this proposes, is the possibility of grow thin films by several inexpensive and scalable methods, such electrodeposition. Nevertheless, the lack in consensus about the electrical properties of this oxide has brought severe obstacles for the application of Cu<sub>2</sub>O [1]. In the specific case of electrodeposited samples, the electrical characterization has proven to be much more complicated, with large dispersion in electrical resistivity reports and unrevealed conduction origin, usually attributed to the difficulty in performing electrical measurements. In general, the p-type conduction of Cu<sub>2</sub>O occurs due the existence of native point defects, such copper vacancies, that induces energy levels inside of bandgap and about 0.2 eV above valence band maximum. For electrodeposited Cu<sub>2</sub>O, these levels occur about 0.6 eV above valence band and the native point defect that generate the conduction remains unknown. Here, using X-Ray absorption spectroscopy (XAS) on electrodeposited samples of Cu<sub>2</sub>O with different thicknesses, we propose a method for evaluate point defects concentration based in the local coordination of the defects. The results indicate high concentration of defects such copper vacancies and interstitials oxygens. A transition in the most concentrated point defect was found changing the thickness of the films, and attributed to the variation of lattice parameter. Theoretical calculations based in density functional methods support the experimental results.

- [1] I.S. Brandt, M.A. Tumelero, S. Pelegrini, G. Zangari, A.A. Pasa, Electrodeposition of Cu<sub>2</sub>O: growth, properties, and applications, J. Solid State Electrochem. 21 (2017) 1999–2020. doi:10.1007/s10008-017-3660-x.

## Properties of hybrid silicas synthesized using different cationic surfactants with cyclic head

Iago W. Zapelini, Laura L. da Silva, Pedro P. Modesto, Paula M. Fukuda, Karen N. Franke,  
Mariana S. Vasconcellos, Dilson Cardoso

*Federal University of São Carlos, Chemical Engineering Department, Catalysis Laboratory, 13565-905, São Carlos,  
Brasil, www.labcat.org  
dilson@ufscar.br*

The M41S materials family consists of mesoporous molecular sieves (MCM-41, MCM-48 and MCM-50) developed by Mobil, that have several applications due to their exceptional characteristics. Recently, the hybrid hexagonal mesoporous silica, MCM-41, was applied as catalyst in base catalyzed reactions. Its activity can be attributed to the presence of siloxi anions inside the pores and on the surface of the silica. Generally, the synthesis of this catalyst uses cetyltrimethylammonium bromide (CTABr) as directing agent of mesopores. However, other works show that CTABr can be substituted by other cationic surfactants, what can improve the structure organization or the catalytic activity of MCM-41. In this sense, this work aims to study the influence of different cationic surfactants with cyclic hydrophilic heads (cetylmethylimidazolium (CMImBr), cetylvinylimidazolium (CVImBr), cetylallylimidazolium (CAImBr) and cetylpyridinium (CPyBr) bromides on the formation of aqueous micelles and mesoporous hybrid silicas synthesized from them. The small angle X-ray scattering (SAXS) curves of aqueous surfactant dispersions showed high scattering intensities to smaller head sizes, indicating that the increasing of the sized of the hydrophilic head hinders the micelle formation. The SAXS curves also show that the increasing of the surfactant concentration reduces de intermicellar distance for all surfactants. The hybrid silicas were synthesized using tetraethyl orthosilicate (TEOS) as silica source and the above surfactant dispersions and were characterized by X-ray diffraction. The results showed the formation of hexagonal MCM-41 structure with CPyBr, CMImBr and CVImBr. The silicas prepared with CAImBr just have a mesoporous structure with low organization. The structural organization depends on the surfactant concentration, which increases by the increasing of available cations to micelle formation.

[1] F. Michaux, N. Baccile, M. Impéror-Clerc, L. Malfatti, N. Folliet, C. Gervais, S. Manet, F. Meneau, J. S. Pedersen and F. Babonneau. *Langmuir* 28, 17477 (2012). [2] J. A. Araújo, F. T. Cruz, I. H. Cruz, D. Cardoso, *Microporous Mesoporous Mater.* 180, 14 (2013).

Acknowledgements: The authors thank to FAPESP (2016/21033-2) and CAPES for the financial support.

# Tambo Colorado pigments: a archaeometric study by synchrotron X-ray diffraction

E. Zeballos-Velásquez<sup>1</sup>, V. Wright<sup>2</sup>, L. Suescun<sup>3</sup> and E. Asto<sup>1</sup>

<sup>1</sup> Universidad Nacional Mayor de San Marcos, Laboratorio de Cristalografía, Lima, Perú; <sup>2</sup> Instituto Francés de Estudios Andinos, Lima, Perú; <sup>3</sup> Universidad De La República, Montevideo, Uruguay.

ezeballosv@unmsm.edu.pe

Tambo Colorado (see Figure) is one of the most impressive archaeological sites in the Southern Peruvian coast, because of its stunning architecture, its extraordinary pictorial decoration, and its strategic location in the section of the Great Inca Road. The Research Project Tambo Colorado considers necessary to conduct a comprehensive analysis encompassing nature of the materials (archaeometric analysis) as well as a proper understanding of their conservation status of its architecture. In this regard interdisciplinary research provides the necessary tools to achieve these goals. Due to of this transdisciplinary approach, one of the main objective is the study of painting technology developed by the craftsmen of the site. The first results obtained using different techniques, in particular **Synchrotron X-Ray Diffraction (SXR)**, allow us to identify the coloring materials used.



Figure. Tambo Colorado. Adobe construction with Inca typical tracing.

The samples which were prepared as powder were then studied by SXR [1] at the Laboratório Nacional de Luz Síncrotron (Brazil), using the XPD beamline, with 4+2 circle Huber diffractometer setup for in-situ diffraction measurements with rapid detection and high resolution. The analysis using SXR are very important since they allowed identifying the presence of mineral components complementing the results from the elemental composition acquired through X-ray Fluorescence. In addition, they allow obtaining quantitative compositional data using the Rietveld method [2]. These data enabled to reconstruct the operational chain followed to elaborate the murals (since the pigments extraction to the making of the murals) but also to consider and develop a suitable surfaces conservation plan.

[1] P.L. Lee, D. Shu, M. Ramanathan, C. Preissner, J. Wang, M. A. Beno, R. B. Von Dreele, L. Ribaud, C. Kurtz, S. M. Antao, X. Jiao, B. H. Toby, J. Synchrotron Rad. 15 (2008) 427-432.

[2] R. A. Young, A. C. Larson, C. O. Paiva-Santos, *User's guide to program dbws-9807a for Rietveld analysis of X-ray and neutron powder diffraction patterns with a PC and various other computers*. School of Physics, Georgia Institute of Technology, Atlanta, GA, E.U.A. (2000).

*Acknowledgements:* This work was supported by Vicerrectorado de Investigación de la Universidad Nacional Mayor de San Marcos. The authors would like to thank to the Laboratório Nacional de Luz Síncrotron by providing facilities for the measures with synchrotron light.